CO and H_2S in H_2: contamination, recovery and mitigation strategies in PEMFCs with ultra-low Pt loaded anode electrodes

Von der Fakultät 4 – Energie-, Verfahrens- und Biotechnik der Universität Stuttgart zur Erlangung der Würde eines Doktors der Ingenieurwissenschaften (Dr.-Ing.) genehmigte Abhandlung

Vorgelegt von

Sebastian Prass

aus Oberwesel am Rhein

Hauptberichter:	Prof. Dr. K. Andreas Friedrich
Mitberichter:	Prof. Dr. Markus Hölzle

Tag der mündlichen Prüfung: 19. März 2024

Institut für Gebäudeenergetik, Thermotechnik und Energiespeicherung (IGTE) der Universität Stuttgart

2024

Declaration of originality in academic work

I hereby declare that I prepared this doctoral thesis independently and did not use any sources or means other than those indicated by me and, furthermore, I cited the passages where I quoted or referred to works by other people and their contents and I comply with the Statutes of the University of Stuttgart on safeguarding good scientific practice in the applicable version.

Ich versichere hiermit, dass ich die Arbeit selbständig angefertigt habe und keine anderen als die angegebenen Quellen und Hilfsmittel benutzt sowie die wörtlich oder inhaltlich übernommenen Stellen als solche kenntlich gemacht habe und die Satzung der Universität Stuttgart zur Sicherung guter wissenschaftlicher Praxis in der jeweils gültigen Fassung beachtet habe.

Freiburg,

_____

Sebastian Prass

Zusammenfassung

Einige der größten Hürden für die Kommerzialisierung von Fahrzeugen mit Brennstoffzellenantrieb (engl. Proton Exchange Membrane Fuel Cell, PEMFC) sind die Kosten und Lebensdauer der Systeme, sowie die fehlende Infrastruktur, die den Wasserstoff (H_2) bereitstellt. Zur Verringerung der PEMFC-Kosten ist eine Reduktion des Gehalts an Katalysatoren der Platin (Pt)-Gruppe nötig, was jedoch durch Vergiftungsmechanismen erschwert wird, deren Wirkung bei niedrigeren Pt-Beladungen pro aktiver Fläche ([$\mu g_{Pt}/cm^2$]) zunimmt. Verunreinigungen im H_2, die durch kostenintensive Reinigungsverfahren herausgefiltert werden, beeinträchtigen die PEMFC-Leistung und Lebensdauer. Sind Kontaminations- und Erholungsmechanismen bekannt, können Betriebsweisen angepasst und der Katalysatorgehalt einerseits verringert, sowie die Herstellung und Aufreinigung des H_2 andererseits kosteneffizienter gestaltet werden. Diese Dissertation untersucht daher die Auswirkung einer Verringerung der Platinbeladung der Anodenelektrode auf die Toleranz gegenüber Kohlenmonoxid (CO) und Schwefelwasserstoff (H_2S) im H_2 anhand von Einzelzellen unter Verwendung klassischer elektrochemischer Charakterisierungsverfahren.

Zunächst ist die Charakterisierung niedrig beladener Elektroden per Zyklovoltammetrie (engl. Cyclic Voltammetry, CV) durch Artefakte erschwert, die normalerweise bei höheren Beladungen (>100 $\mu g_{Pt}/cm^2$) nicht auftreten. Bei niedrigen Beladungen (<50 $\mu g_{Pt}/cm^2$) kann es zu einer spontanen Oxidation von angesammeltem Permeat-Wasserstoff während des kathodischen CV-Vorschubs kommen, was den Pt-Oxid-Reduktionsstrom überlappt und die Bestimmung der aktiven Fläche (engl. Electrochemically Active Surface Area, ECSA) beeinträchtigt.

Werden PEMFCs mit gering beladenen Anodenelektroden (<25 $\mu g_{Pt}/cm^2$) und H_2 betrieben, der CO in Konzentrationen enthält, die gemäß H_2-Qualitätsstandard ISO 14687 zulässig sind, kommt es zu inakzeptablen Spannungsabfällen von bis zu 40%. Dies deutet darauf hin, dass die CO-Toleranz des Katalysators verbessert, oder der ISO-Grenzwert für CO verringert werden sollte. Ist H_2S in Konzentrationen gemäß ISO 14687 im H_2 enthalten, kommt es während chronoamperometrischer Tests zu Spannungseinbrüchen, die bei niedrig beladenen Elektroden schwefeldosisabhängig früher auftreten. Andererseits können sich PEMFCs durch Stopp/Start (engl. Shut-Down/Start-Up, SD/SU)-Prozeduren von Schwefelvergiftungen erholen. Gemeinsam mit den erst nach Dutzenden Stunden auftretenden Spannungseinbrüchen wirft diese Erholung durch SD/SUs die Frage auf, ob der ISO-Grenzwert für Schwefelspezies einer Anpassung bedarf.

Eine Beschichtung des Pt-Katalysators in der Anodenelektrode mit einer Siliziumoxidschicht (SiO_2-Pt/C) verbessert die Leistung und Toleranz der PEMFC beim Betrieb mit reinem und H_2S-kontaminiertem H_2, verschlechtert jedoch deren CO-Toleranz. Während die Verbesserung der Leistung und H_2S-Toleranz auf Einflüsse des SiO_2 auf Wassermanagement und Mobilität oxidierter Schwefelspezies zurückzuführen ist, steht die Verschlechterung der CO-Toleranz im Zusammenhang mit erschwerter Bildung und Mobilität der OH-Gruppen, die für die CO-Oxidation notwendig und in erhöhten Potentialen für CO-Oxidation sichtbar sind.

Abstract

Cost, durability and the hydrogen fuel (H_2) infrastructure are the major challenges for the commercialization of proton exchange membrane fuel cell (PEMFC) vehicles. To lower the PEMFC cost, a decrease in the content of the expensive platinum (Pt) group metal catalysts is required, which is hindered by contaminants leading to performance decrease which become more relevant for lower loadings per active area ([$\mu g_{Pt}/cm^2$)]). Impurities in H_2, whose concentrations can be controlled to a degree at the expense of higher H_2 costs, impede the performance and durability. Knowledge of the contamination mechanisms, but also of processes contributing to a voltage recovery thereof, is important to optimize catalyst content with respect to the cost of the PEMFC system. In addition, it may be possible to improve cost-effectiveness of the H_2 fueling infrastructure. In this dissertation, the effect of lowering the platinum loading of the anode electrode on the tolerance versus carbon monoxide (CO) and hydrogen sulfide (H_2S) in H_2 is investigated experimentally via small scale single cells using classical electrochemical characterization procedures.

First of all, characterization of low-loaded electrodes via cyclic voltammetry (CV) analysis can be biased by artifacts usually not observed for higher loaded electrodes (>100 $\mu g_{Pt}/cm^2$). For low-loaded electrodes (<50 $\mu g_{Pt}/cm^2$), spontaneous oxidation of accumulated crossover hydrogen can occur, overlapping Pt oxide reduction currents during the cathodic transient and potentially interfering with evaluation of the electrochemical surface area (ECSA).

Operating PEMFCs with ultra-low-loaded anode electrodes (<25 $\mu g_{Pt}/cm^2$) and CO-contaminated H_2 at concentrations allowed as per standard ISO 14687 results in severe voltage drops of up to 40%, indicating the need to improve the CO tolerance of the anode catalyst, or to further decrease the ISO limit for CO. Similarly, H_2S at concentrations as per ISO 14687 leads to sulfur poisoning induced voltage break downs during chronoamperometric tests, which occur earlier for lower loaded electrodes and depending on sulfur dose. However, the break downs, appearing after dozens of hours, in combination with a partial recovery from sulfur poisoning with shut-down/start-up (SD/SU) events raise the question, whether the ISO limit for sulfur species needs adaption for lower loadings considering realistic operation in vehicle applications.

Furthermore, coating the anode Pt catalyst with a thin silicon oxide layer (SiO_2-Pt/C) improves the PEMFC performance and durability in neat and H_2S contaminated H_2, but worsens the CO tolerance. The performance improvements are attributed to an improved water retention and mobility of oxidized sulfur species on the SiO_2, while the worse CO tolerance is a result of increased oxidation potential for CO on the SiO_2-Pt/C.

Content

Declaration of originality in academic work VI

Zusammenfassung V

Abstract VII

Content IX

1 Introduction 1

1.1 Background 1

1.2 Challenges for PEMFCs in FCEV 2

1.3 Motivation for this dissertation 4

2 Fundamentals 7

2.1 PEMFC thermodynamics 7

2.2 Voltage losses in PEMFCs 9

2.3 The anode electrode and the opportunities of silicon oxide (SiO_2) coatings 12

2.4 Fuel impurities 14

2.4.1 Carbon monoxide (CO) 16

2.4.2 Hydrogen sulphide (H_2S) 18

2.5 Scope of this dissertation 19

3 Experimental 21

3.1 Fuel cell test bench, platform and characterization methods 21

3.2 Materials 24

3.3 Elemental and morphological analysis via SEM- and TEM-DX 25

3.4 SiO_2 coating process, electrode and CCM fabrication 26

4 Results in the context of PEMFC research 29

4.1 CV analysis of low-loaded PEMFC electrodes 29

4.2 Hydrogen quality standard ISO 14687 and updates thereof 32

4.3 Effect of SiO_2 coating on CO and H_2S fuel contamination 38

5 Conclusions and outlook 49

6 Publications 51

6.1 Hydrogen oxidation artifact during Platinum oxide reduction in cyclic voltammetry analysis of low-loaded PEMFC electrodes 51

6.2 Tolerance and recovery of ultra-low-loaded Platinum anode electrodes upon CO and H_2S Exposure 63

6.3 Tolerance of Silicon Oxide-Coated Pt/C Catalyst Toward CO and H_2S Contamination in Hydrogen for Proton Exchange Membrane Fuel Cells 78

7 References 89
List of abbreviations 97
List of publications 99
Published manuscripts 99
Conferences 99
List of figures 100
List of tables 101
Danksagung 103

1 Introduction

1.1 Background

Over the last couple of decades, increasing evidence points towards the impact humans have made on the climate, calling for more action to minimize this impact. One of the key figures in assessing the state of the climate is the concentration of greenhouse gases (GHG) in the atmosphere, first and foremost carbon dioxide (CO_2), which has increased from somewhat between 250 – 300 to today's more than 400 ppm largely due to combustion of fossil fuels to power industrialization throughout the past two centuries [1]. This change in a seemingly small total concentration is to large parts responsible for the 1°C rise in average global temperature over the same timeframe, which comes with severe consequences for the habitability in various regions on earth. In the United Nations Paris Climate Agreement in 2015 (COP21), 196 parties agreed on a legally binding treaty with the goal to limit global warming to 2°C, preferably 1.5°C, compared to pre-industrial levels in order to reduce the risks accompanied with climate change [2]. To achieve the COP21 goal, anthropogenic GHG emissions are required to be cut by about 50% per decade to reach net-zero emissions around 2050 [3]. In these regards, net-zero signifies actual reductions in GHG emissions by transitioning our fossil fuel-based economy towards a low and zero carbon footprint economy, while creating and maintaining CO_2 sinks to compensate for unavoidable emissions. The complexity of this ambitious goal is exacerbated in light of the expected growth in both the global population and energy demand as projected by the International Energy Agency [4].

On national levels, the COP21 goal translates into individual, more detailed policies towards net-zero emissions. In this spirit, Germany aims to reduce GHG emissions by 65% by 2030 and between 80 – 95% by 2050, respectively, as stated in the Climate Action Plan 2050 [5]. The national goal is broken down into sub-targets for each sector, depending on its current state and possibilities. From 1990 to 2020, the energy related GHG emissions were cut nearly in half from about 1036 to 608 million tons CO_2-equivalents mainly due to reductions in the energy (50% reduction), industry (60%) and housing (31%) sectors, while reductions in the transportation sector were relatively small (11%). The total GHG emission reductions in the transportation sector were small because the improvements in efficiency and average CO_2 emissions of internal combustion engines (ICE) were compensated by more mileage powered by fossil fuels, providing 92% of the energy used in transportation [6]. One of the solutions to cut the emissions in the transportation sector is the electrification of powertrains including battery electric vehicles (BEV), plug-in hybrid electric vehicles (PHEV) and fuel cell electric vehicles (FCEV). The latter, FCEV, are part of the German National Hydrogen Roadmap announced in 2020 to support the cross-sectoral roll-out of hydrogen (H_2) technologies. In this roadmap, H_2 is considered a storage medium for renewable energies that can be used as raw material for industrial processes or as fuel for the energy and transportation to ultimately substitute fossil fuels and decarbonize sectors [7].

1.2 Challenges for PEMFCs in FCEV

Significant technological leaps have pushed PEMFCs closer towards application in mobile or stationary systems, however, several challenges remain to enable a widespread commercial roll-out of FCEVs. As such, important factors are the mass production and the reduction of system cost, the durability particularly of the membrane electrode assembly (MEA), as well as the deployment of the hydrogen infrastructure. These individual fields are often interrelated, as e.g. ramping up mass production or improvements in catalyst durability allow for reductions in material use and the reduction of system cost. Another example, more related to this dissertation, are investigations into contamination mechanisms affecting the MEA, to eventually tolerate less pure hydrogen fuel (H_2) and therefore cheaper infrastructure requirements. From a PEMFC system perspective, H_2 of highest purity would be preferred, whereas from a gas producer perspective, lower H_2 purity requirements would decrease the need for purification and lower the H_2 production cost [8].

In a PEMFC stack, the MEA, which is sensitive to multiple degradation and contamination mechanisms, accounts for about 62% of the stack cost for mass production, of which the content and application of platinum group metal (PGM) catalysts make up to nearly 2/3 of the cost [9]. Two of the main levers to lower this portion of cost are production scale as well as PGM use per stack. With higher production rates, unit costs of an exemplary 80 kW_{net} automotive PEMFC stack are expected to decrease from about 125 to 25 $/kW with the increase in annual production rate from 1.000 to 500.000 units. These reductions are based on benefits from volume material pricing and equipment utilization, improved materials and manufacturing processes. In addition, effort is put into bringing the total PGM loading down to finally reach contents close to state-of-the-art catalytic converters currently installed in internal combustion engines (ICE), which contain about a single digit in grams of PGM per converter in passenger vehicles. At such contents, PGM use, production capabilities and, more importantly, resource extraction are expected to be sustainable, such that PGM availability and prices remain at acceptable levels. The U.S. Department of Energy (DOE) frequently revisits the technical status and cost of PEMFC systems and publishes targets for the PGM loading in the MEA, i.e. the PGM weight per active cell area [10]. More than 20 years ago, PEMFC systems often contained PGM loadings about 2 – 5 times the typical loadings of today's systems, and a reduction of similar magnitude is targeted by the DOE and PEMFC stakeholders to allow for the commercial roll-out of FCEVs. This trend in PGM content is shown in Figure 1, depicting a comparison between the anode and cathode electrode loadings used in selected PEMFC studies and systems referenced in this dissertation, and the past and current DOE targets.

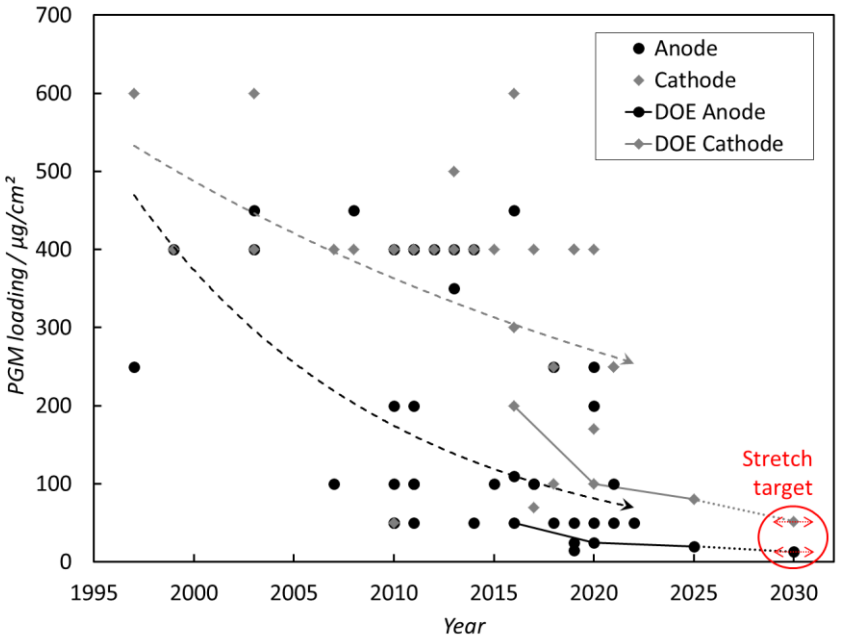

Figure 1 Trend in anode and cathode PGM loading, and the DOE targets for PEMFCs in automotive applications. Adapted from selected publications including in-situ PEMFC testing on contamination [11,12,21–30,13,31–34,14–20]

This striking figure visualizes the development towards MEAs with low (< 125 µg/cm²) and ultra-low (<62.5 µg/cm²) total PGM loadings, which generally is enabled by improvements in PEMFC materials, designs and operating strategies. Although the majority of the PGM content usually is in the cathode electrode (about 60 – 80%) of a MEA, it is worth looking into how to further decrease the anode content towards low and even ultra-low loadings, that are 25 and 12.5 µg/cm², respectively, and possibly even lower values [35]. In the anode, it is not the necessary activity of the hydrogen oxidation reaction (HOR) limiting the PGM loading reduction. Specific degradation and contamination effects make higher loadings necessary to provide a loading buffer to compensate for losses in catalytic active surfaces over the PEMFC lifetime. Technically, on anode side, low double and even single digit µg/cm² PGM loadings would be sufficient to provide HOR for power densities of about 1 W/cm² comparable to state-of-the-art MEA designs [36,37]. In practice, though, irreversible degradation due to imperfect transient operation or fuel starvation events, but also reduced fuel efficiency as a result of contamination effects eventually arise in the anode electrode. The former, transient operation and particularly fuel starvation, can be harmful because in times of current production while fuel is lacking, the anode potential is driven to levels where electrolysis and oxidation of the carbon support occurs, which finally leads to the “consumption” of the anode electrode and the irreversible loss of electrochemically active surface area (ECSA) [34]. The latter, fuel impurities, can reversibly or irreversibly contaminate the MEA. Several species adsorb on catalyst surfaces in the anode electrode and hinder the HOR, while few species additionally affect the either ion transport or water management, or even the reaction kinetics on the cathode side [38,39]. For example, carbon monoxide (CO) and hydrogen sulfide (H_2S), two species eventually present in H_2 produced from methane reformation or as a by-product in industrial processes [40], affect the PEMFC performance

already at extremely low concentrations as they readily adsorb onto the catalyst surfaces blocking it for HOR. To compensate for such losses, PEMFC manufacturers usually employ anode PGM loadings ranging from 50 to 100 µg/cm² to achieve reasonable PEMFC durability and efficiency upon operation with contaminated H_2. By lowering the electrode loading of a selected metal catalyst without enhancing its ECSA, e.g. by decreasing particle size to achieve higher surface areas, and durability, the active area for HOR and the contamination tolerance eventually decreases [14,41]. To further reduce the costly PGM loading in the anode towards the DOE targets, two alternative pathways exist on how to deal with the effect of fuel contamination: either the maximum concentrations of critical impurities allowed in H_2 for automotive low temperature PEMFCs have to be lowered, or catalysts with an improved tolerance have to be employed. In this context, this dissertation provides contamination tests with CO and H_2S using MEAs with low and ultra-low anode loadings, studies of mitigation strategies, and artifacts limiting electrode characterization methods.

1.3 Motivation for this dissertation

In order to find the optimal trade-off between PEMFC contaminant tolerance and fuel purity, it is necessary to build a database of the contaminant tolerance of state-of-the-art and targeted MEA materials. The contamination mechanisms and recovery strategies from species eventually contained in H_2, as summarized in the fuel quality standard ISO 14687, are generally known and described in literature [39,42–44], but the magnitude of their effects on new MEA designs, including ultra-low anode loadings, can vary and calls for frequent re-evaluation. While the contamination mechanisms remain unchanged, effects relieving from contamination or extending lifetimes eventually gain in relevance, such that fuel purity requirements could be adapted. Such measurements were conducted in this dissertation with carbon monoxide (CO) and hydrogen sulphide (H_2S), representing species that reversibly and irreversibly contaminate PEMFCs, as a starting point for discussions on fuel purity adaptions. Furthermore, sulfur contamination of anode and cathode electrodes generally is considered irreversible during operation, but specific situations like shut-downs and start-ups (SD and SU), regularly taking place in automotive PEMFC systems, are assumed to alleviate from sulfur contamination, but literature was lacking experimental evidence for this assumption.

In-situ experiments with ultra-low electrode loadings are challenging because of the low current magnitudes associated to processes happening on catalyst surfaces, such that typical electrode characterization techniques require refinement. Specifically, the evaluation of the electrochemically active surface area (ECSA) via cyclic voltammetry (CV) is biased for ultra-low catalyst loadings. CV is indispensable for analysis of the redox reactions on electrocatalyst surfaces in the potential window of interest, but for an adequate analysis, the knowledge of artifacts and thresholds for CV analysis is required. The difficulties mainly stem from artifact currents gaining in relevance as well as unfavorable signal to noise ratios at low current magnitudes. Investigations into such limitations were part of this dissertation, since unreported artifacts arose during CV analysis of ultra-low-loaded anode electrodes, which also can occur during analysis of low-loaded cathode electrodes.

Furthermore, alternatives to manipulate the tolerance versus contamination such as alloying the catalyst or selecting adequate MEA designs exist, but in recent years, an additional option evolved:

functional coatings added on the electrocatalyst surface. As such, a coating based on silicon oxide (SiO_2) fabricated via hydrolysis of silicon precursors (essentially a sol-gel-process) has received significant attention. When applied on electrocatalysts, the SiO_2 coating was found to stabilize catalyst and support particles versus degradation mechanisms, affect the performance during specific operating conditions or alter the handling of the materials for electrode fabrication. In addition, a comparable SiO_2 coating is often applied on metal tubing in process engineering applications as an adsorption barrier versus gaseous sulfuric species such as H_2S. Although a different branch, it raises the question whether a similar effect could be achieved with SiO_2 coated electrocatalysts. Investigations into the effect of the coating on CO and H_2S contamination in PEMFCs have not been conducted yet, and therefore were added to this dissertation as an additional means to manipulate the electrocatalyst tolerance.

This dissertation is divided into 6 main chapters. Chapter 1 introduces to the background and states the motivation for this dissertation. Chapter 2 contains the PEMFC basics including a literature review specifically on topics pertaining to the anode electrode and the SiO_2 coating, as well as on CO and H_2S contamination. Chapter 3 describes the experimental setups with a focus on the test bench and the methods used for in-situ characterization, the fabrication procedure and ex-situ analysis of the SiO_2 coating and materials. Chapter 4 summarizes and discusses the three publications produced during the course of this dissertation in the overall context of PEMFC research, with the conclusions and the outlook provided in chapter 5. The three full publications are reproduced in chapter 6.

2 Fundamentals

2.1 PEMFC thermodynamics

Proton exchange membrane fuel cells (PEMFCs) are multiphase electrochemical systems comprising of two electrodes, the anode and cathode, separated by the proton exchange membrane (PEM). The electrodes are continuously supplied with hydrogen (H_2) as the fuel and oxygen (O_2) in air as the oxidant. At the anode, H_2 is oxidized via the hydrogen oxidation reaction (HOR) to form protons and electrons (2-1).

$$2H_2 \rightarrow 4H^+ + 4e^- \tag{2-1}$$

The electrons are conducted through electrically conducting components and an external circuit, and protons are transported through the proton conducting PEM to the cathode. At the cathode, O_2 recombines with electrons and protons to water (H_2O) via the oxygen reduction reaction (ORR) (2-2).

$$4H^+ + 4e^- + O_2 \rightarrow 2H_2O \tag{2-2}$$

The overall reaction is the redox reaction between O_2 and H_2 to H_2O, which releases electric and thermal energy as products (2-3).

$$2H_2 + O_2 \rightarrow 2H_2O \tag{2-3}$$

The electric and to some extend the thermal energy can be used, while the product water is exhausted from the PEMFC. Redox reactions are driven by a potential difference between the states of the reactants and products. For electrochemical systems, the reversible cell potential E^o is given by the change in Gibb's free energy of formation (2-4), with the superscript 0 representing values at standard conditions (298.15 K and 101325 Pa).

$$E^0 = -\frac{\Delta G^o}{zF} \tag{2-4}$$

With Gibb's free energy ΔG^0, the number of electrons transferred z (2 in case of H_2/O_2 PEMFCs) and the Faraday's constant F (96485.33 C mol^{-1}). The Gibb's free energy is given as the difference between the enthalpy of reaction ΔH^0 and the change in entropy ΔS^0 at temperature T (2-5).

$$\Delta G^0 = \Delta H^0 - T\Delta S^0 \tag{2-5}$$

As the enthalpy of reaction and entropy depend on the phase of reactants and products, individual reversible cell potentials can be calculated for the case of liquid water and steam given the values in Table 1.

Table 1 Specific enthalpy and entropy for O_2, H_2 and H_2O in gaseous (g) or liquid (l) states

Species	$\boldsymbol{\Delta H^0}$ $\boldsymbol{\frac{kJ}{mol}}$	$\boldsymbol{S^0}$ $\boldsymbol{\frac{J}{mol\ K}}$	$\boldsymbol{\Delta G^0}$ $\boldsymbol{\frac{kJ}{mol}}$
H_2(g)	0	130.68	0
O_2(g)	0	205.14	0
H_2O(l)	-285.83	69.91	-237.13
H_2O(g)	-241.82	188.83	-228.57

Using equation (2-4), the reversible cell potentials for liquid product water $E^0_{H_2O(l)}$ and steam $E^0_{H_2O(g)}$ are calculated as follows (2-6).

$$E^0_{H_2O(l)} = -\frac{-285.83\frac{kJ}{mol} - 298.15K * \left(-0.1633\frac{kJ}{mol\ K}\right)}{2 * 96485.33\frac{C}{mol}} = 1.229V$$
$$E^0_{H_2O(g)} = -\frac{-241.82\frac{kJ}{mol} - 298.15K * \left(-0.0445\frac{kJ}{mol\ K}\right)}{2 * 96485.33\frac{C}{mol}} = 1.184V \quad (2\text{-}6)$$

The actual PEMFC operating conditions and consequently the Gibb's free energy and entropy though typically differ from standard conditions, such that the reversible cell potential deviates from the one calculated at standard conditions. The reversible cell potential as a function of pressure p and temperature T is can be calculated using the transformed Nernst-equation (2-7), assuming the gases act as ideal gases [45].

$$E(T,p) = E^0 + (T - T^0)\frac{\Delta S^0}{2F} - \frac{RT^0}{2F} ln\frac{p}{p^0} \quad (2\text{-}7)$$

Based on this expression, the temperature dependency of the reversible cell potential is given as (2-8)

$$\frac{dE}{dT} = \frac{\Delta S^0}{2F} = \frac{-0.1633\frac{kJ}{mol\ K}}{2 * 96485.33\frac{C}{mol}} = -0.85\frac{mV}{K} \quad (2\text{-}8)$$

With an increase in temperature of 1 K, the reversible cell potential decreases by 0.85 mV. On the other hand, the pressure dependency based on the molarity for product water in liquid ($\Delta n = -\frac{3}{2}mol$, (2-9)) and gaseous ($\Delta n = -\frac{1}{2}mol$, (2-10)) phase is given as follows:

$$\frac{dE}{d\log(p)_{H_2O(l)}} = \frac{\Delta nRTln(10)}{2F} = \frac{-\frac{3}{2}mol * 8.314\frac{J}{mol\,K} * 298.15K * \ln(10)}{2 * 96485.33\frac{C}{mol}} = 44\frac{mV}{dec} \quad (2\text{-}9)$$

$$\frac{dE}{d\log(p)_{H_2O(g)}} = \frac{-\frac{1}{2}mol * 8.314\frac{J}{mol\,K} * 298.15K * \ln(10)}{2 * 96485.33\frac{C}{mol}} = 15\frac{mV}{dec} \quad (2\text{-}10)$$

An increase in gas pressure by a factor of 10 results in an increase in the reversible cell potential by 44 mV and 15 mV in case of liquid product water and steam, respectively. The reversible cell potential resembles the maximum possible potential, which could be reached in a PEMFC operated with H_2 and O_2. In practice, however, the actual cell potential U measured at the PEMFC terminals is lower than the reversible cell potential E due to several voltage losses.

2.2 Voltage losses in PEMFCs

As every electrochemical system, polarization curves of PEMFCs show a non-linear relationship between current density i and potential U (Figure 2) because of several types of voltage losses dominating at different domains.

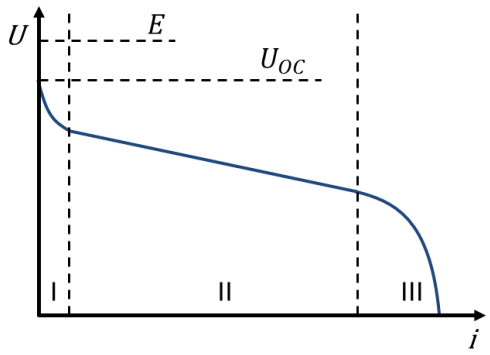

Figure 2 Schematic PEMFC polarization curve and voltage loss domains (I activation, II ohmic and III diffusion)

Already at zero current, the open circuit voltage U_{OC} is lower than the reversible cell potential E and typically reaches values close to 1 V with current state-of-the-art MEA designs. The difference between E and U_{OC} is a result of mixed potentials at the electrode mainly due to gas crossover and shorting currents through the thin PEM of thicknesses ranging from 8 to 25 µm for current automotive designs. As soon as current is drawn, multiple voltage losses due to overpotentials η in addition to the ohmic cell resistance lower the measured cell potential (2-11).

$$U = U_{OC} - \left(\eta_{act,ORR} + \eta_{act,HOR} + \eta_{Lim} + iR\right) \quad (2\text{-}11)$$

At low currents densities (domain I), the voltage loss is dominated by the ability of the catalysts to catalyse the charge transfer across electrode and electrolyte interfaces, referred to as kinetic overpotentials $\eta_{act,HOR}$ and $\eta_{act,ORR}$ for the HOR and ORR in the anode and cathode, respectively. Generally, the activation overpotential η_{act} for every electrocatalytic reaction on a catalyst surface is related to the current density i as given by the Butler-Volmer equation (2-12).

$$i = i_0 \left[exp\left(\frac{\alpha_a z F}{RT}\eta_{act}\right) - exp\left(-\frac{\alpha_c z F}{RT}\eta_{act}\right)\right] \tag{2-12}$$

With α_a and α_c as the anodic and cathodic charge transfer coefficients, z as the electrons transferred during the electrochemical reaction, the ideal gas constant R, temperature T and the exchange current density i_0 of the reaction on the catalyst surface. Using this equation, the net current density i can be calculated as a function of η_{act}. The exchange current density i_0 is the magnitude of the anodic and cathodic current density on a catalyst surface at zero overpotential (or zero net current) and resembles the intrinsic charge transfer rates between catalyst surface and electrolyte. The exponentials in the Butler-Volmer equation take into account both the anodic and cathodic reactions on an electrode surface. At high overpotentials (η_{act} > 70 mV), the anodic reaction dominates and the second exponential term can be neglected, and the Butler-Volmer equation simplifies to the Tafel equation (2-13).

$$\eta_{act} = \frac{RT}{\alpha_a z F} * ln\frac{i}{i_0} \tag{2-13}$$

During regular operation of a PEMFC with H_2 and O_2, the activation overpotentials $\eta_{act,HOR}$ and $\eta_{act,ORR}$ differ significantly. For example, at the cathode, $\eta_{act,ORR}$ accounts for about 70% of the total overpotential at 0.5 A/cm² as compared to 10% for $\eta_{act,HOR}$ at the anode [46]. The reason can be found in the exchange current density i_0 being orders of magnitude higher for HOR/HER as compared to the sluggish ORR/OER on Pt. On Pt, $i_{0,HOR/HER}$ can reach values as high as 200 - 600 mA/cm^2 (at temperatures of 313 to 353 K) as compared to 0.1 mA/cm^2 for $i_{0,ORR/OER}$, which is why the anode overpotential $\eta_{act,HOR}$ at typical current densities is comparably low and often neglected in PEMFC research [47,48]. This circumstance though changes during specific situations, e.g. if the PEMFC is operated in dry conditions or with fuel impurities, or if the anode electrode degrades and catalyst surfaces are irreversibly lost upon fuel starvation [39,46,49]. In such situations, the catalytically active surfaces in the anode are lost or blocked, such that i_0, being the product of the specific exchange current density and the surface roughness (actual catalyst surface area per geometric cell area), significantly decreases.

As soon as charges are transported through PEMFC components, ohmic resistances R give rise to the ohmic overpotential η_{Ohm}, which dominates at intermediate current densities (domain II) and is visible in the linear decline of the cell potential according to Ohm's law (2-14).

$$iR = i * (R_\Omega + R_{Ion}) \tag{2-14}$$

While the electronic resistances R_Ω due to electron transport through electrodes, gas diffusion layers, bipolar plates and across interfaces are independent of the current density, the ionic resistances R_{Ion} due to ion transport through the electrolyte in the PEM and electrodes is not. The ionic transport is facilitated by water via the Grotthuss-mechanism, where excess protons diffuse along the hydrogen bond network of neighboring water molecules. With increasing current density, water production and consequently ionic conductivity through the ionomer in PEM and electrodes increases, such that the ohmic voltage drop iR eventually decreases.

At high current densities (domain III), reactant consumption exceeds the diffusion towards the electrode surface. Macro and micro pores of the GDL and electrodes, product water in these pores or on surfaces, as well as the electrolyte covering catalyst surfaces impede the diffusion and cause the mass transport limited overpotential η_{Lim}. This is relevant mainly for the cathode, because it is usually supplied with air containing about 21% oxygen (O_2) and 78% nitrogen (N_2) instead of pure O_2, diffusion pathways are eventually blocked by product water especially at high current densities, and the thin ionomer film on catalyst material in the cathode impedes oxygen diffusion. The total O_2 transport resistance R_T can be estimated using the approach of Baker et al. with the oxygen partial pressure in the channel $p_{O2,ch}$ and a measured limiting current density i_{lim} (2-15) [50].

$$R_T = \frac{4Fp_{O_2,ch}}{RTi_{lim}} \tag{2-15}$$

When measuring limiting current densities at various partial pressures of oxygen and total gas pressures, this approach allows the separation of R_T into pressure independent diffusion, i.e. diffusion through water, ionomer thin films and micro pores, and into pressure dependent diffusion due to intermolecular interaction through macro pores. Considering that the O_2 concentration difference between channel and catalyst surface affect the kinetic overpotential $\eta_{act,ORR}$ and the reversible cell potential according to the Nernst-equation, Zihrul et al. derived equation (2-16) to estimate the overpotential η_{Lim} using the total O_2 transport resistance R_T.

$$\eta_{Lim} = \frac{RT}{F} * \left(\frac{1}{4} + \frac{\gamma}{\alpha}\right) * ln\left(\frac{p_{O_2,ch} - \frac{RT}{4F} * R_T * i}{p_{O_2,ch}}\right) \tag{2-16}$$

With γ as the reaction order of the ORR (with a value of 0.54 in Zihrul's studies) and α as transfer coefficient (at a value of 1). The reactant diffusion is strongly affected by the water management of the PEMFC, and usually the inlet gas humidity on one, and the water retention capability of the MEA on the other hand, have to be well selected to avoid flooding and excessive diffusion resistances. On the anode side, diffusion resistances usually are not an issue because the highly diffusive H_2 is pure or eventually diluted by N_2 up to 30% due to accumulation in the anode loop, while water is transported with the electroosmotic drag away from the anode alleviating from flooding issues. However, freeze start-ups or imbalanced transient operation can lead to fuel starvation events, practically depicting infinite diffusion resistances as H_2 is locally lacking. Furthermore, contamination effects in both anode and cathode

electrodes can give rise to mass transfer overpotentials, because catalyst surfaces are partially blocked by adsorbed contaminant species, such that reactants must travel longer paths through progressively smaller cross sections to reach vacant, active catalyst sites [51].

2.3 The anode electrode and the opportunities of silicon oxide (SiO_2) coatings

This dissertation focusses on fuel impurities and consequently on the anode electrode in PEMFCs. Current automotive state-of-the-art anode and cathode catalysts employed in PEMFCs are predominantly based on Pt or Pt alloy nanoparticles on carbon supports, as these materials provide good activities for the oxygen reduction reaction (ORR) and exceptional activity for the hydrogen oxidation reaction (HOR). To give an idea, the exchange current density (the reaction rate at zero external current) for ORR and HOR on Pt is in the order of 0.1 and 200 mA/cm² metal catalyst surface area, respectively, although ORR catalysts are preferably classified by activity measurements at 0.9 V (i.e. at low current densities) to avoid the necessary but error-prone extrapolation of the measured currents in Tafel-plots [47]. Significant effort is put into further improving the activity and durability of catalysts for the ORR, as the cathode typically dictates performance and lifetime during regular operation with neat hydrogen and air, when overpotentials arising from catalyst activation for ORR and oxygen mass transport dominate the voltage losses. Specific situations, like cell-reversal due to fuel starvation [52], shut-downs and start-ups (SD/SU) [31], and operation with contaminated fuel impair the functionality of the anode and eventually cause a loss or blockage of the catalyst material with the risk of full cell voltage break downs. To accommodate such losses, the anode electrode typically contains more Pt catalyst material, i.e. a higher loading per geometric cell area, as operation with neat reactant gases would require. The anode Pt loading of state-of-the-art automotive MEAs typically ranges somewhere between 50 – 100 µg/cm², while loadings as low as 5 – 30 µg/cm² with acceptable or even outstanding power densities up to 2.5 W/cm² have been accomplished on lab-scale, indicating that such low anode loadings generally can suffice [36]. Ultra-low loadings on anode side ranging from 12.5 – 25 µg/cm² in combination with cathode loadings between 50 to 100 µg/cm² are envisioned by the DOE to meet the cost target of \$40/kW_{net} by 2025 [9,53]. With respect to the anode, the question is how to protect the electrode versus fuel starvation and impurity effects, to allow for such a significant loading reduction.

During fuel starvation, the hydrogen supply of the anode is disturbed due to liquid water or ice blocking diffusion pathways through the flow field and GDL, or due to imbalanced fuel distribution during transient operation. If current is drawn while fuel is lacking, a mass transfer induced overpotential drives the anode potential to levels where water electrolysis eventually commences (>1.23 V), which provides protons and electrons and is measurable as a negative cell voltage due to $E_{cell} = E_{ca} - E_{an}$ [52]. At high electrode potentials, though, oxidation of the carbon support with water according to equations (2-17) and (2-18) is severely accelerated. Over extended period of times, fuel starvation therefore essentially leads to the irreversible loss of catalyst support in the anode electrode.

$$C + 2H_2O \rightarrow CO_2 + 4H^+ + 4e^-, \text{ E}^0 = 0.207 \text{ V (vs. standard hydrogen electrode, SHE)} \quad (2\text{-}17)$$

$$C + H_2O \rightarrow CO + 2H^+ + 2e^-, \text{ E}^0 = 0.518 \text{ V (vs. SHE)} \quad (2\text{-}18)$$

Strategies to mitigate cell reversal events range from cell voltage monitoring systems to prompt current interruption as a response to negative cell voltages, the implementation of an OER catalyst into the anode electrode such as iridium oxide (IrO_2) to promote electrolysis, referred to as reversal tolerance additive (RTA) [34], or the addition of H_2 spillover materials such as tungsten oxide (WO_3), which incorporate H_2 in times of excess and release it during starvation events [54]. Particularly RTAs are increasingly implemented into state-of-the-art automotive anode electrodes, though RTAs also suffer from deactivation during starvation phases primarily due to species generated via carbon corrosion, but also due to the collapse of the electrode and loss of the connection between carbon and RTA particles [55]. During fuel starvation, the longevity of the RTA and consequently the anode depends on the amount and distribution of RTA, but also on the water content in the electrode [52,56]. Ideas to protect the RTA versus deactivation are scarce, but range from optimization of RTA particle size and distribution, to adding a thin silicon dioxide (SiO_2) protective coating onto the RTA [57]. Such SiO_2 coatings generally have shown to improve the stability of carbon supported electrocatalysts versus degradation mechanisms like catalyst dissolution and carbon corrosion, while the activity is barely or not at all affected, because the few nanometer thick porous coating still allows for sufficient reactant diffusion [58–60]. Two methods for fabrication of SiO_2 coatings on catalyst powders have been employed: first the conventional sol-gel chemistry method comprising the adsorption of multiple Si-containing nucleating agents on the catalyst powder in a dispersion, and second, the atomic layer deposition (ALD) method coupled with a fluidized bed reactor to whirl the catalyst powder during the deposition process [61]. Especially the sol-gel method has been used on PEMFC electrocatalysts over the last 15 years, since Takenaka et al. reported their works on SiO_2 coated Pt deposited on carbon nano tubes (CNT) in 2008 [62]. Since then, variations in carbon support and catalyst types, silicon precursors and additives have shown that the integrity, porosity and hydrophobicity of a sol-gel based SiO_2 coating can be modified and with that, the impact it has on PEMFCs [58,60,63–65]. For example, if the SiO_2 coating completely or partially covers a carbon supported catalyst (schematically shown in Figure 3), depends on the interactions between solid surfaces and the silicon precursors during the hydrolysis, and seems to be affected by the combination of catalyst and support types on one hand, and Si-precursors on the other.

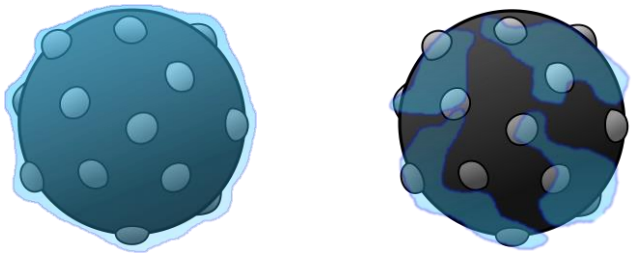

Figure 3 Illustration of Pt/C particle fully or partially covered with SiO_2

Graphitic carbon surfaces, having fewer defects and elements other than carbon in the lattice, eventually provide different sites for adsorption of OH-groups and silicon precursor molecules as compared to carbon particles with higher specific surface areas, defect densities and different elemental compositions. Furthermore, the pore sizes in the SiO_2 layer appear to depend on the combination of the

precursors such as 3-aminopropyltriethoxysilane (APTES), triethoxysilane (TEOS) and methyltriethoxysilane (MTEOS) [66]. SiO_2 coatings based on APTES and TEOS revealed lower oxidation currents for alcohols with larger molecule sizes as compared to coatings based on APTES and MTEOS, indicating smaller pores for the coating of the former combination. Intuitively the question arises, whether SiO_2 coatings also could act as adsorption barriers versus impurity species in a PEMFC operated with contaminated H_2. This question is encouraged by the fact that the stainless steel tubes used to supply contaminants for in-situ PEMFC tests at Fraunhofer ISE are coated with SilcoNert®, a coating based on SiO_2, to minimize the adsorption particularly of sulfuric species on the metal surfaces. Hence, this question was picked up within this dissertation, in which a coating based on the hydrolysis of APTES and TEOS was employed on a Pt/C catalyst used in the anode electrode, to investigate its effect on fuel impurities, namely carbon monoxide (CO) and hydrogen sulfide (H_2S).

2.4 Fuel impurities

Hydrogen (H_2) is produced in large scales over a variety of processes from both fossil fuels and renewable sources, and it is a crucial feedstock for many industrial sectors. In 2019, steam methane reformation (SME) and partial oxidation (POX) of coal provided about 76% and 23%, of the 70 Mt of commercially used H_2, respectively, while water electrolysis only accounted for up to 2% of the global H_2 production [8]. Of course, each process delivers a product of a specific purity making purification indispensable for further usage. For example, carbon monoxide (CO), methane, formaldehyde, nitrogen (N_2), argon and water (H_2O) resemble the most likely occurring impurities in H_2 from SME even after purification, as compared to H_2O, oxygen (O_2), N_2 and carbon dioxide (CO_2) from electrolysis [40]. When H_2 incurs as a by-product from chemical processes, or is produced from biomass or coal gasification, additional species like sulfuric or halogenated species, or formic acid are possible. Depending on the feedstock, the production process, the infrastructure including transportation, conditioning and dispensing, additional trace amounts of elements or compounds stemming from odorants, cleaning agents or chemicals can be introduced into the H_2 fuel.

Most impurities are removed subsequent to production down to concentrations of a few parts per million (ppm) or billion (ppb) via pressure or temperature swing adsorption processes (PSA and TSA) to achieve H_2 purities of about 99 to 99.999%. However, purification comes at a cost, because every purification cycle requires energy to compress or heat the gas, while a fraction of the product is lost during frequent system purges. About 74% of the annual H_2 production is consumed in processes, where purity is less of a concern such as oil refining or the production of ammonia, methanol or steel. For many other processes, however, purity is of crucial importance to prevent undesired losses in system efficiency or lifetimes. Fuel cells, particularly PEMFCs used in automotive applications, are extremely sensitive to specific impurities and therefore require H_2 of high purity with very low concentrations of these species, which are listed in the quality standard ISO 14687:2019 for H_2 dispensed at refilling stations (Table 2).

Table 2 Hydrogen for automotive application: ISO 14687:2019 fuel purity standard [40]

Characteristics (assay)[a]	Type I, Type II, Grade D
Hydrogen fuel index (minimum mole fraction)[b]	99.97%
Total non-hydrogen gases	300 ppm
Maximum concentration of individual contaminants	
Water (H_2O)	5 ppm
Total hydrocarbons except methane (C1 equivalent)[c]	2 ppm
Methane (CH_4)	100 ppm
Oxygen (O_2)	5 ppm
Helium (He)	300 ppm
Nitrogen (N_2)	300 ppm
Argon (Ar)	300 ppm
Carbon dioxide (CO_2)	2 ppm
Carbon monoxide (CO)[d]	0.2 ppm
Total sulfur compounds (S1 equivalent)[e]	0.004 ppm
Formaldehyde (HCHO)	0.2 ppm
Formic acid (HCOOH)	0.2 ppm
Ammonia (NH_3)	0.1 ppm
Total halogenated compounds (Halogenat ion equivalent)[f]	0.05 ppm
Maximum particulates concentration	1 mg kg^{-1}

[a] For the constituents that are additive, such as total hydrocarbons and total sulphur compounds, the sum of the constituents shall be less than or equal to the acceptable limit.

[b] The hydrogen fuel index is determined by subtracting the "total non-hydrogen gases" in this table, expressed in mole percent, from 100 mole percent.

[c] Total hydrocarbons except methane include oxygenated organic species. Total hydrocarbons except methane shall be measured on a C1 equivalent (µmol/mol).

[d] The sum of measured CO, HCHO and HCOOH shall not exceed 0,2 µmol/mol.

[e] As a minimum, total sulphur compounds include H2S, COS, CS2 and mercaptans, which are typically found in natural gas.

[f] All halogenated compounds which could potentially be in the hydrogen gas [for example, hydrogen chloride (HCl) and organic chlorides (R-Cl)] should be determined by the hydrogen quality control plan discussed in ISO 19880-8. Halogenated compounds shall be measured on a halogen ion equivalent (µmol/mol).

[g] Particulate includes solid and liquid particulates comprises of oil mist. Large particulates can cause issues with vehicle components and should be limited by using filter as specified in ISO 19880-1. No visible oil shall be found in fuel at a nozzle.

Next to the general hydrogen purity of 99.97%, this standard names several specific components with maximum concentrations, which are known to be particularly harmful for PEMFC efficiency or lifetime, or which constitute an issue for other system components and typical system operation modes. H_2O for

example, actually required for humidification and proper performance of the PEM, can eventually generate ice crystals during refilling at gas stations, which can damage the H_2 tank. Inert components such as He, Ar, N_2, and also CO_2 or CH_4 up to a certain concentration, can accumulate in the anode recirculation loop if not purged frequently to maintain proper PEMFC efficiency. Most other species, though, directly affect the electrochemical reactions in the MEA by either promoting dissolution and the loss of catalyst material (in case of halogenated compounds), or by lowering the protonic conductivity of the electrolyte (ammonia, in form of the ammonium ion, NH_4^+) or by adsorbing on catalysts and blocking active sites (formic acid, formaldehyde, sulfuric species and CO). For an extensive description of the poisoning mechanisms of (fuel) contaminants, the reader is forwarded to reviews in literature [38,39]. In this dissertation, CO and H_2S, two species frequently investigated in the past, have been used to examine the tolerance of the Pt catalyst anode electrodes versus reversible and irreversible poisoning effects and therefore are discussed in more detail in the next sections.

2.4.1 Carbon monoxide (CO)

CO is a strong poison for Pt electrocatalysts with severe effects on the PEMFC performance even at trace concentrations. In the anode electrode, CO adsorbs on the catalyst surfaces and competes with the hydrogen oxidation reaction (HOR) for active sites (2-19).

$$Pt + CO \rightarrow Pt - CO \tag{2-19}$$

The bonding mode, i.e. the number of Pt sites blocked by a CO molecule, depends on the coverage of catalyst by CO, and shifts from bridge-bonded, $(Pt)_2$–CO, to linear-bonded species, Pt–CO, with increasing coverage [67]. The CO coverage, i.e. the fraction of the total catalyst surface covered by CO, is a function of both, the rates of CO adsorption and of mechanisms contributing to a recovery from CO poisoning. At a given current density, these mechanisms are at equilibrium and a somewhat stable cell voltage is reached, which is below the voltage reached upon operation with neat H_2.

A crucial recovery mechanism is based on the dissociation of H_2O on Pt or other metals to forming hydrous oxide, and the subsequent oxidation of the adsorbed CO with the OH-molecule towards CO_2, (2-20) and (2-21).

$$Pt + H_2O \rightarrow Pt - OH + H^+ + e^- \tag{2-20}$$

$$Pt - CO + Pt - OH \rightarrow 2Pt + CO_2 + H^+ + e^- \tag{2-21}$$

These reactions usually require elevated potentials, because the equilibrium potential E^0 for oxidation of CO on Pt is about 0.611 V vs. RHE. In practice, though, the oxidation occurs already at lower potentials, because temperature, relative humidity or catalyst nanoparticle facets and catalyst alloy compositions affect the oxidation potential and shift it to values as low as 0.3 V vs RHE [68]. A second recovery mechanism involves the (electro-)chemical oxidation of CO with O_2, diffusing from the cathode to the

anode or present in trace amounts in the H_2 fuel, which adsorbs on Pt in the anode to react with CO to CO_2, (2-22) and (2-23).

$$2Pt + O_2 \rightarrow Pt - O_2 + Pt \rightarrow 2(Pt - O) \tag{2-22}$$

$$Pt - O + Pt - CO_{ads} \rightarrow 2Pt + CO_2 \tag{2-23}$$

With decreasing PEM thickness (automotive state of the art is between 8 – 25 µm, with 8 or even 5 µm as viable targets for reinforced membranes) and ionomer materials of higher diffusivity for O_2 [69,70], this mechanism is expected to gain in significance because more O_2 would diffuse through the PEM and be available in the anode loop. Apart from the passive addition of O_2 to the anode, this mechanism can also intentionally be provoked via air bleeding, i.e. an active addition of air to the anode recirculation loop to oxidize CO (and other unwanted species that can be oxidized), while accepting the loss in efficiency due to H_2 reacting with O_2 in the anode. However, the increased O_2 content in the anode can come with the downside of a promoted ionomer degradation, because hydrogen peroxide and radical formation, and consequently PEM degradation are enhanced [24].

An elegant means to mitigate CO contamination is the addition of transition metals more oxophilic than Pt, which attract H_2O and facilitate formation of OH-groups (referred to as bifunctional mechanism, similar to equation (2-20)), or which modify the electronic properties of the catalyst such that the bonding energy of CO on Pt is lowered and CO oxidation commences at lower potentials. Alloys of Pt with ruthenium (Ru), often employed in direct methanol FCs or PEMFCs operated with reformate gas, but also molybdenum (Mo), cobalt (Co), nickel (Ni) and iron (Fe) or a mixture thereof have shown to improve the CO tolerance of PEMFC anodes [74]. These alloys are sufficiently stable at normal operating conditions and anodic potentials below 0.5 V, but the alloying element usually exhibits increased dissolution rates upon exposure to high potentials, e.g. during shut-down and start-up (SD/SU) and fuel starvation events, or because of their lower stability in acidic media [68]. Therefore, despite their enhanced tolerance versus CO contamination, these catalyst alloys are usually not regularly employed in low temperature PEMFCs for automotive applications. With increasing operating temperatures, the tolerance of catalysts towards CO contamination is promoted, owing to increased reaction rates of CO oxidation in addition to the thermal desorption of CO [71], however, elevated temperatures usually lower the stability of PFSA based ionomers. Moreover, high water contents also enhance the CO tolerance of the anode electrode, because water molecules are required for the generation of OH-groups. Both temperature and humidity effects on CO oxidation potentials are visible in the shift of the oxidation peak towards lower potentials during CO stripping measurements [72]. Moreover, fuel utilization in the anode electrode affects the CO poisoning dynamics, as in-plane gradients in stoichiometry, CO concentration and water content affect the local CO coverage and anode overpotential [15,73].

Of course, reducing the PGM loading in the anode electrode also lowers the tolerance visible in the lower measured cell potential as a result of the higher anode overpotential, because contaminant species and H_2 are competing for fewer active sites [41]. If the loading is to be further reduced in order to reach ultra-low loadings, the maximum allowable CO concentration might have to be adapted, but this requires extensive in-situ testing, which is part of this dissertation.

2.4.2 Hydrogen sulphide (H_2S)

H_2S adsorbs and dissociates to elemental sulfur on catalyst surfaces, which blocks active Pt sites for HOR and accumulates in the anode electrode over extended times of operation at finite load (2-24).

$$Pt + H_2S \rightarrow Pt - S + 2H^+ + 2e^- \quad (2\text{-}24)$$

Similar to CO contamination, sulfur blocks one or two sites via linear-bonded, Pt–S, and bridge-bonded species, $(Pt)_2$–S, which affects the energy required to remove the sulfur from Pt via oxidation [75,76]. During operation of a PEMFC, sulfur contamination is predominantly irreversible and leads to a complete cell voltage break down, if no measures are taken to recover the cell performance. Generally, adsorbed sulfur can undergo oxidation in presence of oxygen species to yield water soluble sulfur oxides, but usually requires high electrode potentials above 0.8 – 1.2 V. At such potentials, sulfur is oxidized with water to sulfur dioxide (2-25), which dissolves in water forming sulfites (2-26) or sulfates (2-27) [20]. These species are eventually flushed out of the PEMFC with water, and the poisoned electrode recovers [44].

$$Pt - S + 2H_2O \rightarrow Pt + SO_2 + 4H^+ + 4e^- \quad (2\text{-}25)$$

$$SO_2 + H_2O \rightarrow SO_3^{2-} + 2H^+ \quad (2\text{-}26)$$

$$SO_2 + 2H_2O \rightarrow SO_4^{2-} + 4H^+ + 2e^- \quad (2\text{-}27)$$

Potentials above 0.8 – 1.2 V though are typically not reached by the anode electrode during regular operation, except during fuel starvation and SD/SU events, or if such potentials are enforced via an external power supply. Nevertheless, this process usually is not considered a feasible measure for automotive systems and furthermore leads to a gradual destruction of the electrode by accelerating carbon corrosion. However, steady-state or periodic polarizations to potentials as high as 1.4 or even 1.5 V have shown to recover somewhat close to 100% of the original ECSA and PEMFC performance, indicating that sulfur contamination is to a degree reversible [20,30,77,78]. Besides such polarizations, the interruption of the operation alone and maintaining OCV at otherwise constant conditions also has shown to partially alleviate from sulfur poisoning by allowing adsorbed sulfur to react with H_2 back to H_2S [13]. Furthermore, since water is always present in the PEMFC, sulfur species eventually oxidize and dissolve at low rates even during operation with H_2S, with the state of the species being governed by the pH [79]. For example, an increase in RH from 50 to 100% during operation with 2 ppm H_2S was found to decelerate the current decay rate by 60%, which indicates that oxidation and dissolution processes of sulfuric species are also occurring at regular anode potentials [80]. Another example is the active introduction of air or ozone (O_3) into the anode compartment delaying the inevitable cell voltage break with H_2S, because O_2 and O_3 oxidize adsorbed sulfur to soluble species [20,81]. These species are ultimately flushed out with excess reactant gas streams and water from the anode compartment, but also from the cathode compartment if dissolved species are transported through the PEM. Contrary to CO contamination, though, an increase in PEMFC operating temperature has a negative effect on sulfur contamination, visible in the 69% faster voltage decay for a PEMFC operated at 90°C compared to 50°C [82]. Higher temperatures accelerate the rates of

H_2S dissociation to forming elemental sulfur on Pt, however, higher temperatures also facilitate sulfur oxidation at potentials above 0.8 V, because the Pt–S bond is weakened [20,76].

Possibilities for H_2S or sulfur contamination tolerant catalysts are much scarcer as compared to CO contamination. The aforementioned CO tolerant catalyst alloys (Pt with Ru, Mo, Co or Fe) do not influence the tolerance versus H_2S contamination [30]. Catalysts alloyed with palladium (Pd) and copper (Cu) have shown to improve the H_2S tolerance, but these alloys are rather suited for use in HT-PEMFCs and not in automotive LT-PEMFCs, because of the excellent HOR activity of Pt catalysts and the negative effect of Cu on electrolyte stability [83,84]. The reduction in anode loading also generally shortens the durability of a PEMFC upon continuous operation with H_2S contaminated fuel [14]. This points towards a reconsideration of the allowed concentration for sulfuric species to allow for ultra-low anode loadings, but it leaves the question whether realistic PEMFC operations according to automotive drive cycles including regular events such as SD/SU alleviate from the necessity to lower the ISO 14687 limit for sulfuric species.

2.5 Scope of this dissertation

As outlined in the previous sections, PEMFC cost and durability including the tolerance versus contaminants are closely related to the PGM content, namely the Pt loading of the MEAs. In order do find the optimal trade-off between durability and cost, it is necessary to understand the underlying degradation and contamination mechanisms and assess whether their effects on PEMFC performance are within acceptable ranges. With respect to fuel contamination, this means that not only the Pt content is considered a variable, but also the impurity concentration, which is allowed in the fuel at dispensing stations. If reductions in Pt loadings are targeted, concentration limits eventually have to be reconsidered based on PEMFC tests with the possible outcome, that the limits require adaption. In these regards, the tolerance of low and ultra-low-loaded anode electrodes versus CO and H_2S contamination were investigated as a starting point for discussions on the necessity to tighten the fuel quality standard ISO 14687 on these species. Furthermore, SD/SU events are expected to show beneficial effects on sulfur contaminated electrodes, and therefore were included in the testing procedure to confirm the expectation.

In the course of these investigations, electrochemical characterization methods like CV and EIS were employed to investigate parameters like the ECSA and electrode resistances of ultra-low-loaded electrodes. With lower loadings, the ratio between the currents of the processes of interest and artifacts became disadvantageous, such that these methods required adaption and a new artifact eventually was observed in CV measurements. In light of the aforementioned reductions on PGM content in the MEA, such artifacts are expected to be observed more often in future and clarification might be required.

When conducting contaminant testing at low concentrations, test bench components such as tubes and fittings are often coated with a thin SiO_2-layer as an adsorption barrier for impurity species. Such SiO_2 coatings also can be applied on electrocatalysts, where this topic already received noteworthy attention due to the stability enhancing and wettability changing effects. However, the impact of a SiO_2 coating on CO and H_2S contamination was not investigated yet. Considering the fact that water content has such a significant influence on the tolerance versus contamination, an improvement with a SiO_2 coating appeared likely and was investigated within this dissertation.

These three investigations are represented by separate publications summarized by this dissertation. Prior to the summary, the experimental procedures are laid out and subsequently, the investigations and conclusions are presented and discussed in the scientific context.

3 Experimental

This dissertation investigates the effect of fuel impurities on PEMFC experimentally. All in-situ experiments were carried out with single test cells by means of classical electrochemical characterization techniques. The PEMFC components used in chapter 4.1 and 4.2 were acquired from project partners and suppliers, while the catalyst material employed in chapter 4.3 required modifications and subsequent electrode and CCM fabrication. These in-house prepared materials were analysed by scanning and transmission electron microscopy with energy dispersive X-ray spectroscopy (SEM and TEM-EDX). In the following, the test bench and cell designs, testing procedures, electrode fabrication and material analysis are described.

3.1 Fuel cell test bench, platform and characterization methods

The in-situ tests were conducted on an in-house built test bench equipped with a Zahner Zennium Pro potentiostat and a Kikusui PLZ664WA electric load for electrochemical measurements. Gas flows and humidity of the reactant gases are controlled via multiple mass flow controllers (MFCs), where part of the gas is channeled through a bubbler and mixed subsequently with the dry gas fraction to achieve a required humidity. The addition of impurities (GasX) is controlled via two additional MFCs, each one for non-adsorbing (e.g. CO, CO_2) and adsorbing species (sulfuric or halogenated compounds, NH_3) with the point of gas injection into the dry gas stream to bypass the bubbler and avoid dissolution of the GasX in bubbler water (Figure 4).

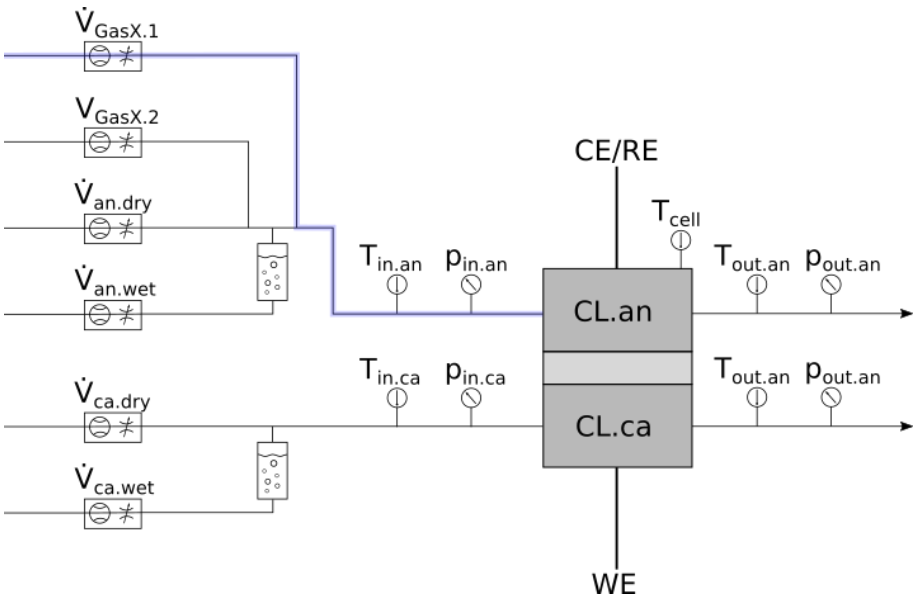

Figure 4 Test bench schematic with two MFCs for impurities (GasX.1 and GasX.2) and SilcoNert® coated tubing (in blue), and the PEMFC with anode and cathode catalyst layers (CLs)

Moreover, the stainless steel tubing and components for GasX species, which tend to adsorb on metal surfaces (like sulfuric species or NH_3), were coated with a SiO_2 coating (SilcoNert® prepared by SilcoTek GmbH) as adsorption barrier.

The typical in-situ procedures for MEA characterization required adaptions to accommodate the investigations of the contaminated anode electrodes. For cyclic voltammetry (CV) analysis of the anode, the working, counter and reference electrodes (WE, CE and RE) have to be exchanged, for which there exist three options (Figure 5).

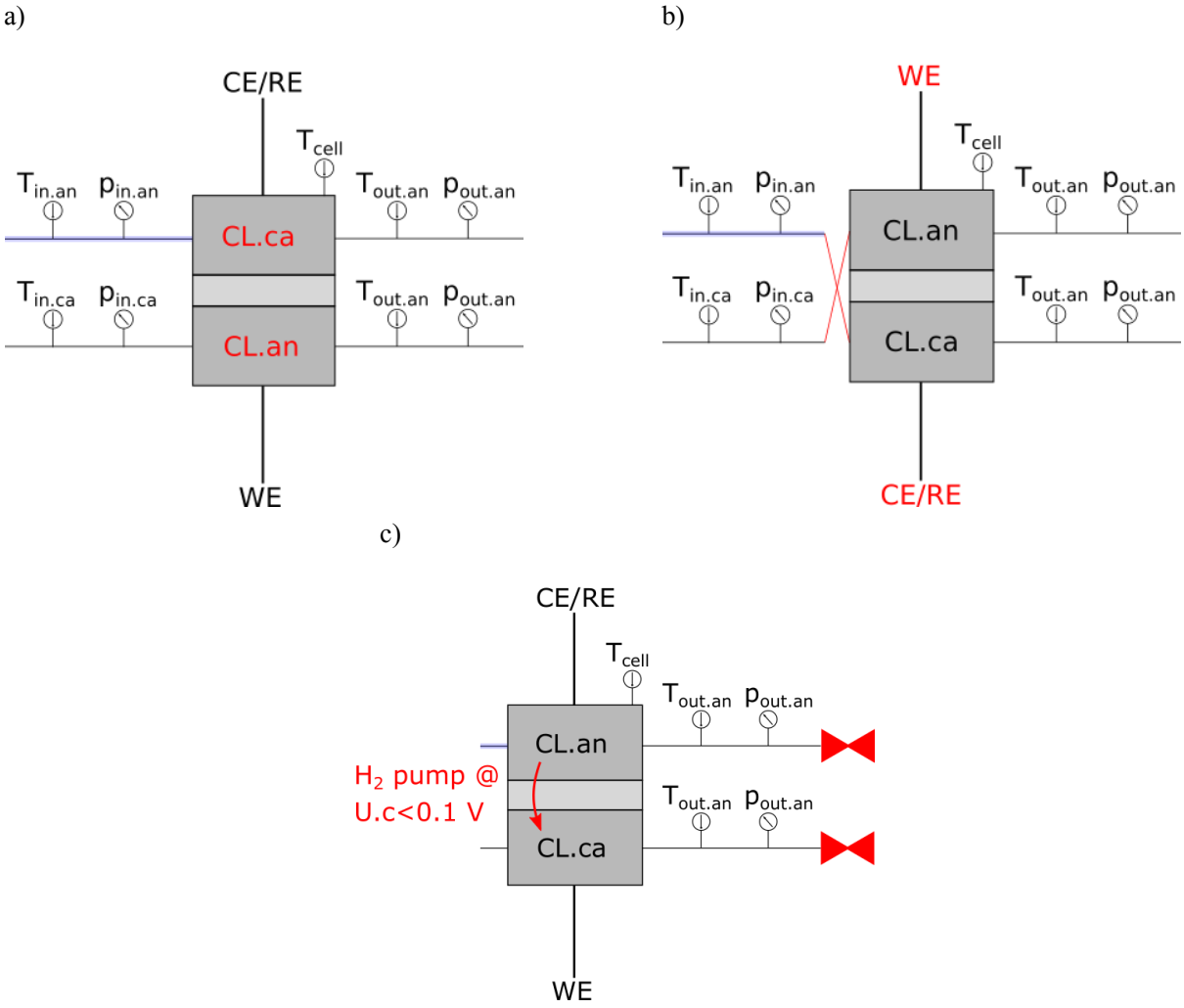

Figure 5 Alternatives of cell preparation for CV analysis of the anode electrode, a) MEA rotation, b) switch of gas supply and electrical connections and c) H_2 pumping and N_2 purge of both electrodes, closure of back pressure valves and subsequent CV in negative potential ranges (e.g. from -0.05 – 0.9 V)

The first option is a simple rotation of the MEA after a shutdown of the cell, such that the actual anode electrode becomes the WE (Figure 5 a). The second option comprises the exchange of the H_2 and N_2 supply and of the electrical WE, CE and RE connections (Figure 5 b). Due to safety precautions, the test

bench design did not provide for an automated exchange of the H_2 and N_2 supply and therefore manual modifications were obligatory. The third option requires electrochemical pumping of H_2 towards the cathode at cell potentials (U.c) below ~0.1 V, the purging of the anode with N_2, and a CV measurement between potentials of e.g. -0.05 to -0.9 V, while gas flows are switched off and back pressure valves closed to minimize gas agitation in both compartments. The advantage of the latter is the possibility for a fully automated operation, however, the conditions during the CV are comparably instable due to the lack of controlled gas flows, while additionally the test bench electric hardware limited from this option, hence, it was not considered for this work. Which option suits best for fuel contamination studies depends on test bench capabilities and whether the MEA is exposed to ambient air and temperatures during the preparation for the anode CV, which eventually would recover the MEA from contamination. For studies investigating the ECSA at begin-of-life (BOL) or tests without contamination, option a) was deemed sufficient. Measurements including contamination, particularly H_2S and its effect on the ECSA, required option b) to minimize exposition of the MEA towards air. In addition to the configuration, the timing of the different characterization methods after contamination can be of relevance. For example, for CV analysis of sulfur contaminated anode electrodes, the method should be timed such that the test bench downtime is kept as short as possible for the necessary modifications to prevent unwanted recovery from sulfur contamination.

The single cell platform used for in-situ testing was updated in the course of the project from a differential test cell provided by an industry project partner (with 20.25 cm² active area) to the current standard single cell test platform at Fraunhofer ISE, the balticFuelCells GmbH qCF Liquid Cooling High Amp (with 12 cm² active area). Both test platforms are differential cells, which are operated at high gas flow rates to minimize in-plane gradients in reactant composition, humidity and temperature over the active area. Operating parameters were adapted to eventually correlate to specific publications in literature, or according to the research question of the respective chapter (Table 3). For example, during the studies focussing on the correlation between Pt loading and contamination effect, the operating conditions were adjusted to publications by Hashimasa et al. [14,41], because the authors investigated the reduction of the anode loading down to 50 µg/cm^2, and this dissertation continued to even lower loading values. On the other hand, for the study focusing on the effect of the SiO_2 coating on contamination, the relative humidity was varied as the interplay between the SiO_2 and water was of interest.

Table 3 Operating parameter ranges

Parameter	Chapter 4.1	Chapter 4.2	Chapter 4.3
Cell type (active area)	Baltic qCF highAmp (12 cm²)	Baltic qCF confidential (20.25 cm²)	Baltic qCF highAmp (12 cm²)
Flowrate an	2 l/min	3 l/min	2 l/min
Flowrate ca	5 l/min	7 l/min	5 l/min
Cell temperature		80°C	
Rel. humidity an	95-100%		40 / 70 / 100%
Rel. humidity ca	75-100%		40 / 70 / 100%
Inlet pressure an		1.05-2 bara	
Inlet pressure ca		1.05-2 bara	

Contamination tests in literature usually include polarization curves with and without, or before and after the exposition to contaminant gases to evaluate the performance difference with the contaminant [81,85], or static operation at a fixed current or potential to measure the performance decay over time [15,86]. In addition, electrochemical impedance spectroscopy (EIS) can also be employed to further investigate the contamination mechanism of a contaminant [87], however, as the mechanisms of CO and H_2S are already well known, EIS was predominantly used to assess the high frequency resistance (HFR) during polarization curves and only added during the contaminant tests with SiO_2 coated catalyst material in chapter 4.3. CV can be employed to determine the oxidation potentials of CO [29,68] or sulfur [20,30], which gives information on the energy required to oxidize adsorbed species from the catalyst surfaces. The testing sequences used in this dissertation are combinations of these methods, and the detailed sequences and parameters are given in the respective publications.

3.2 Materials

The materials used in chapters 4.1 and 4.2 were provided by associated project partners, whereas the materials for chapter 4.3 required partial modification with subsequent in-house electrode and CCM fabrication. Generally, all MEAs comprised of electrodes with low anode and high cathode Pt loadings, state-of-the-art automotive PEMs and a comparably hydrophobic GDL (Table 4). Low anode and high cathode loadings were selected to focus on contamination effects of the anode electrode and to minimize the influence of the cathode electrode. For example, sulfur contaminated fuel will predominantly affect the HOR kinetics at the anode electrode by adsorption of elemental sulfur on the catalyst surface. However, sulfuric species can diffuse or be transported through the PEM to the cathode electrode, where they eventually affect the ORR kinetics [80]. In addition, a hydrophobic GDL (i.e. with a relatively high amount of hydrophobic agent) was chosen to allow for performance tests at or close to 100% RH without the risk of flooding the MEA at high current densities.

Table 4 Cell platform and MEA specifications

	Chapter 4.1 and 4.2	Chapter 4.3
Catalyst (an/ca)	Pt nanoparticles on C support	
Pt loading an	15 / 25 / 50 µg/cm²	70 µg/cm²
Pt loading ca	400 µg/cm²	550 µg/cm²
C support an	Graphitized carbon (confidential)	Graphitized carbon (Umicore Elyst Pt20 0390)
C support ca	High surface area carbon (confidential)	High surface area carbon (Umicore Elyst Pt50 0550)
PEM	15 µm, reinforced (confidential)	15 µm, reinforced (Fumatech FS-715-RFS)
GDL (an/ca)	Freudenberg H23C9	

The CCMs supplied by associated project partners were protected by a non-disclosure agreement (NDA) and therefore further details about electrodes and the PEM are confidential. In contrast, the materials modified and processed in-house were analysed via SEM and TEM-EDX to assess structures, average compositions and distribution of the elements and the material details could be named.

3.3 Elemental and morphological analysis via SEM- and TEM-DX

Scanning electron microscopy coupled with energy dispersive X-ray spectroscopy (SEM-EDX, FEI Quanta 400 with EDAX detector system for EDX spectrometry) was primarily employed to analyse the elemental composition and structures of fabricated catalyst powders and electrodes. SEM imaging and EDX analysis were conducted at high acceleration voltage (30 kV) and spot sizes on piles of catalyst powders to acquire average material compositions and assess powder and decal structures. For elemental analysis of catalyst materials, inductively coupled plasma mass spectroscopy (ICP-MS) or optical emission spectroscopy (ICP-OES) are often employed because of their high sensitivity to low concentrations of a broad range of elements, but these destructive methods require the dissolution of the solid material in a mixture of hydrofluoric, nitric and/or hydrochloric acid. The advantage of SEM-EDX over ICP-MS/OES lies in the simultaneous morphological and elemental analysis, while sample material is not destroyed and available for further usage. As the amount of the modified catalyst materials were barely sufficient for the in-house electrode paste fabrication, SEM-EDX was employed to evaluate the average compositions.

Scanning transmission electron microscopy (STEM) coupled with EDX (ThermoFisher Scientific Talos F200X STEM, equipped with Bruker Super-X four silicon drift detectors for EDX spectrometry) was employed to investigate the local distribution of the SiO_2 coating on the catalyst particles or agglomerates and furthermore evaluate the Pt particle size distribution at high resolution. As such STEM-EDX images usually often represent agglomerates or even single catalyst particles, multiple images were acquired and analysed to achieve adequate statistics.

3.4 SiO_2 coating process, electrode and CCM fabrication

SiO_2 coated electrocatalysts are commercially not available and hence, the coating and subsequent electrode and CCM fabrication was performed in-house. The complete description of the SiO_2 coating on electrocatalysts can be found in the publication in chapter 4.3, however, additional relevant information is provided in the following. In short, the SiO_2 coating process is based on the hydrolysis of silicon-containing precursors on carbon supported platinum electrocatalysts (Pt/C) dispersed in water and ethanol, the subsequent phase separation via centrifugation, and the drying and calcination of the slurry. To exert a similar heat treatment on the reference anode catalyst material, Pt/C powder without SiO_2 was added in a separate tray into the oven during calcination of the SiO_2-Pt/C. After calcination, the SiO_2 coated product contained agglomerates and chunks in sizes up to several mm in diameter (Figure 6 a). This material was ball milled to acquire a fine SiO_2-Pt/C catalyst powder prior to the subsequent paste and electrode fabrication processes.

a) b)

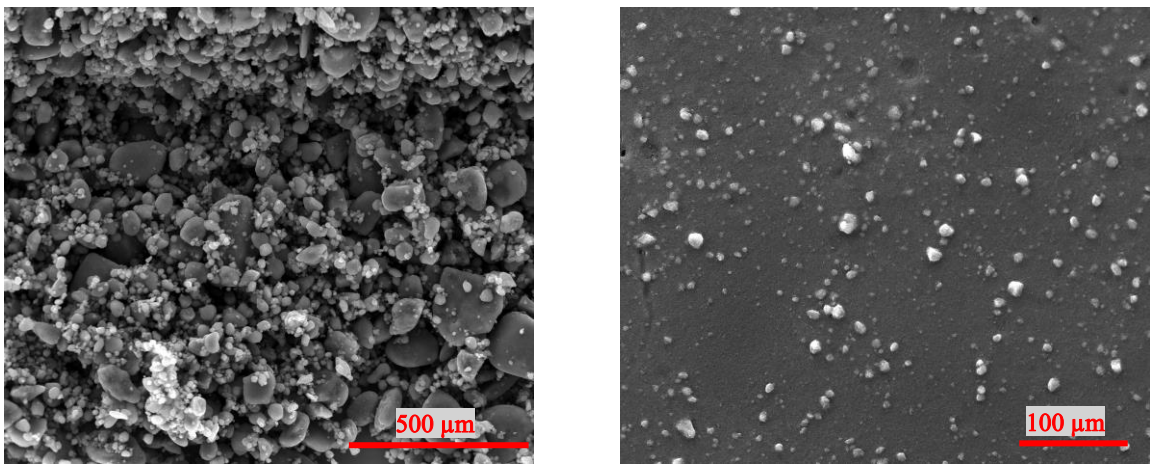

Figure 6 SEM images of a) the SiO_2-Pt/C agglomerates after calcination and b) the dried electrode surface on the decal after ball milling, paste fabrication and printing

Catalyst pastes for anode and cathode electrodes were generally prepared in a similar manner by mixing the respective catalyst powder with ionomer in water and alcohols using an axisymmetric centrifuge and magnetic stirring. For all pastes, the same solvents and ionomer content in the electrode (30 wt.%) were employed. The pastes were screen printed on substrates to generate electrode decals with target loadings of 0.07 and 0.55 mg_{Pt}/cm^{-2} for anode and cathode electrodes, respectively. SEM images of the electrodes containing Pt/C and SiO_2-Pt/C revealed agglomerates of catalyst particles in sizes up to 20 µm diameter despite the ball milling (only conducted on SiO_2-Pt/C material) and mixing steps for all electrodes (Figure 6 b). Agglomerates or defects in electrodes are subject to current research at Fraunhofer ISE, since their influences on PEMFC performance and durability are not yet fully understood. Agglomerates in the electrode eventually exert mechanical strain on the PEM, and electrode delamination from the PEM amplifies mechanical-chemical degradation of the ionomer [88,89]. Catalyst material inside of these agglomerates eventually lacks of contact to the proton conducting ionomer, but this role can be

adopted by water penetrating into these particles during PEMFC operation. Since these agglomerations were visible for all electrodes in this work, they were considered negligible, and the electrodes accepted for further testing. For fabrication of the catalyst coated membrane (CCM), each an anode and cathode decal were hot pressed onto an automotive PEM. The CCMs were framed using laser cut polyethylene naphthalate (PEN) foils and assembled with the GDLs to form the membrane electrode assembly (MEA).

4 Results in the context of PEMFC research

This dissertation is a composite of three publications investigating the effects of fuel contaminants, namely CO and H_2S, on PEMFCs with low-loaded anode electrodes, the CV analysis thereof and an alternative route to manipulate the tolerance versus fuel contamination. In the following, the main results of the three publications are summarized and embedded into the general context of PEMFC research and development. The conclusions and outlook are provided in Chapter 5, whereas the full length publications can be found in Chapter 6.

4.1 CV analysis of low-loaded PEMFC electrodes

Cyclic voltammetry (CV) analysis, one of the most important methods for the characterization of electrocatalysts, provides information on oxidative and reductive charge transfer processes on electrode surfaces. Knowledge of the limitations and the influence of measurement conditions are indispensable to investigate a process of interest. Works in literature provide guidelines on how to conduct CV analysis of electrochemical systems in general [90,91], or in more detail, which artifacts can occur during CV analysis of PEMFC electrodes [92,93]. However, with new materials or setups, re-evaluation of the limitations and measurement conditions eventually is required. For the specific case of low-loaded PEMFC electrodes, several best practices for CV analysis were re-evaluated in the course of this dissertation because of difficulties arising from unfavorable ratios between the currents from electrochemical processes of interest and from artifacts or noise. One of the measures to manipulate the shape of a CV is the potential sweep rate, which determines the time for an electrochemical process to develop and complete. Faster sweep rates eventually shorten the time for potentially disturbing processes to unfold while processes of interest are emphasized. Therefore, to accentuate particularly hydrogen adsorption and desorption and to facilitate the determination of the ECSA from hydrogen underpotential deposition (H_{UPD}), the sweep rate was raised from the often used 20 to 100 mV/s. Furthermore, the WE requires purging with N_2 for removal of the oxidant, however, maintaining the N_2 purge flow during the CV increases the Nernst potential for H_2 evolution, which is proportional to the ratio of H_2 concentrations in CE and WE (2-11).

$$E_{Nernst} \propto Log\left(\frac{C_{H_{2,CE}}}{C_{H_{2,WE}}}\right) \tag{4-1}$$

With N_2 purge switched on during the CV, the evolving H_2 is removed from the WE and additional H_2 is "electrochemically pumped", i.e. transported from CE to WE. Currents associated to H_2 pumping and the reverse process of oxidation of accumulated H_2 in the WE, sometimes referred to as "concentration cell effect", were found to affect particularly H-desorption charges relatively more severe for low-loaded anode as compared to high loaded cathode electrodes as shown in Figure 7.

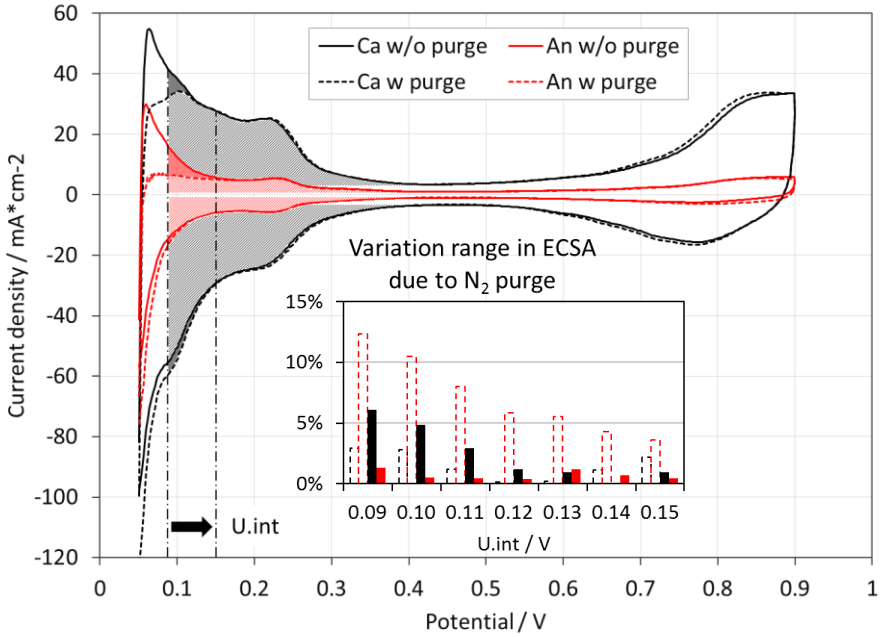

Figure 7 CV measurements of high loaded cathode and low-loaded anode electrodes (400 vs. 50 µg/cm² Pt/C, respectively) with the variation range in ECSA based on total ECSA value due to N_2 purge on or off (dark vs. bright transparent areas) for different lower charge integration limits U.int shown in the inset

To improve statistics, the ECSA can be averaged from both H-adsorption and desorption of multiple CV cycles, which ideally yields similar values, i.e. low variation ranges. However, for CV analysis of low-loaded electrodes, the variation range was at unfavorable levels with N_2 purge of the WE switched on during the CV, and consequently the purge was omitted. An alternative to minimizing variation range due to the influence of the concentration cell effect is to increase the lower potential limit for integration (U.int in Figure 7) of the H_{UPD} charge transfer, e.g. from 0.09 to 0.15 V, which in turn results in the underestimation of the ECSA. During these re-evaluation tests, an artifact was observed, which could not be fully explained by works in literature and therefore was investigated in more detail. The artifact shows itself as an oxidation peak overlapping the Pt oxide reduction during the cathodic CV transient, and is described in the publication "**Hydrogen oxidation artifact during Platinum oxide reduction in cyclic voltammetry analysis of low-loaded PEMFC electrodes**", provided in Chapter 6.1. [94]. The artifact significantly affected the ECSA evaluation from H_{UPD}, specifically from H-adsorption and therefore was investigated within this dissertation. Through a parametric study, this oxidation peak could be associated to the spontaneous HOR of previously accumulated crossover hydrogen (H_{2X}), for which specific criteria have to be fulfilled that it can be observed. First, the artifact predominantly occurs during CV analysis of low-loaded electrodes composed of catalyst material, whose oxide is completely inactive towards HOR. Second, the potential window and sweep rate have to be appropriate for catalyst oxide formation and the accumulation of H_{2X}, e.g. with the upper potential limit >0.9 V for Pt. Third, the CV measurement must be carried out without N_2 purge of the WE, such that H_2 can accumulate and is not purged prior to the Pt oxide reduction. For higher loaded electrodes, the artifact is usually not observed as Pt or alloys including Pt either are not fully covered by an oxide layer, such that H_{2X} is continuously oxidized, and/or the currents

associated to the oxide reduction are much larger than the spontaneous HOR of H_{2X}, and the oxidation peak is barely, if at all, noticed. Although this artifact does not provide any further information on catalyst structures or parameters besides the fact that Pt (or other catalyst) oxides are eventually inactive towards H_2 oxidation, it might interfere with the ECSA determination from H-adsorption and furthermore with the analysis of the currents associated to Pt oxide reduction. Knowledge of this artifact and the selection of appropriate conditions for CV analysis of low-loaded electrodes are indispensable, especially when considering the targeted PGM contents for the anode and cathode electrodes, for which the artifact might be observed more often in the future. If CV conditions are appropriate, i.e. high CV upper potential limit as it is eventually used for investigations into sulfur oxidation or metal oxide development, and the N_2 purge is switched off, this peak can overlap the currents associated to metal oxide reduction. Further, it might emanate into the double layer potential window, where it disturbs the evaluation of the double layer charge transfer and consequently the ECSA determination from H-adsorption as shown in Figure 8.

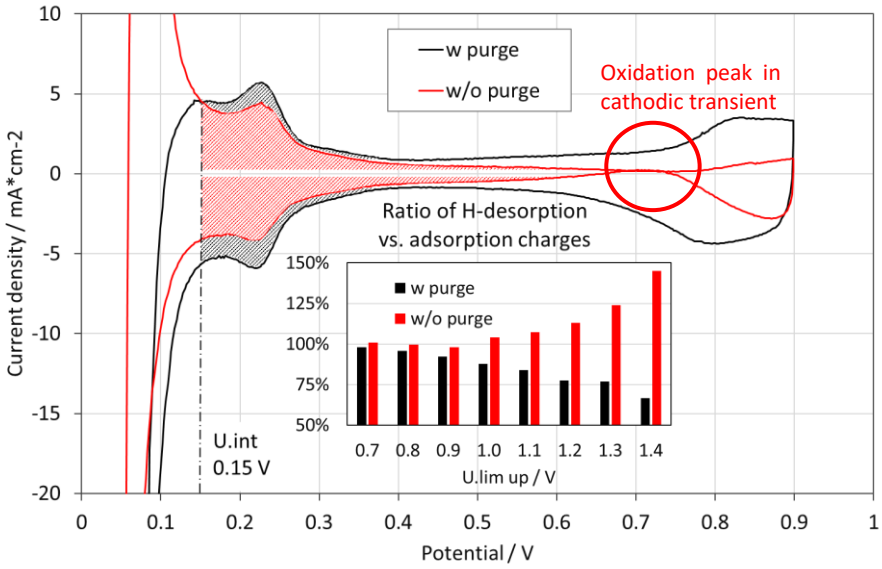

Figure 8 CV measurements of low loaded anode electrode (50 µg/cm² Pt/C) with and without N_2 purge and upper potential limit (U.lim) of 0.9 V, with the ratio of H-desorption vs. adsorption charges shown in the inset for U.lim upt to 1.4 V (U.int for ECSA determination 0.15 V). The oxidation peak in the cathodic transient leads to the increase in the ratio if N_2 purge is switched off, while the concentration cell effect causes the decrease with N_2 purge switched on.

As shown in the inset, the ratio of H-adsorption vs. desorption increases in consequence of the oxidation peak occurring in the cathodic transient, which complicates the evaluation of the double layer charge transfer currents when the N_2 purge is switched off. Vice versa, if purge is switched on, the ratio decreases due to the concentration cell effect altering specifically H-desorption charges despite the selection of a lower charge integration limit U.int of 0.15 V.

Comparable oxidation peaks in the cathodic transient of CVs were reported for Pt catalysts by Tahmasebi et al. [95] and for Pd based electrodes by Zhao et al. [96] as shown in Figure 9, which the authors though observed in electrochemical systems different from H_2 and air PEMFCs. Tahmasebi et al.

investigated oxidative and reductive processes on Pt electrodes in a rotating disk electrode (RDE) setup purged either with N_2, O_2 or H_2, which is where the authors noticed the oxidation peak during Pt oxide reduction in the cathodic transient (Figure 9 a). They attributed this peak to a short-lived increase of the ECSA, or to a synergetic effect arising from changes in surface electronic structure in the presence of dissolved H_2 during Pt oxide reduction. Though possible, the more applicable explanation might be related to the work by Zhao et al. on the origin of an oxidative peak in the cathodic transient referred to as J_b in their study.

a) b)

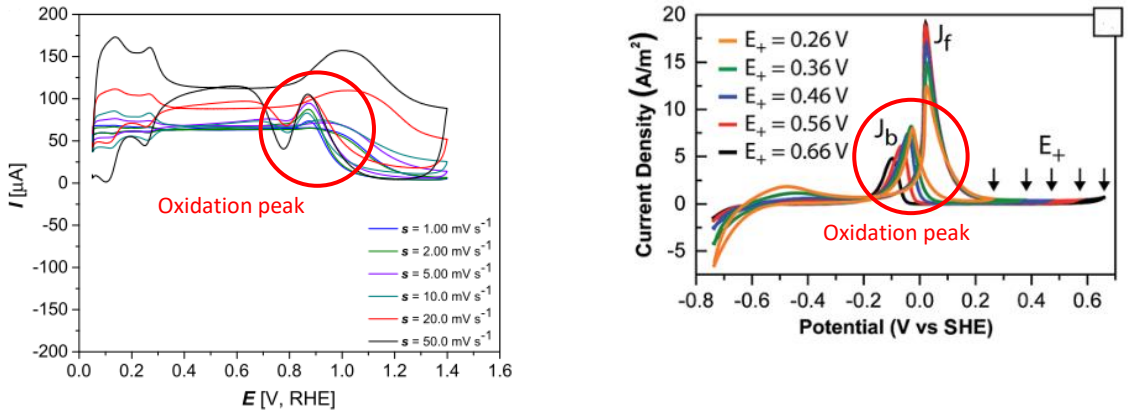

Figure 9 CV profiles of a) Pt(poly) in 0.5 M aqueous H_2SO_4 saturated with H_2, and b) of methanol oxidizing on a Pd electrode taken from Tahmasebi et al. [95] and Zhao et al. [96], respectively, with the oxidative peak marked in red.

Zhao et al. investigated the oxidation of alcohols on noble metal electrodes, where the ratio of J_f/J_b, with J_f as the oxidation peak current in the anodic scan (Figure 9 b), is used as an indicator for the carbon monoxide tolerance of the catalyst. However, the authors concluded that the peak simply arises from fresh alcohols oxidizing on the metal catalyst surfaces once the surface oxides are reduced during the cathodic scan. A comparable explanation likely applies for the peak reported by Tahmasebi et al., where H_2 dissolved in the RDE electrolyte solution near the catalyst surfaces is eventually oxidized during Pt oxide reduction. Further studies reporting this oxidation peak, also on low-loaded electrodes tested in-situ in PEMFCs operated with H_2 and air, were not found in literature, either because N_2 purge is usually activated during CV analysis, and/or electrode loadings investigated via CV are larger than the anode loadings employed in this dissertation.

4.2 Hydrogen quality standard ISO 14687 and updates thereof

The tolerance of a PEMFC electrode towards specific contaminants is closely related to the electrode loading and ECSA, because nominally larger catalyst surface areas provide a larger buffer versus contaminant coverage and therefore endure higher contaminant dose. With the target to lower the amount of PGMs in PEMFCs, the surface area and hence, the tolerance eventually decreases such that the acceptable limits for contaminants have to be reassessed. In this context, the International Organization for

Standardization (ISO) frequently revisits and updates the hydrogen quality standard for PEMFC vehicles ISO 14687. This standard, created in 1999 and revisited in 2001, 2008, 2012, 2014, 2019, is currently being updated in the technical committee (TC) working group (WG) ISO/TC 197/WG 27 by stakeholders from industry and research institutes concerned with H_2 production, infrastructure and usage in PEMFC vehicles [97]. To justify possible adaptions of the standard, committee members conduct tests, but also include literature references into their decision-making. These tests often follow the guidelines for PEMFC contamination tests outlined in a standard published by the Society of Automotive Engineers, the SAE J3219, which summarizes best practices for PEMFC fuel quality screening [98]. The results of the ISO/TC 197 revision will be published in the committee draft (CD), ISO/CD 14687, on which national bodies can vote and comment, and which upon approval will replace the former version of ISO 14687:2019. In this context, the target of low and ultra-low-loaded anode electrodes for PEMFCs requires contaminant testing to assess whether adaptions of impurity limits are necessary.

H_2 for PEMFC vehicles can contain a multitude of impurities, such as oxidized, sulfuric, halogenated, or inert species, and their occurrence and concentrations depend on the H_2 feedstock, production, and purification processes. The occurrence of several species is considered unlikely owing to alternative, "clean" H_2 production or efficient purification systems [40], however, impurity testing is still required because the ISO 14687 ultimately states all relevant impurities and their limits irrespective of the H_2 source. In this dissertation, carbon monoxide (CO) and hydrogen sulfide (H_2S), species only possible in H_2 stemming from fossil fuel-based processes, were used as contaminants because these species are known strong catalyst poisons and the severity on MEAs with ultra-low-loaded anode electrodes as well as the effect of shut-down and start-up (SD/SU) events on sulfur contaminated electrodes required evaluation. These investigations are described in the publication "**Tolerance and recovery of ultra-low-loaded platinum anode electrodes upon CO and H_2S exposure**" [99], provided in Chapter 6.2. This publication is related to the works by Hashimasa et al. [14,41], who reported the PEMFC tolerance decreasing effect by lowering the Pt based anode electrode loading from 400 to 50 $\mu g_{Pt}/cm^2$. The in-situ contamination tests included galvanostatic operation of single cells comprising of low-loaded anode electrodes with 50, 25 and 15 $\mu g_{Pt}/cm^2$, and using fuel contaminated either by CO or H_2S in concentrations at or close to the respective limits, i.e., 0.2 ppm for CO and 0.004 ppm for sulfuric species (e.g. H_2S). In addition, the effect of SD/SU events on sulfur contaminated anode electrodes was investigated by means of CV analysis to assess the catalyst surface covered and freed from sulfur by the SD/SU.

First, the publication establishes the difficulties arising from the evaluation of the ECSA from CVs of ultra-low-loaded electrodes, because artifacts and noise gain in relevance in consequence to the low currents from electrochemical processes on the small Pt and carbon surface areas (see chapter 4.1). Critical parameters and options for CV analysis usually are the cell temperature and gas humidity, the sweep rate, the potential window for the sweep on one and for the ECSA determination on the other hand, and whether the cathode electrode is continuously purged with N_2 during the CV. For the contamination studies in this dissertation, these operating parameters were varied to find the parameters giving most reproducible CV measurements of ultra-low-loaded electrodes. Main differences to regularly employed parameters were a comparably high sweep rate of 100 mV/s (versus 20 mV/s often employed in literature) to minimize the significance of current noise, the deactivation of the N_2 purge during the CV due to extreme H_2 evolution currents as soon as purging was activated, and a decrease of the potential window to 0.15 – 0.3 V used for

ECSA determination. Especially the latter leads to an underestimation of the ECSA, however, it still allows for a relative comparison of the ECSA of an electrode before and after (sulfur) contamination.

Second, the PEMFC performance, evaluated via polarization curves and chronoamperometric operation at 1 A/cm² in neat H_2, shows that the performance and voltage decay rates over time are independent of the anode electrode loading and no increase in anode overpotential due to ultra-low loadings is observed. This is in line with the study by Kinoshita, reporting no significant increase in overpotential and current decay rate for loadings above 10 µg/cm² [100]. This observation changes dramatically upon the introduction of 0.4, 0.2 or 0.1 ppm CO in H_2, which causes the voltage to decrease by 25 – 60%, 10 – 50% and 5 – 40%, respectively, for the MEAs with the three different anode loadings of 50, 25 and 15 $\mu g_{Pt}/cm^2$. In literature, a threshold often used as a maximum for contamination induced effects in chronoamperometric measurements is 50 mV, which resembles 7% based on the measured 700 mV at 1 A/cm² in neat H_2 for all tested anode electrodes. If these results were used for discussions on adaptions of the ISO 14687 CO limit, only the 50 µg/cm² anode electrode and a CO concentration of 0.1 ppm would pass the test. For all other loadings and CO concentrations, the results would indicate the necessity to either reduce the CO limit or adapt the anode electrode design.

Third, the decrease in anode loading results in a decrease of the durability upon H_2S contamination, however, this decrease is disproportional to the sulfur dose (molar mass of H_2S until a voltage drop by 30 mV is reached), indicating a relaxation of the contamination mechanism for lower loaded electrodes, where the loading reduction is achieved by reducing the electrode thickness. In addition, SD/SU events were found to recover sulfur contamination visible in a slight increase in ECSA of a poisoned anode electrode after the event. The nominally recovered ECSA was in comparable ranges for the three types of anode electrodes (approximately 2.7 – 4.4 m^2/g_{Pt}), corresponding to an almost full ECSA recovery for the lower loadings based on the higher values after contamination. In combination, both findings allow for the hypothesis that interfacial effects either between the PEM and electrode, or the electrode and MPL play a role in sulfur contamination and recovery thereof, which would affect thinner electrodes to larger extend as thicker electrodes at otherwise similar electrode designs. For catalyst dissolution during ASTs, an analogue observation can be observed: Pt dissolved upon potential cycling is transported into the PEM, which was more profound in proximity to the PEM and ultimately resulted in a Pt depleted zone in the catalyst layer (CL) at the CL/PEM interface [25]. A comparable mechanism appears possible for oxidized and dissolved sulfur species at the electrode interfaces, where these species are eventually transported within water from the electrode.

In terms of discussions on adaptions of the ISO 14687, these results are controversial. On one hand, sulfur contamination still leads to complete voltage break downs during operation for lower loadings, while on the other hand, typical SD/SU events recover from the poisoning and eventually relax from the necessity to lower the ISO limit for sulfuric species. In addition, further mechanisms can contribute to a recovery from CO and H_2S contamination in automotive PEMFC systems, which should be included in discussions on ISO 14687 adaptions. Table 5 lists several relevant studies investigating contamination by CO and H_2S in the fuel, however, further works are available in literature and summarized in the reviews from Shabani et al. [38] and Zamel et al. [39].

Table 5 Publications on CO and H_2S contamination, and effects contributing to a recovery thereof.

Author	Year	Title	Species: conc.	Testing type	Electrodes	Conclusion	Ref.
			[ppm]		[µg/cm²]		
Koski	2022	Dynamic Load Cycle Effects on PEMFC Stack CO Tolerance under Fuel Recirculation and Periodic Purge	CO: 2	Static / dynamic load cycling	An: 50 Pt Ca: ?	Dynamic load cycling decreases impact of CO due to increased CO oxidation rates during high load points.	[101]
Papasavva	2021	Impact of anode catalyst loadings and carbon supports to CO contamination in PEM fuel cells	CO: 0.1 - 0.4	Chronoamp. at 0.1 - 1.7 A/cm²	An: 50 - 100 Pt Ca: 250 Pt	Pt supported on high surface area carbon revealed higher CO tolerance compared to Pt on highly graphitized carbon support.	[21]
Erbach	2018	CO_2 Enrichment in Anode Loop and Correlation with CO Poisoning of Low Pt Anodes in PEM Fuel Cells	CO: 0.05 - 0.1 CO_2: 400 – 800	Chronoamp. at 1 A/cm²	An: 50 Pt Ca: 250 Pt	Accumulation of CO_2 and reverse water gas shift reaction leads to CO in anode loop, with 400 ppm CO_2 comparing to 0.04 ppm CO.	[19]
Matsuda	2016	Adsorption behavior of low concentration carbon monoxide on polymer electrolyte fuel cell anodes for automotive applications	CO: 0.2 - 1.0	Chronoamp. at 1 A/cm²	An: 110 Pt Ca: 300 Pt	Linear and bridge bonded CO covering 60% of anode Pt surfaces, with large excess of oxygen at anode outlet due to oxygen permeation.	[86]
Wang	2016	The effects of hydrogen dilution, carbon monoxide poisoning for a Pt–Ru anode in a proton exchange membrane fuel cell	CO: 50		An: 450 PtRu Ca: 600 Pt	Dilution by N_2 and contamination by CO "magnify their effects" when mixed in H_2.	[28]
Perez	2014	Effect of fuel utilization on the carbon monoxide poisoning dynamics of Polymer Electrolyte Membrane Fuel Cells	CO: 0.18 – 1	Chronoamp. at 1 A/cm²	An: 50 Pt Ca: 400 Pt	Higher fuel utilization leads to increased CO contamination effect, with CO being measured almost immediately at the outlet of the anode.	[15]
Reshetenko	2014	Study of low concentration CO poisoning of Pt anode in a proton exchange membrane fuel cell using spatial electrochemical impedance spectroscopy	CO: 20	Chronoamp. at 0.8 A/cm² Spatially resolved	An: 400 Pt Ca: 400 Pt	CO contamination decreases cell voltage at H_2 inlet, while it increases at the outlet. Recovery from CO occurs mainly with permeate oxygen due to low anode overpotential.	[102]
Hashimasa	2011	PEFC Power Generation Performance Degradation by Hydrogen Sulfide and Ammonia—Effects of Lowering Platinum Loading	H_2S: 0.5 - 2 NH_3: 1 – 5	Chronoamp. at 1 A/cm²	An: 50 - 400 Pt Ca: 400 Pt	Amount of H_2S supplied to cell until voltage breaks down (by 30 mV) proportional to anode loading. Effect of NH3 independent of concentration and anode loading but depends on cathode loading.	[14]
Lopes	2011	The effects of hydrogen sulfide on the polymer electrolyte membrane fuel cell anode catalyst: H_2S--Pt/C interaction products	H_2S: 8	Chronoamp. at 0.65 A/cm² UI curves	An: 400 Pt Ca: 400 Pt	H_2S dissociated on Pt to sulfur, which can be electrochemically oxidized to SO_2 via CV. Air bleeding improves tolerance versus H2S contamination.	[20]
Hashimasa	2010	Effects of Platinum Loading on PEFC Power Generation Performance Deterioration by Carbon Monoxide in Hydrogen Fuel	CO: 1	Chronoamp. at 1 A/cm²	An: 50 - 400 Pt Ca: 400 Pt	Decreasing the anode loading increases the effect of CO contamination, with higher degree of oxidation of CO towards CO_2 for lower loadings.	[41]
Inaba	2008	Impacts of air bleeding on membrane degradation in polymer electrolyte fuel cells	CO: 5 – 150		An: 450 PtRu Ca: 400 Pt	Air-bleeding with negligible effect on PEM degradation up to 2000 h of operation, afterwards degradation increased due to anode catalyst degradation and enhanced H_2O_2 formation.	[24]
Imamura	2007	Effect of sulfur-containing compounds on fuel cell performance	H_2S: 0.5 – 5	Chronoamp. at 1 A/cm²	An: 100 Pt Ca: 400 Pt	No recovery from sulfur poisoning upon operation with neat H_2, but during OCV sulfur reacts back to H_2S and partially recovers cell. Ionomer degradation with sulfur contamination was observed.	[13]
Mohtadi	2003	Effects of Hydrogen Sulfide on the Performance of a PEMFC	H_2S: 50	Potentiostatic at 0.69 and 0.67 V UI curves	(1) An: 450 PtRu Ca: 600 Pt (2) An: 400 Pt Ca: 400 Pt	PtRu does not improve H_2S tolerance, but operation with neat H_2 partially recovers performance. Almost full recovery after sulfur oxidation via anode CV.	[30]

Contaminant testing is often being conducted in single-cells at static load points following the SAE J3219 to improve testing reproducibility, however, realistic automotive drive cycles usually include variable load, start/stop procedures, purging of the anode recirculation loop, reactant starvation events or temperature and humidity excursions, all of which can alleviate from reversible contamination mechanisms [44,103]. To this effect, Koski et al. reported that dynamic drive cycling alleviates from CO contamination as compared to moderate, static load cycling, because fast load cycling periodically elevates the anode potential to levels, where CO is oxidized such that the average performance improves as shown Figure 10 [101].

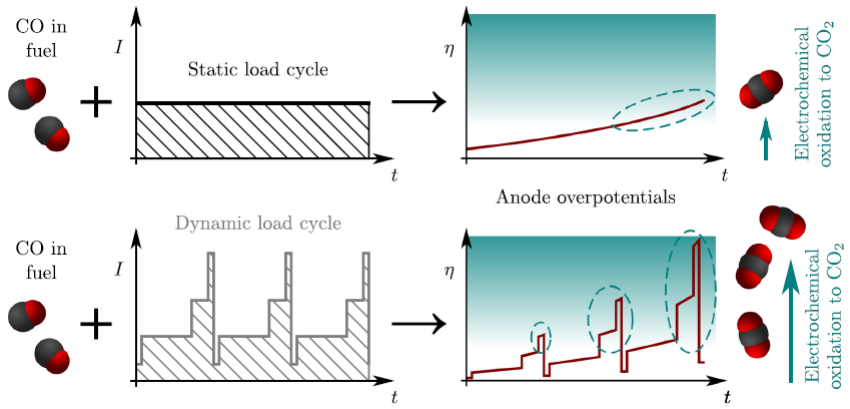

Figure 10 Schematic of the influence of dynamic vs. static load cycling (DLC vs. SLC) on CO fuel contamination, where periodic high anode overpotentials lead to electrochemical oxidation of CO and to higher performance for the DLC at equal average current density, taken from Koski et al. [101].

Such variations in current densities including short excursions to high load and consequently high anode overpotential for a contaminated electrode can help to recover the anode catalyst surfaces from poisons that are oxidized at comparably moderate potentials such as CO. These tests by Koski et al. were conducted with fuel recirculation close to realistic automotive PEMFC systems, where fuel impurities and gases permeating from the cathode, i.e., N_2 or CO_2, eventually accumulate in the loop, dilute H_2 and intensify contamination effects. N_2 is inert, however, at concentrations as high as several dozens of vol.%, it was found to "magnify" the effect of catalyst poisons such as CO due to different gas velocities at equal fuel utilization, and thus influences on PEMFC water management and mechanisms recovering from CO [28]. CO_2 can be of harm, because CO can be formed from CO_2 and H_2 via the reverse water gas shift reaction (RWGS, (4-2)), with CO concentrations as high as 0.04 ppm from 400 ppm CO_2, which is its concentration in air that could permeate from cathode to anode.

$$CO_2 + H_2 \rightarrow CO + H_2O \tag{4-2}$$

To relieve from the accumulation of unwanted species, frequent purges of the anode loop are employed in automotive PEMFC systems, which releases some of the unreacted H_2 into the atmosphere and lowers fuel efficiency, but therefore decreases diluent and contaminant concentrations. Purge

strategies can be based on mathematical models with operating conditions including the H_2 concentration measured by designated sensors and stack performance as input parameters, and the goal to maximize fuel efficiency [104,105]. High fuel utilization, i.e., a low ratio of H_2 supplied to the anode versus H_2 consumed, and low purge rates, can improve fuel efficiency. However, if contaminants such as CO are present, their effect can be magnified since the contaminant partial pressures increase to the anode outlet upon consumption of the H_2, which eventually extends the influence of CO on the current density distribution from H_2 inlet to the outlet [15,102]. Along with PEMFC system operating strategies, the electrode and MEA designs with parameters such as catalyst alloy, ionomer to carbon ratio, catalyst support or ionomer type, membrane thickness and composition, influence the contaminant tolerance, because activity and accessibility of catalyst particles for reactants and contaminants, oxygen permeation and water management, and consequently the coverage of catalysts by contaminants varies [21,85].

For sulfur contamination of the anode electrode, the operating strategy appears to be the main lever to improve the system tolerance. Operation at elevated RH or oxygen content in the anode either stemming from permeation from the cathode or air bleeding alleviates from sulfur poisoning [20], though air bleeding also decreases fuel efficiency and potentially enhances PEM degradation [24]. Supplying neat H_2 to the anode and maintaining OCV can recover from sulfur contamination by reaction of adsorbed sulfur back to H_2S [13], whereas continuous operation with neat H_2 after supply of contaminated fuel appears to be discussed controversial in literature as shown in Figure 11.

a) b)

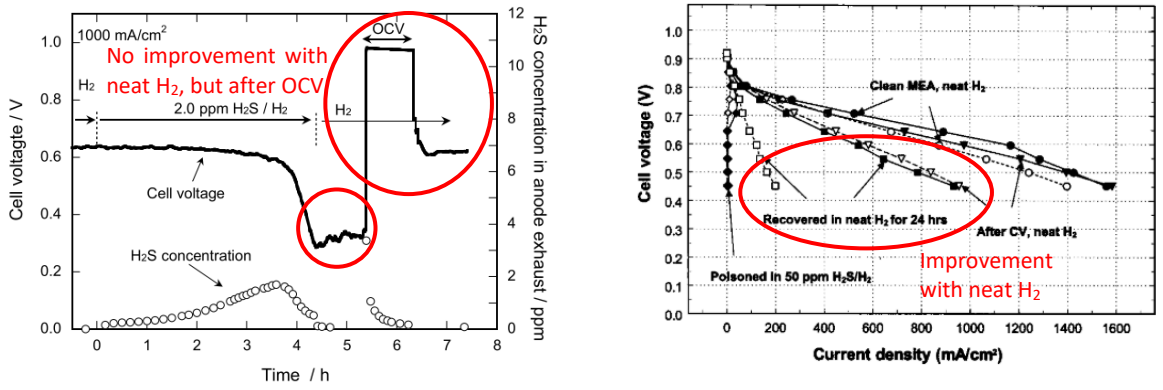

Figure 11 H_2S contamination tests showing a) cell voltage drop due to H_2S, where no (significant) recovery upon introduction of neat H_2 can be seen, but OCV-hold recovered the cell performance, and b) polarization curves of Pt (full symbols, e.g. ♦) and PtRu (open symbols ◊) anode electrodes, each one before and after H_2S contamination, 24 h recovery at 0.67 – 0.69 V potentiostatic operation in neat H_2 and after sulfur oxidation via CV, taken from Imamura et al. [13] and Mohtadi et al. [30].

Imamura et al. reported that the cell performance did not improve upon introduction of neat H_2 during chronoamperometric tests [13], whereas Mohtadi et al. indicated a partial recovery after extended potentiostatic operation visible in the polarization curves, where oxidation of adsorbed sulfur at low reaction rates recovered the contaminated anode electrode [30]. The difference between these studies lies in the significantly longer time for recovery with neat H_2 for the study by Mohtadi et al. (24 vs. ~1 h),

which indicates that a recovery from sulfur contamination during operation generally is possible, but just requires a remarkably long operation time.

Whether the ISO 14687 requires adaption for ultralow anode loadings, should ultimately be based on a larger selection of contamination studies including PEMFC stack tests at various operation strategies coupled with fuel recirculation, to enable testing as close as possible to automotive application. If done so, an outcome could be the recommendation to alleviate impurity limits, such as e.g. reported by Viitakangas et al. for the cases of formic acid (HCOOH) and formaldehyde (HCOH) shown in Figure 12 [106].

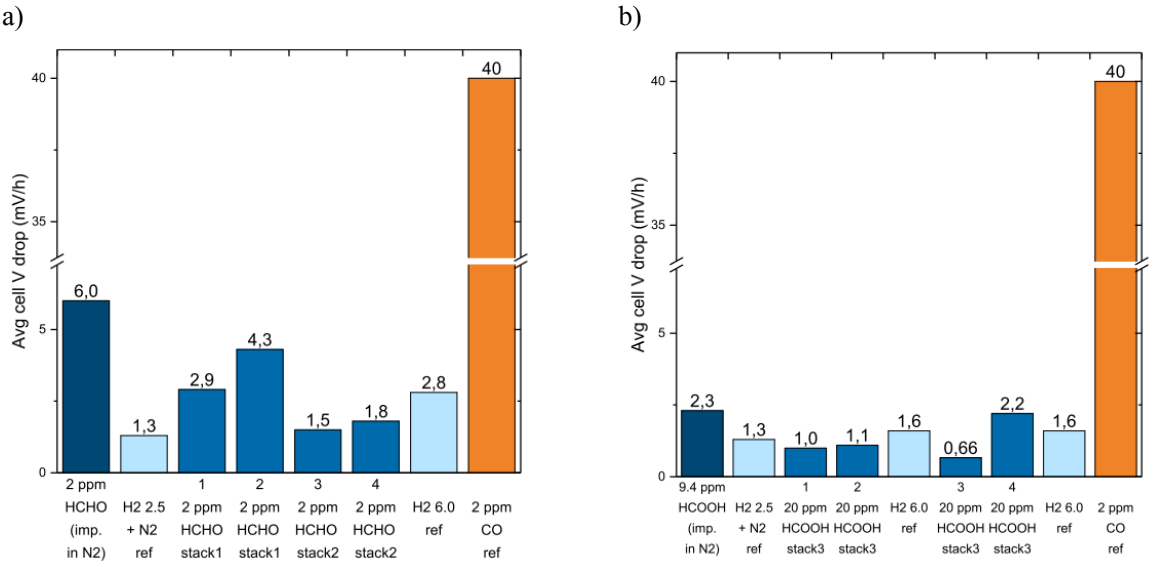

Figure 12 Average cell voltage drops of stacks in chronoamperometric measurements at 0.6 A/cm² upon operation with a) HCOH and b) HCOOH as compared to the voltage drop in neat H_2 and reference measurement with 2 ppm CO, taken from Viitakangas et al. [106].

In ISO 14687, both species HCOH and HCOOH are named separately with comparably low maximum limits of 0.2 ppm. However, the results by Viitakangas et al. acquired with PEMFC stacks, fuel recirculation and high fuel utilization do not support the tight threshold. Even at concentrations 200 and 100 times larger than allowed by the ISO standard for HCOH and HCOOH, respectively, the voltage drops were insignificant and close to the values for reference tests with neat H_2, and a relaxation of the ISO 14687 was recommended. Similarly, the species investigated in this dissertation, CO and H_2S, ultimately require stack tests equipped with MEAs including ultra-low loaded anode electrodes, ideally including fuel recirculation and automotive drive cycling, to decide for adaptions of the ISO 14687.

4.3 Effect of SiO_2 coating on CO and H_2S fuel contamination

A viable alternative to improve the tolerance of PEMFC electrodes and allow for lower anode electrode loadings from the perspective of contamination, is to use alloys that alleviate from specific poisoning effects. Specifically, Pt alloys with oxophilic transition metals, as e.g. Ru or Mo, have shown to improve the tolerance versus CO contamination. On the downside, these alloying elements eventually leach out of

the catalyst particle leaving a Pt enriched shell without the beneficial effect of the alloy, while effects by other impurities such as sulfuric species are not affected by it. An approach that could target both, preventing the catalyst material from dissolution and structural damage, while simultaneously affecting contaminant tolerance, are thin functional coatings on the catalyst particles. Coatings based on silicon oxide (for simplicity referred to as SiO_2, though it exists non-stoichiometric in thin films), oxides of other metals or transition metals, polymers or ceramics have been used as a means to modify catalyst surfaces, also for the application as PEMFCs electrodes [61]. Particularly SiO_2 has received significant attention as a coating on electrocatalysts, where it can be employed to alter the performance at specific operating conditions, or to stabilize the catalyst material versus degradation mechanisms. However, its effect on contamination from impurities in H_2 and air has not been subject to investigations yet, though multiple mechanisms are possible that could contribute to a tolerance enhancement as shown in Figure 13.

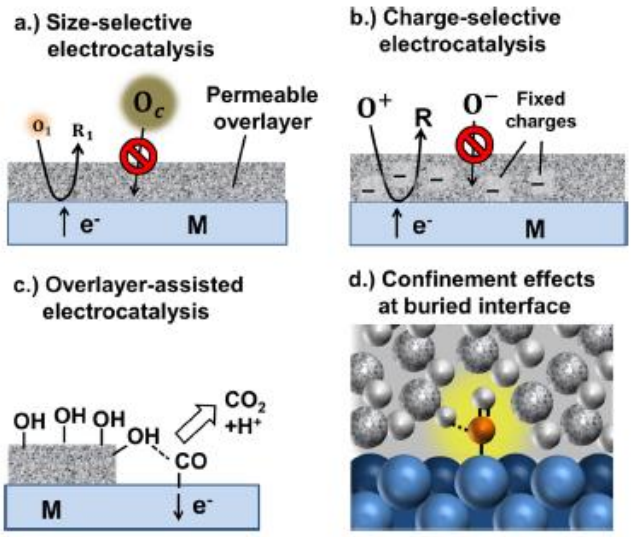

Figure 13. Mechanisms on how functional coatings can affect reaction mechanisms on an active metal (M). Depicted is the reduction of an oxidant species (O_1) to forming the reductant species (R_1). Contamination mechanisms can be affected by a) size-selection and rejection of a competing oxidant species (O_c) with spheres symbolizing hydration spheres, b) charge-selection, c) overlayer-assisted electrocatalysis and d) confinement of a reactant species (here: CO molecule) buried at the interface between metal M and the coating, taken from Esposito [107].

Either the coating (overlayer in Figure 13) selectively enables reactant transport based on differently sized hydration spheres or charges of the species to the catalyst surface (Figure 13 a. and b.), the coating directly participates in reaction steps, e.g. by hydration and provision of OH-groups (Figure 13 c.), or it modifies energy barriers for reactions at the confined interface between coating and electrocatalyst, and alters reaction energetics and pathways (Figure 13 d.) [107]. SiO_2-coatings possibly interact with contaminants via multiple of the proposed mechanisms, and therefore were investigated in this dissertation as a means to alter contaminant tolerance, which is described in the third publication "**Tolerance of silicon oxide coated Pt/C catalyst versus CO and H_2S contamination in hydrogen for PEMFCs**" provided in

chapter 6.3 [108]. The hypothesis that this coating affects contamination mechanisms is supported by the common practice to coat tubes in fluidic engineering applications with SiO_2, e.g. SilcoNert® offered by SilcoTek GmbH, as adsorption barriers against sulfuric species, which in fact gave rise to the idea behind the third publication.

The publication introduces to the fabrication and quality analysis of the SiO_2 coating and compares the results to works in literature and listed in Table 6 [58–66]. The coating is based on the hydrolysis of silicon precursors with subsequent phase separation, drying and calcination, and the final product is used like any other catalyst powder for catalyst ink and electrode fabrication. Each step in this process and the selection of chemicals offer the possibility for variations, but the process and chemicals employed in this dissertation were generally kept as close as possible to the works in literature with the only difference being the amounts of chemicals used, the type of phase separation and the addition of a ball milling step to break down SiO_2-Pt/C agglomerates. The Pt particle size distribution of the SiO_2-Pt/C was found to be comparable to the Pt/C distribution and therefore appears to be unaffected by the coating process. However, in comparison to works in literature, the silicon content was relatively low (~0.6 versus 0.3-40 wt.%), which deposited in clusters in proximity to catalyst particles, whereas thicker and homogeneous layers were reported for most of the reported studies. Whether a complete or selective, thick or a thin SiO_2 coating is preferred depends on its purpose and is part of an ongoing discussion in literature. The former, a thick and complete coating, is expected to be beneficial for durability enhancements because there is a greater chance that vulnerable Pt or carbon surfaces are protected from degradation mechanisms. However, it comes with greater impacts on reactant diffusion through the thicker SiO_2 layer to active catalyst sites. On the other hand, the catalyst surface wettability and therefore water management can be already affected by a thin or inhomogeneous, selective coating, while the impact on reactant diffusion by the coating is kept at a minimum. Contamination mechanisms and a recovery thereof usually depend on the availability of water, e.g. as a prerequisite for the formation of OH-groups required for CO oxidation, or for the dissolution of soluble species, and hence, the fabricated SiO_2-Pt/C with comparably low content and irregular distribution of SiO_2 was used for the anode electrode in the subsequent in-situ tests.

Other than expected, the CV analysis of the SiO_2-Pt/C anode electrode revealed an about 10% larger ECSA as compared to the reference Pt/C throughout the relative humidities (RH) of 40, 70 and 100%, which is attributed to the water retaining effect of SiO_2 and an improved protonic connection to particles otherwise not in contact to the ionomer. This effect is noticeable in polarization curves in neat H_2 at 40, 70 and 100% RH, showing an about 1 – 3% lower high frequency resistance (HFR) and a marginally better performance for the SiO_2-Pt/C. Upon operation with 1 ppm CO in the fuel, the performance of the SiO_2-Pt/C MEAs was worse at high RH (70 and 100%), and almost comparable at low RH (40%) conditions, suggesting a negative influence of the SiO_2 coating on the CO tolerance. This was not expected because, first, the SiO_2-Pt/C showed higher ECSA from H_{UPD} and therefore should provide a higher nominal catalyst surface area at similar catalyst loadings, and second, the water retention by the SiO_2 should help with the recovery from CO contamination. CO stripping measurements though revealed an elevated onset for CO oxidation on the SiO_2-Pt/C, which increased with higher RH, and which can be associated either to a hindrance of formation of OH-groups from water, a lower OH-mobility on or in proximity to the SiO_2, or a stronger bond between CO and Pt. For the SiO_2-Pt/C MEAs, this essentially indicates a lower CO tolerance and explains the observed worse performance with CO in H_2. For low RH conditions, both effects, water

retention and CO tolerance reduction, counter each other such that SiO_2-Pt/C and Pt/C MEAs show similar performance.

In contrast, the SiO_2-Pt/C revealed an about 20% extended durability in chronoamperometric tests until the voltage break down was observed upon operation with 75 ppb H_2S in the fuel. Similar to CO, sulfur contamination strongly depends on the availability of water in the electrode, although the reason lies less so in the provision of water for electrooxidation with OH-groups, but more so in the dissolution of already oxidized sulfur species and the transport from the electrode surfaces [110,111]. Electrooxidation of adsorbed sulfur on Pt requires potentials between 0.8 – 1.1 V and therefore is not expected to commence at the low anode potential at a sufficient rate. Nevertheless, at low rates, oxidation of sulfuric species can still occur, and when there are higher water contents in the SiO_2-Pt/C electrode, the dissolution and transport from the electrode are enhanced. In addition, Bounechada et al. reported that the mobility of oxidized sulfuric species on SiO_2 surfaces was considerable [112], which could further add to the explanation for the extended durability versus H_2S contamination by the SiO_2 coating.

Overall, the SiO_2-Pt/C employed as anode catalyst in this work was found to negatively influence the CO tolerance, but positively the HFR and H_2S tolerance, which is attributed to its water retaining character and its possible effect on the mobility of oxidized sulfur species. Compared to the literature works listed in Table 6, these findings are to some extend controversial, because several studies reported beneficial effects of SiO_2 towards (electro-)oxidation of CO on Pt, while others showed a shift towards higher oxidation potentials in CO stripping measurements, i.e. negative effects, without further discussing this observation. Note: the listed studies employ the terms SiO_2, SiOx, silica or silicon oxide to refer to the same material. SiO_2 applied as thin films on complex surfaces forms non-stoichiometric structures, and hence, SiOx, silica or silicon oxide would be the more correct terms, but most studies used SiO_2 to describe the coating material and therefore this term is used throughout the following section.

Table 6 Publications on SiOx serving as coating, additive or support in electrocatalysis.

Author	Year	Publication	Coating method	Catalyst	Si-content / thickness	Conclusion	Ref.
					[wt.%] / [nm]		
Park	2021	Influence of Cathode Catalyst Layer with SiO_2-Coated Pt/Ketjen Black Catalysts on Performance for Polymer Electrolyte	Sol-gel	Pt/C		SiOx coated catalyst maintained good dispersion over time in catalyst ink and showed higher porosity and pore sizes in electrode. Performance was worse at high RH attributed to pores blocked by SiOx, while performance at low RH improved.	[65]
Archeampong	2020	An Organosilane-Based Fuel Cell Ionomer that Mitigates Carbon Corrosion	Sol-gel	Pt/C	40 / NA	Electrode made with organosilicate based ionomer instead of PFSA improved stability in ASTs by suppression of catalyst dissolution, agglomeration, carbon corrosion.	[113]
Park	2019	Improvement of cell performance in catalyst layers with silica-coated Pt/carbon catalysts for polymer electrolyte fuel cells	Sol-gel	Pt/C	12.5 - 23 / NA	SiOx coating inherited protonic conduction of PFSA in electrode. Performance was worse at high RH attributed to water retention, while performance at low RH improved.	[64]
Robinson	2018	Silicon Oxide-Encapsulated Platinum Thin Films as Highly Active Electrocatalysts for Carbon Monoxide and Methanol Oxidation	Spin coating UV conv.	Pt/Ti/Si wafer	NA / 2.4 - 5.4	Higher SiOx layer thicknesses revealed lower CO oxidation potentials during CO stripping, which is attributed to CO oxidation with silanol-groups on coating surfaces. SiOx coated Pt showed improved alcohol oxidation rates.	[114]
Labrador	2018	Hydrogen Evolution at the Buried Interface between Pt Thin Films and Silicon Oxide Nanomembranes	Spin coating UV conv.	Pt/Ti/Si wafer	NA / 9.5 - 107	Hydrogen evolution reaction (HER) not hindered by SiOx coating, while coating served as a barrier against Cu^{2+} ions used as model poison.	[115]
Yu	2018	SiO_2 decoration dramatically enhanced the stability of PtRu electrocatalysts with undetectable deterioration in FC performance	Sol-gel	Pt/C	NA / 2	SiOx improved stability and maintained good CO tolerance of PtRu catalyst upon potential cycling. CO stripping though revealed a shift in oxidation potential towards higher values with coating.	[63]
Aoki	2018	Durability Improvement of Pd Core-Pt Shell Structured Catalyst by Porous SiO_2 Coating	Sol-gel	PtRu/C	17 - 33 / NA	Coating made from MPTES compared to APTES selectively coated catalyst particles, which improved suppression of agglomeration and mitigated ECSA decay in ASTs.	[59]
Fujii	2015	Performance and durability of Pd-C catalyst covered with SiO_2 layers in PEMFCs	Sol-gel	Pt/C PtRu/C	40 / 5	Improved durability upon potential cycling because coating prevented dissolution and diffusion of Pd species. SiOx coated catalyst showed better performance at initial state, eventually owing to protection from adsorption of sulfonic acid groups on catalyst.	[58]
Takenaka	2013	Catalytic activity of highly durable Pt/CNT catalysts covered with hydrophobic silica layers for the oxygen reduction reaction in PEFCs	Sol-gel	Pt/CNT	10 - 11 / 1 - 3	SiOx coating made from MTEOS is more hydrophobic due to incorporated methyl groups, and shows larger pores as compared to coating made from TEOS. Durability in AST improved with SiOx for both coating types.	[66]
Velan	2011	Effect of SiO_2 additives on the PEM fuel cell electrode performance	Silica added as particles to electrode	Pt/C + Silica		SiOx particles added to the anode electrode improved performance with increasing concentration, Addition to the cathode decreased performance at high RH. Addition to both electrodes showed improvement in performance at low RH conditions.	[116]
Takenaka	2011	Highly durable carbon nanotube supported Pd catalysts covered with silica layers for the oxygen reduction reaction	Sol-gel	Pt/CNT	20 / NA	ORR activity unaffected by coating but coating improved durability during AST. SiOx layer promoted four-electron instead of two-electron oxygen reduction. CO stripping revealed slightly higher CO oxidation potentials for SiOx coated catalyst.	[60]
Su	2010	Self-humidification of a PEMFC using a novel Pt/SiO_2/C anode catalyst	Sol-gel	Pt/C	0.3 - 3 / NA	SiOx coated anode catalyst eliminated the need for external humidification due to hydrophilic character of coating and improved water retention.	[109]
Takenaka	2008	Preparation of C nanotube-supported metal nanoparticles coated with silica layers	Sol-gel	Pt/CNT	26.3 - 47.4 / 2 - 15	SiOx coating thickness controllable by TEOS concentration. Coating improved catalyst particle resistance vs. sintering, but no prevention of adsorption of CO on catalyst.	[62]
Fukuoka	2007	Preferential Oxidation of Carbon Monoxide Catalyzed by Platinum Nanoparticles in Mesoporous Silica	Sol-gel (Pt growth in silica)	Pt/Si		Pt supported on mesoporus silica improved CO oxidation due to support oxygen in silica lattice participating in reaction.	[117]

Preferential oxidation (PROX) of CO on catalyst materials is a commonly employed process to purify H_2 rich product streams from CO [118]. In this context, Pt nanoparticles confined in mesoporous silica (SiOx) structures were found to show exceptional activity and selectivity for CO PROX, because oxygen incorporated in the silica structure, but also surface silanol-groups within the SiOx-mesopores partake in CO oxidation [117]. PROX of CO on a catalyst is a chemical process excluding the influence of an electrolyte and, hence, an alkaline or acidic environment. However, also for electrochemical processes on catalysts in acidic media, SiO_2-coatings were found to ease from contamination effects by CO, but also from metal ions such as Cu^{2+} as shown in Figure 15.

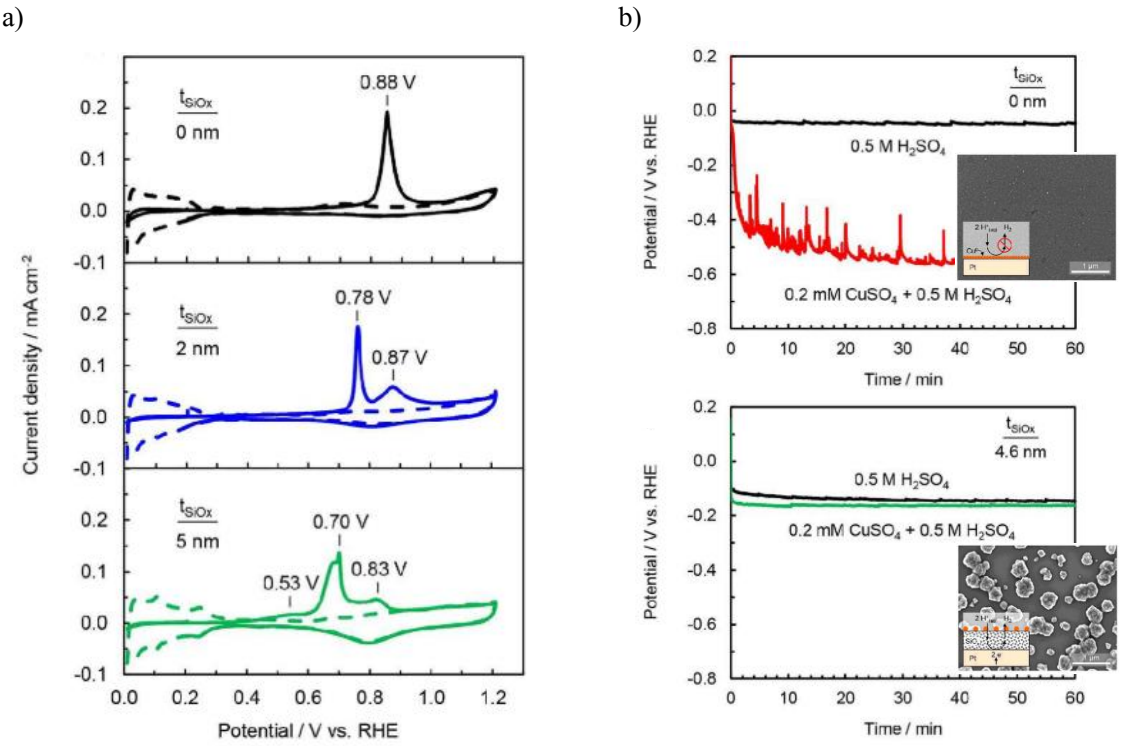

Figure 14 Investigations on Pt and Ti thin films supported on a Si-wafer and coated with SiO_2 of thickness t_{SiOx}, a) CO stripping measurements showing the shift in CO oxidation towards lower potentials for thicker SiO_2-coatings, and b) HER rate at -5 mA/cm² with and without copper sulfate ($CuSO_4$) forming Cu^{2+} in aqueous solution as model contaminant, with SEM images of catalyst surfaces showing contaminant deposition after testing, taken from Robinson et al. [114] and Labrador et al. [115].

Robinson et al. investigated the effect of SiO_2-coatings on Pt towards the oxidation of CO and methanol, and found that the coating improved activity and selectivity of the catalyst visible in the shift in CO oxidation towards lower potentials (Figure 14 a) [114]. They attributed this shift to silanol-groups forming on the SiO_2 (SiOx), which react with CO or methanol oxidation intermediates adsorbed on Pt.

$$SiO_x + H_2O \rightarrow SiO_x - OH + H^+ + e^- \tag{4-3}$$

$$Pt - CO + SiO_x - OH \rightarrow Pt + SiO_x + CO_2 + H^+ + e^- \quad (4\text{-}4)$$

In addition, the same group of researchers also investigated the effect of the coating on hydrogen evolution reaction (HER) in presence of copper ions (Cu^{2+}) used as model species to simulate the poisoning of an electrode surface by metal contaminants (Figure 14 b) [115]. The SiO_2-coating acted as a barrier for the Cu^{2+} ions visible in the similar potentials with and without Cu^{2+} for the coated Pt, whereas the potential decreased for the non-coated catalyst. The authors associated this to the different sizes of the hydrated ions of 2.82 Å vs. 4.19 Å for H^+ and Cu^{2+}, respectively. Interestingly, the Cu^{2+} deposited in clusters on the SiO_2 instead of forming a homogeneous layer, thereby leaving sufficient coating surfaces free for the transport of H_2/H^+ to and from the buried catalyst. For these studies, the main reason for the observed beneficial effects by the SiO_2 coating could be attributed to the fabrication procedure, which appears to result in well-defined catalyst and coating layers. Robinson et al. and Labrador et al. coated a Si-wafer with thin films of Ti and Pt, acting as support layer and catalyst, respectively, and finally a silicon precursor (trimethylsiloxy-terminated polydime-thylsiloxane, PDMS), which was applied in different thicknesses and converted to SiO_2 via ultraviolet (UV) ozone treatment.

These works generally demonstrate that SiO_2 used as catalyst support or coating can exhibit beneficial effects towards CO and metal ion contamination, but the fabrication method and testing setup appear to dictate the outcome. Coating catalyst powders requires a different procedure such as the sol-gel process, where a powder is coated via hydrolysis in a dispersion of solvents and silicon precursors with subsequent drying. This sol-gel process was employed for all studies investigating SiO_2-coated catalyst powders used for H_2 and air PEMFC electrodes [58–66]. Within few of these studies, CO stripping was conducted, and the CO oxidation peak usually showed a shift towards higher potentials as shown in Figure 15, indicating a negative influence of the SiO_2-coating on CO tolerance in contrast to the work by Robinson et al.

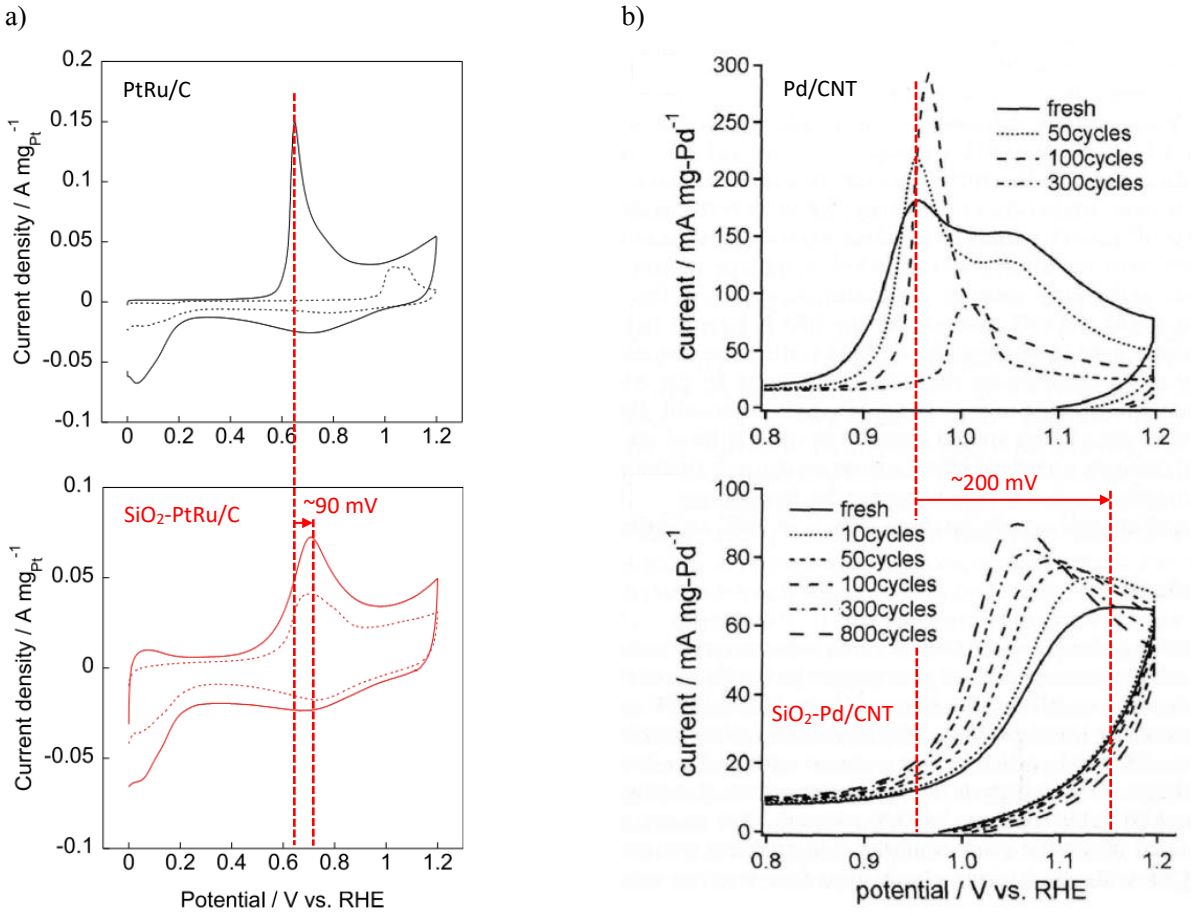

Figure 15 CO stripping measurements showing the 90 and 200 mV shifts in CO oxidation towards higher potentials and stability enhancing effect (solid lines for fresh catalyst, dashed lines for degraded) for SiO_2-coated catalyst materials, taken from a) Yu et al. for a PtRu/C catalyst evaluated per RDE in 0.5 M H_2SO_4 [63], and b) Takenaka et al. for a Pd/CNT catalyst also evaluated per RDE in 0.1 $HClO_4$ [60].

Both, the study by Yu et al. [63] and Takenaka et al. [60], reported the stability enhancing effect of the SiO_2-coating with CO stripping measurements as characterization method, where the smaller shift in CO oxidation potential indicates the improved stability of the SiO_2-coated catalyst. When comparing the CO oxidation potentials of coated vs. uncoated PtRu and Pd catalysts before the cycling (solid lines in all CVs shown in Figure 15), a shift towards higher potentials with the coating can be seen. This is in line with the results of this dissertation, and several reasons could explain this different behaviour as compared to the studies by Robinson and Labrador et al. First, the fabrication method affects the catalyst powder in such a way, that it undergoes noteworthy structural changes with the hydrolysis and calcination, which possibly affects catalyst facets, surface compositions and in consequence the formation of the electrode structure with the ionomer. Second, the homogeneity of the SiO_2-clusters or layers plays a role, i.e. SiO_2 rather forms clusters or inhomogeneous, thick layers on the carbon supported catalyst as compared to homogeneous layers on Pt/Ti/Si wafers. Thick SiO_2 clusters could partially block catalysts on carbon and reduce the ECSA, though this explanation is countered by the higher ECSA and approximately similar CO

oxidation currents evaluated for the SiO_2-Pt/C in this dissertation. Third, SiO_2 influences reaction oxidation mechanisms of CO on Pt by interaction with oxygen species, possibly hindering mobility or formation of OH groups on Pt, or in addition, a spillover of CO adsorbed on the SiO_2 onto the Pt catalyst.

In contrast, the PEMFC sulfur tolerance increased with the coating, which can be attributed to both, the water content in the anode electrode affecting sulfur contamination mechanisms, as well as interactions of sulfur species with the SiO_2 as exemplarily shown in Figure 16.

a) b)

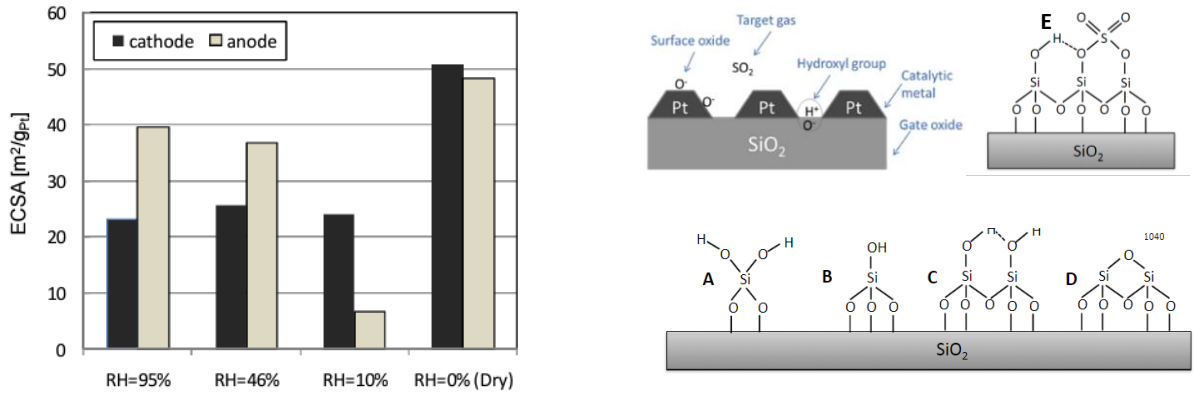

Figure 16 Influences of water and SiO_2 on contamination by sulfur species, a) ECSA of anode and cathode electrodes after exposure of the cathode to SO_2 at different relative humidities, taken from Tsushima et al. [111], and b) schematic cross-section of the Pt catalyst supported on SiO_2, and representation of terminal silanol groups (A-C), siloxane (D) and surface sulfate groups (E) on SiO_2, taken from Bounechada et al. [112].

Several studies reported the influence water has on sulfur contamination irrespective of the species (H_2S, SO_2 or COS), as e.g. reported by Tsushima et al. [111] for SO_2 introduced to the cathode electrode at varying relative humidities. In the PEMFC environment, sulfur species can react with water to soluble species and/or diffuse between electrodes, such that the electrode opposing the point of introduction is eventually affected. For SO_2 introduced to the cathode, the cathode ECSA was found to decrease by similar nominal values (~24 m^2/g_{Pt}) for all RH values, whereas the anode ECSA decreased to greater extends with the decrease in humidity (Figure 16 a). If water is lacking (0% RH), no drop in ECSA was visible, suggesting that residual water in the MEA is required to forming HSO_3^- or SO_3^- ions with sulfur contamination, that can adsorb and poison the catalyst. The SiO_2-Pt/C in the anode supports water retention and consequently, influences on sulfur contamination by retained water are likely [109]. In addition, direct interactions between sulfur species and the coating are possible as reported by Bounechada et al. [112]. The authors investigated the adsorption and interaction of SO_2 on Pt supported on SiO_2 (schematically shown in Figure 16 b) and found that oxidized sulfuric species, specifically SO_3, are withdrawn from Pt surfaces to forming sulfate species by removal and rearrangement of silanol groups. Hence, a spillover of sulfuric species from Pt sites onto the SiO_2-coating is possible that could further improve sulfur tolerance of the PEMFC anode electrode.

Based on these results, catalyst coatings used in PEMFCs should be evaluated from various perspectives, i.e. whether the performance in neat or contaminated reactants, the degradation mechanisms, and also the handling of the materials is altered, before coatings are applied in larger scales in stacks or systems. If these metrics are optimized, the subsequent step would be an upscaling of the coating process, and a minimization of the losses of expensive catalyst material throughout the process steps.

5 Conclusions and outlook

This dissertation deals with fuel contamination being one of the obstacles towards *ultra-low-loaded anode electrodes* as targeted for 2025 (and beyond) by the DOE for automotive PEMFCs on grounds of cost calculations. Lowering catalyst loadings in both anode and cathode electrodes generally decreases the tolerance towards impurities in fuel and air, however, this does not necessarily exclude low loadings from implementation. The contaminant tolerance ultimately depends on the interplay between the MEA design, i.e. ECSA, catalyst composition, PEM diffusivity and selection of GDL, and the operating strategy including measures to recover from fuel and air contaminants. For optimization of the cost, performance and durability, new MEA designs require extensive in-situ testing aiming on evaluation of contamination tolerance next to material stability, and in this context, this dissertation investigates the effect of CO and H_2S in fuel on PEMFCs with ultra-low-loaded anodes.

First of all, for low-loaded electrodes, whether they are the anode or cathode, specific in-situ characterization methods can be challenging. Particularly CV analysis requires knowledge of limitations or artifacts, and of measures to counter these. One of such artifacts can occur during the cathodic transient of CV analysis of low-loaded electrodes, when crossover hydrogen accumulated in the working electrode spontaneously oxidizes, and the oxidation peak overlapping Pt oxide reduction currents eventually diminishes the validity of the CV measurement. This artifact is considered of interest for the research community, particularly in light of the targeted loading reductions for both, anode and cathode electrodes, for which such artifacts are expected to be observed more often in the future.

Operating PEMFCs with ultra-low-loaded anode electrodes (<25 $\mu g_{Pt}/cm^2$) and CO contaminated fuel at concentrations at or close to the levels allowed as per H_2 quality standard ISO 14687, results in severe and unacceptable voltage losses, which indicates the need to either significantly improve the tolerance of the anode catalyst, or to lower the concentration limit for CO in the fuel. Similarly, H_2S in the fuel at concentrations as per ISO 14687 shortens the durability until voltage break downs are observed, however, the break downs occur after dozens of hours even for the lowest anode loading (15 $\mu g_{Pt}/cm^2$) investigated, while shut-down and start-up events recover part of the poisoned ECSA. Automotive PEMFC systems, providing a certain capability for self-recovery from contamination depending on operating strategy [44,103], eventually can withstand such H_2S concentrations, though this would require confirmation by experiments closer to realistic application, e.g. via (short-)stack testing including H_2 recirculation and load cycling simulating practical application.

An interesting approach to stabilize electrocatalysts versus degradation mechanisms are functional coatings, and naturally the question arises, whether such coatings also affect the tolerance versus contaminants. In this dissertation, a relatively common coating made from SiO_2 was employed on the Pt/C in the anode electrode, but the results on CO and H_2S tolerance are controversial. The SiO_2 coating negatively influenced the CO, but positively the H_2S tolerance, which is attributed to its water retaining character and a possible effect of the SiO_2 on the mobility of oxidized sulfur species. CO stripping measurements revealed elevated onsets for CO oxidation on the SiO_2-Pt/C, indicating a higher CO coverage during operation in contaminated H_2, and consequently a worse performance. Selecting the appropriate materials and coating method could potentially deliver a coated electrocatalyst with both, improved stability and tolerance at once, which could support the development towards low and ultra-low-

loaded electrodes in PEMFCs. Nevertheless, a more facile way to achieve comparable results in terms of water retention can be achieved by simply adding silica powder to the electrodes [116], though the effects on electrode stability and contaminant tolerance are unknown and could be investigated in future works.

In summary, from a performance perspective, *ultra-low-loaded anode electrodes* appear to be a viable option, if the effects of contamination or the loss of the anode electrode due to fuel starvation are minimized or even eliminated. During the course of this dissertation, though, business strategies of original equipment manufacturers shifted towards the implementation of PEMFC systems in heavy duty instead of passenger vehicle applications, where durability and efficiency are more important than system cost. Cutting the system cost by implementation of low or ultra-low-loaded electrodes therefore appears to have lost in importance in short-term, but plays a role in medium to long-term developments.

6 Publications

The publications including the results of this dissertation are reproduced in the following.

6.1 Hydrogen oxidation artifact during Platinum oxide reduction in cyclic voltammetry analysis of low-loaded PEMFC electrodes

Sebastian Prass, Jean St-Pierre, Matthias Klingele, Kaspar Andreas Friedrich, Nada Zamel

Electrocatalysis, 12 (1), 45-55 (2020)
Special Issue Proton Exchange Membrane Fuel Cells (PEMFCs)
https://doi.org/10.1007/s12678-020-00627-6

Electrocatalysis
https://doi.org/10.1007/s12678-020-00627-6

ORIGINAL RESEARCH

Hydrogen Oxidation Artifact During Platinum Oxide Reduction in Cyclic Voltammetry Analysis of Low-Loaded PEMFC Electrodes

S. Prass[1] · J. St-Pierre[2] · M. Klingele[1] · K. A. Friedrich[3,4] · N. Zamel[1]

Accepted: 12 October 2020

Abstract
An artifact appearing during the cathodic transient of cyclic voltammograms (CVs) of low-loaded platinum on carbon (Pt/C) electrodes in proton exchange membrane fuel cells (PEMFCs) was examined. The artifact appears as an oxidation peak overlapping the reduction peak associated to the reduction of platinum oxide (PtOx). By varying the nitrogen (N_2) purge in the working electrode (WE), gas pressures in working and counter electrode, upper potential limits and scan rates of the CVs, the artifact magnitude and potential window could be manipulated. From the results, the artifact is assigned to crossover hydrogen (H_{2X}) accumulating in the WE, once the electrode is passivated towards hydrogen oxidation reaction (HOR) due to PtOx coverage. During the cathodic CV transient, PtOx is reduced and HOR spontaneously occurs with the accumulated H_{2X}, resulting in the overlap of the PtOx reduction with the oxidation peak. This feature is expected to occur predominantly in CV analysis of low-loaded electrodes made of catalyst material, whose oxide is inactive towards HOR. Further, it is only measurable while the N_2 purge of the WE is switched off during the CV measurement. For higher loaded electrodes, the artifact is not observed as the electrocatalysts are not fully inactivated towards HOR due to incomplete oxide coverage, and/or the currents associated with the oxide reduction are much larger than the spontaneous HOR of accumulated H_{2X}. However, owing to the forecasted reduction in noble metal loadings of catalyst in PEMFCs, this artifact is expected to be observed more often in the future.

Keywords Cyclic voltammetry · Oxidation artifact · Platinum electrode · Low loading · Hydrogen crossover

Introduction

Cyclic voltammetry (CV) analysis is a widely used technique to examine the electrochemical active surface area (ECSA) of proton exchange membrane fuel cell (PEMFC) electrodes [1]. During CVs, currents associated to adsorption limited electron-transfer reactions on the catalyst surfaces are measured as a response to potential scans. The ECSA is then determined either from the electrical charges transferred during the under-potential deposition of hydrogen (H_{UPD}) or from the charges associated to the oxidation of adsorbed carbon monoxide (CO) referred to as CO-stripping [2, 3]. The former is conducted in an atmosphere of hydrogen (H_2) and nitrogen (N_2) in the counter and working electrode (WE), respectively, while the latter requires a CO adlayer adsorbed on the electrocatalyst in the WE prior to the actual CV. For alloyed electrocatalysts and/or supports, CO-stripping or a combination of both methods is preferable, as the charge transfer reactions and therefore CV profiles often are affected by the added alloy elements [4–6]. In contrast, for pure polycrystalline platinum supported on carbon (Pt/C), ECSA determination via H_{UPD} often is considered sufficient as it eliminates the provision of an additional CO/N_2 gas mixture required for CO-stripping. For Pt/C electrocatalysts, the basic reactions during H_{UPD} are the adsorption/desorption of atomic hydrogen (H) and the oxidation/reduction of platinum (Pt) and its oxide (PtOx), respectively, as shown in Fig. 1a.

From these CV profiles, the ECSA is determined via integration of the H-adsorption and/or H-desorption currents

✉ S. Prass
sebastian.prass@ise.fraunhofer.de

[1] Fraunhofer Institute for Solar Energy Systems ISE, Heidenhofstr. 2, 79114 Freiburg, Germany

[2] Hawaii Natural Energy Institute, University of Hawaii, Manoa, 1680 East-West Road, POST 109, Honolulu, HI 96822, USA

[3] Institute of Engineering Thermodynamics, German Aerospace Center, Pfaffenwaldring 38-40, 70569 Stuttgart, Germany

[4] Institute of Building Energetics, Thermal Engineering and Energy Storage (IGTE), University of Stuttgart, Pfaffenwaldring 31, 70569 Stuttgart, Germany

Published online: 31 October 2020

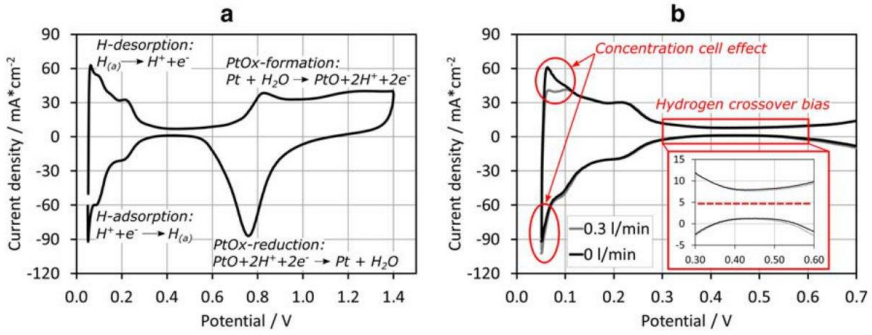

Fig. 1 Typical CV profile of a Pt/C electrocatalyst (**a**) and its artifacts such as the "concentration cell effect" and "hydrogen crossover bias" (here: ~ 5 mA/cm^2 as shown in the inset) (**b**). The formation and reduction of PtOx is presented figuratively by the reactions including PtO; however, further oxide species such as PtOH or PtO_2 are present depending on the upper potential sweep limit and catalyst material. Scan rate: 100 mV/s; N_2 purge: 0 and 0.3 l/min; p_{an}/p_{ca}: 50/50 mbar

(between ~ 0.08 and 0.4 V) by subtraction of the charge transfer associated to the double-layer charging (typically between 0.3 and 0.6 V) [3]. In contrast, the currents associated to formation (anodic transient, above 0.7 V) and reduction of PtOx (cathodic transient, between 0.5 and 1 V) are of interest, if the reversibility of structural and chemical changes in the catalyst [6–11] or support surfaces [12] or the presence of impurities on these surfaces [13, 14] are to be examined. These oxide formation and reduction processes are more complex as H-adsorption/desorption, as they often include the ad- or desorption of water, subsequent multi-step electron transfer reactions via hydroxide formation, and different oxidation states of the catalyst depending on the potential range [15–19].

As several research groups have already reported, artifacts during CV measurements distort the CV profiles and thereby affect extracted information such as the ECSA [20, 21]. One of these artifacts is the "concentration cell effect" shown in Fig. 1b, caused by the superposition of molecular H_2 evolution current, which depends on the partial H_2 pressure in the WE, and currents from H-adsorption/desorption [22]. With higher N_2 flowrates, molecular H_2 is purged from the WE, the partial H_2 pressure decreases, and more H_2 evolves in the WE showing as increased negative currents in CV profiles below 0.1 V. Another artifact arises due to molecular H_2 crossing over through the membrane to the WE (H_{2X}), where it readily oxidizes at potentials above 0.1 V, generating a bias current that shifts the center of the CV profile away from the *x*-axis (e.g., 5 mA/cm^2 in Fig. 1b).

In addition to these two well-known phenomena, we observed another artifact during CV analysis of low- and ultra-low-loaded electrodes during the cathodic scan at potentials between 0.6 and 0.8 V, which is shown in Fig. 2. The artifact is visible as a positive oxidation peak where the negative PtOx reduction peak would be expected, which is more pronounced for lower Pt loadings in the electrode (Fig. 2b). Understanding this type of artifact is particularly important as low-loaded electrodes (loadings ≤ 100 μg/cm^2 of an electrocatalyst) are increasingly employed especially in the anode electrode of automotive catalyst-coated membranes (CCMs) [23]. Platinum loadings of 50 μg/cm^2 are already often considered state-of-the-art, with even lower (ultra-low) loadings forecasted for the near future. Although the majority of studies in literature focuses on the cathode electrode including higher catalyst loadings and its decay during accelerated stress tests (ASTs), the anode electrode is of interest especially when investigating the effect of startup/shutdown cycles [24] or impurities [25, 26] on the anode compartment, or the cell reversal tolerance upon freeze start-ups and successional reversal effects [27, 28]. Therefore, thorough understanding of CVs of low- and ultra-low-loaded electrodes is of great interest.

In literature, few comparable oxidation peaks during the reverse (cathodic) scan of CVs have been reported. Tahmasebi et al. [29] investigated electrocatalytic reactions occurring on a Pt wire acting in an all-glass electrochemical cell under atmospheres saturated with N_2, oxygen (O_2), or H_2 and found this oxidation peak during the cathodic scan, once the setup and electrode was saturated with H_2. They associated this peak to an "increased catalytic activity" towards H_2 oxidation reaction (HOR), which indicates the necessity of H_2 to be present for the artifact to occur. For PEMFCs operating with alcohols such as methanol (MeOH), Zhao et al. [30] discussed a comparable oxidation peak during the cathodic scan regularly observed for MeOH-PEMFCs [31–33], as there exist two theories on its origin. The older theory associates this peak to the oxidation of CO forming inevitably during the reaction of MeOH on electrocatalysts, while the newer theory demonstrates that the peak is caused by MeOH reacting on freshly formed sites after the reduction of the catalyst oxides during the cathodic CV transient. For PEMFCs operated with H_2 and O_2/air (H_2 and N_2 during CVs), to the best of our

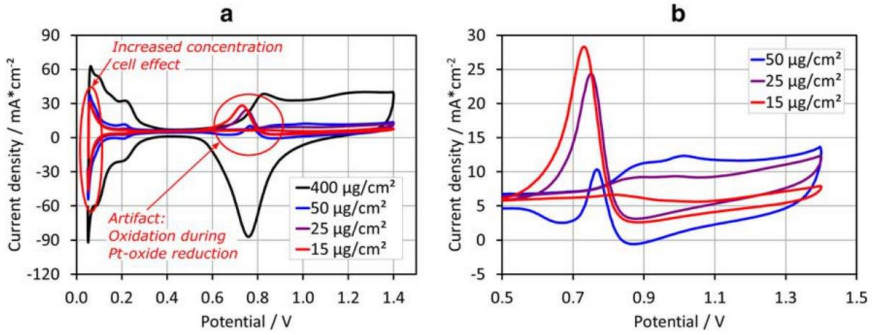

Fig. 2 CVs of a high-loaded electrode (400 µg/cm^2) versus CVs of low and ultra-low-loaded electrodes (50, 25, and 15 µg/cm^2) in comparison (**a**). For the low-loaded electrodes, the concentration cell effect appears increased in comparison to currents associated to H-adsorption and H-desorption, and additionally the artifact peak shows where the PtOx reduction is expected during the cathodic scan (**b**). Scan rate: 100 mV/s; N_2 purge: 0 l/min; p_{an}/p_{ca}: 50/50 mbar

knowledge, this oxidation peak during the cathodic transient has not yet been reported in literature.

The intuitive assumption that this artifact could originate from the oxidation of carbon surface species such as carbon oxides formed on the support of catalyst particles, is comprehensible. Carbon surface oxides, which are regarded as reaction intermediates during the carbon corrosion process, can form at elevated potentials depending on the type and surface defect density of the carbon support and the presence of catalyst material [34–39]. Maass et al. [37] characterized five distinct carbon corrosion processes in different potential regimes, of which three processes could be linked to the artifact described in our study as they eventually occur at elevated potentials during potentiodynamic measurements. At potentials above 0.207 V vs. RHE, carbon oxidation to carbon dioxide (CO_2) generally takes place either directly according to reaction (1) or indirectly with carbon surface oxides (O_{ad}) forming as intermediate species according to reactions (2) and (3), respectively.

$$C + 2H_2O \rightarrow CO_2 + 4H^+ + 4e^- \quad (1)$$

$$C + H_2O \rightarrow C{-}O_{ad} + 2H^+ + 2e^- \quad (2)$$

$$C{-}O_{ad} + H_2O \rightarrow CO_2 + 2H^+ + 2e^- \quad (3)$$

Moreover, carbon monoxide (CO) can form at potentials above 0.518 V vs. RHE according to reaction (4).

$$C + H_2O \rightarrow CO + 2H^+ + 2e^- \quad (4)$$

Luckily the reaction kinetics of carbon oxidation are sluggish at potentials below ~ 0.9–1 V enabling the use of carbon as catalyst support material for PEMFCs [40]. At higher potentials and especially in presence of Pt, the reaction kinetics significantly increase, which results in significant corrosion rates and the loss of carbon support material [34, 38]. If O_{ad} or CO species formed via reactions (2) and (4) and remained stable long enough even at elevated potentials during potentiodynamic cycling, these species could oxidize with hydroxyl groups on Pt surfaces stemming from the reduction of PtOx according to reaction (5), which could result in the artifact peak in the potential window of ~ 0.6–0.8 V.

$$C{-}O_{ad} + Pt{-}OH_{ad} \rightarrow Pt + CO_2 + H^+ + e^- \quad (5)$$

Carbon oxidation is expected to proceed to a certain degree during elevated potential cycling of Pt/C electrodes. Consequently, some carbon oxide species could form and be available for oxidation during the reduction of PtOx causing the artifact peak. Another alternative explanation could be linked to the study by Yamashita et al. [41]. The authors investigated carbon corrosion mechanisms during shut-down and start-up procedures while varying the atmosphere in the WE and formulated three different carbon corrosion mechanisms correlated to PtOx reduction. These mechanisms are all based on shortages of either gaseous H_2 or protons and electrons required for the chemical reaction or reduction of PtOx and which are inherently generated by the oxidation of the carbon support. With respect to the artifact, some of these generated protons and electrons could be transferred towards the CE compartment instead of reducing PtOx, resulting in the artifact peak. However, based on the experiments conducted in our study, these alternative explanations including carbon corrosion processes seem unlikely as compared to the accumulation and spontaneous HOR of crossover hydrogen outlined in the following section.

In this paper, we present the results from the investigations into the artifact visible during CV analysis of low-loaded PEMFC Pt/C electrodes. CV as well as linear sweep voltammetry (LSV) measurements have been conducted on electrodes with different Pt/C loadings while varying the measurement

parameters such as the N_2 purge rate and gas pressures in anode and cathode (p_{an}/p_{ca}) as well as the CV settings such as the upper potential limit and scan rate. These variations aim on elucidating the correlation between cell environment and artifact occurrence and magnitude to clarify its origin.

Experimental

For this study, all CV and LSV measurements were conducted in a balticFuelCells GmbH qCf *Liquid Cooling high amp* differential cell at 80 °C cell temperature in a fuel cell test bench designed and built in-house. For each measurement, the cell was purged with fully humidified (100% relative humidity) H_2 (quality 5.0, Linde AG) and N_2 (quality 6.0, Air Liquide) prior to the CV or LSV. Unless noted otherwise, the N_2 purge of the WE was switched off 5 s prior to starting the CV measurement, allowing stagnant N_2 in the compartment. The CE was purged with 0.3 l/min H_2. Also, for most CV measurements, the gas pressure in both electrodes was set to 50 $mbar_g$ during the CV to avoid intrusion of ambient air. CV analysis was performed by cycling the potential between 0.05 and the respective upper potential limit vs. reversible hydrogen electrode (RHE) at varying scan rates for 5 full cycles. Any variations in measurement parameters or CV settings are given in the figure captions and corresponding text.

The measurements were conducted on three different CCMs (provided by Greenerity GmbH) with equal membranes and cathode catalyst layers (CLs), but with different low loadings on the anode. In all CCMs, the cathode contained the same 400 μg/cm^2 of Pt on highly graphitized carbon, while the anode contained either 50, 25, or 15 μg/cm^2 of Pt on high surface area carbon. All electrodes were fabricated in a similar manner, but the different loadings were achieved by varying the thicknesses of the electrodes. Freudenberg H23 C9 was employed as gas diffusion layer (GDL) material in both anode and cathode compartments. All CV measurements on low-loaded electrodes were carried out with the anode as working electrode (WE).

Results and Discussion

As can be seen in Fig. 2b, the artifact was visible for all low-loaded electrodes (50, 25, and 15 μg/cm^2). However, it appeared the strongest for the electrode with the lowest loading of 15 μg/cm^2. Therefore, in order to enhance the visibility of effects due to parameter variation, we present predominantly the results of CV analysis of this electrode in the following sections.

Most studies in literature employ CV scan rates between 1 and 100 mV/s [20, 21, 26, 42, 43]. At higher scan rates, current magnitudes arising from electrochemical surface processes generally increase. Simultaneously, depending on the reaction rate of the process, the potentials at which these magnitudes are reached can shift while transferred charges associated to a process can decrease if the process is not given sufficient time to terminate. However, for ultra-low-loaded and thin electrodes, relatively high scan rates were found to enhance the distinction of electrochemical processes from CV profiles for subsequent analysis. Additionally, higher scan rates allow for shorter dwell times of the WE at potentials > 0.85 V avoiding unnecessary carbon corrosion of the catalyst support. Therefore, to investigate the artifact, we conducted and analyzed CV profiles predominantly taken at relatively high scan rates of 100 and 400 mV/s. However, the artifact peak was also observed for lower CV scan rates of 20 mV/s as can be seen in Fig. 4a.

N_2 Purge and Upper Potential Limit Variations

Figure 3 presents CV profiles taken at 400 mV/s of the lowest electrode loading (15 μg/cm^2) with varying upper potential limits (0.7 to 1.4 V in 0.1 V steps), when the N_2 purge was switched on and off.

In Fig. 3a and b, the features of the anodic and cathodic transients in the potential range from 0.1 to 0.3 V correspond to desorption and adsorption of H_{UPD}, whereas the relatively large currents below 0.1 V correspond to H_2 evolution at the WE. With N_2 purge being switched off, H_2 evolves and accumulates in the WE resulting in the oxidation currents at the onset of the anodic transient. At potentials of 0.8–1.4 V in the anodic transient, Pt oxidizes to form PtOx, which is reduced at potentials of 0.5–1.0 V in the cathodic transient mainly visible in the CV profiles taken with N_2 purge being switched on. In contrast, with the N_2 purge being switched off, the artifact peak occurred as shown in Fig. 3b at potentials below 0.8 V including a relatively steep incline and drop in current partly overlapping the PtOx reduction potential, as well as a gradient decline in current in the double-layer region at potentials of 0.3–0.6 V. All shown CV profiles include a positive bias due to crossover hydrogen (H_{2X}), which should be similar for all CV profiles as measurements were typically conducted successively on one CCM sample. Although CV profiles generally can be corrected via subtraction of the bias, the artifact oxidation peak would not allow for clear evaluation of the bias magnitude according to the inset of Fig. 1b. Therefore, all CV profiles reported here are not centered on the *x*-axis.

Evidently, the artifact peak only becomes visible when the N_2 purge is switched off. Furthermore, the current magnitude of the artifact increases while the peak potential decreases, when the upper CV potential limit reaches further into PtOx formation potentials. Firstly, this observation hints towards a gaseous species required for the artifact to occur, as such a species could be purged out of the WE with N_2. Presumably, carbon oxide species residing on the surface of the carbon

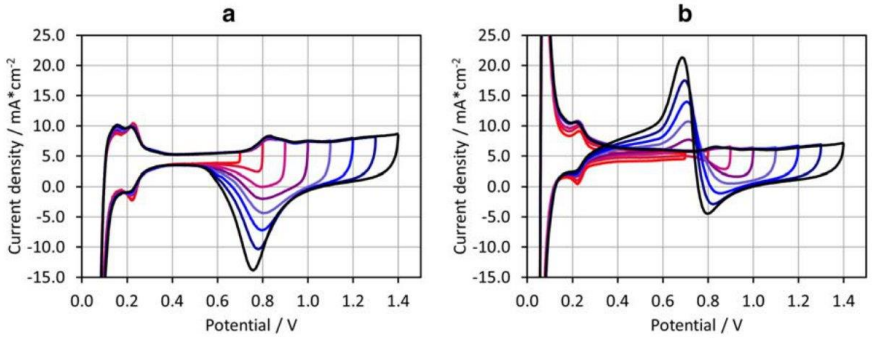

Fig. 3 Variation of the upper potential limit with N_2 purge on the WE switched on (**a**) and off (**b**). Electrode: 15 μg/cm^2; scan rate: 400 mV/s; P_{an}/P_{ca}: 50/50 mbar

support near Pt particles would not be affected by the N_2 purge, thus eliminating the theory including such carbon surface oxides. Secondly, the growth in artifact magnitude with increasing CV upper potential limit indicates a dependency of the artifact either on the PtOx layer and/or on the dwell time the WE remains at specific potentials, during which a species could form. Though carbon corrosion takes place and eventually produces carbon dioxide, the formation of gaseous trace carbon monoxide seems unlikely considering its instability at elevated potentials especially in the presence of Pt.

Scan Rate Variations

One way to investigate electrochemical processes and to distinguish between Faradaic and surface electrochemical reactions is to conduct CVs at different potential scan rates, since changes in current magnitudes or transferred charges with scan rate variations can offer valuable information about the origin of an observed process. For this purpose, Fig. 4a presents CV profiles of the 15 μg/cm^2 electrode obtained at different potential scan rates (20 mV/s and 100 to 800 mV/s in 100 mV/s steps), without N_2 purge of the WE.

Again, in Fig. 4a, both desorption and adsorption of H_{UPD} are visible between potentials of 0.1 and 0.3 V, while the large currents below 0.1 V correspond to H_2 evolution at the WE. At potentials of 0.8–1.4 V, PtOx formation occurs, which shows as increasing positive currents in CV profiles conducted at scan rates > 300 mV/s. At lower scan rates, the currents in the potential window decrease due to the decrease in H_{2X} bias as a result of PtOx formation, which will be explained in more detail in the following section. During the cathodic CV transient, PtOx reduction proceeds at potentials of about 0.7 to 1.1 V. Typically, the reduction would continue to even lower potentials of about 0.6 [29], but the artifact appears as a positive oxidation peak overlapping the reduction current. With higher scan rates, the artifact starts at lower potentials (E_{Red}), inset of Fig. 4b) and reaches lower peak currents (i_{Peak}) at lower peak potentials (E_{Peak}), which coheres with the decrease in PtOx reduction currents reached at lower E_{Red} potentials. Furthermore, the potential at which the artifact finishes (E_{Int}) decreases with higher scan rates. However, for few CV

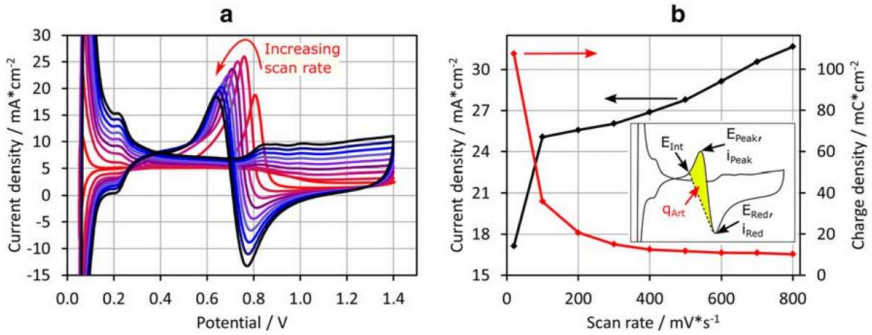

Fig. 4 Scan rate variation (20, 100–800 mV/s in 100 mV/s steps) without N_2 purge on the WE (**a**) and peak current of the artifact as well as the transferred charge from areas integrated as shown in the inset (**b**). Electrode: 15 μg/cm^2; P_{an}/P_{ca}: 50/50 mbar

profiles taken at relatively low scan rates, the latter value (E_{Int}) is difficult to extract and, hence, the potential was arbitrarily selected as the potential where the steep decline in current after the artifact peak ends.

Typically, in case of only oxidation or reduction processes eventually overlapping (such as adsorption/desorption of H_{UPD} and double-layer charging), the change in current magnitude would be of interest when conducting CV scan rate variations. Unfortunately, in case of the artifact, the artifact oxidation current overlaps partially with the PtOx reduction current, which significantly affects the magnitude i_{Peak}. However, as a substitute and to predominantly examine the current associated with the artifact, the difference in currents i_{Art} ($= i_{Peak} - i_{Red}$) between the onset and completion was extracted instead and plotted in Fig. 4b along with the charge q_{Art}. For q_{Art}, the integration area as shown in the inset of Fig. 4b is based on the assumption that the lowest PtOx reduction current (i_{Red}, E_{Red}) marks the starting point of the artifact, while the end point is resembled by the change in inclination in the declining branch (E_{Int}). This area is selected arbitrarily and likely includes errors arising from the overlap with the PtOx reduction currents or the difficulty to assess the true boundaries of the artifact. However, for most observed artifact peaks, the boundaries distinctly marked an area of positive oxidation currents especially for the electrode loadings of 50 and 25 μg/cm^2 as can be seen in Fig. 6. Table 1 lists the respective values for i_{Art}, E_{Peak}, E_{Red}, and E_{Int} as well as the transferred charges q_{Art} of the CV profiles in Fig. 4a.

Generally, if the current associated to a process increases proportionally with the increase in scan rate, while simultaneously the transferred charges integrated between potential limits remain approximately constant, the process can be associated to either a non-Faradaic or a Faradaic process controlled by surface electrochemical processes as e.g. double-layer charging or H-adsorption. For example, if all Pt sites are occupied by atomic hydrogen, the doubling in scan rate will result in twice the current magnitude in the potential range of 0.1–0.3 V, while integration would result in an almost constant charge transfer as H-adsorption and double-layer charging are relatively fast processes [29]. Vice versa, a disproportional change in current and significant differences in transferred charges would hint towards a Faradaic process, which is controlled or dominated by the diffusion of reactants and/or products. From Fig. 4b, the artifact current i_{Art} shows a rather disproportional increase, while the transferred charges q_{Art} decrease exponentially. Therefore, both the unsteady increase in artifact current i_{Art} and exponential decay of the charge q_{Art} with increasing scan rate rather support the definition of Faradaic reactions. The large offset of i_{Art} for the scan rate of 20 mV/s presumably is a result of the interplay between PtOx reduction and artifact oxidation processes at different reaction rates, which emerges at relatively low scan rates.

To confirm whether PtOx is responsible for the decrease in H_{2X}-related bias at scan rates < 300 mV/s in Fig. 4a, we conducted LSVs with all three low-loaded electrodes in comparison to the high-loaded electrode of 400 μg/cm^2 at a scan rate of 1 mV/s as shown in Fig. 5.

The response of the low-loaded electrodes upon the potential increase is a direct decrease in the H_{2X}-related current at potentials > 0.5 V and a flattening of the current towards the upper potential limit of 1 V. In comparison, the current of the 400 μg/cm^2 electrode first increases and then drops after potentials above 0.7 V, but it does not level out at about 1 V. Higher potentials were avoided during these LSV measurements, as the scan rate of 1 mV/s would be inevitably accompanied with unnecessary dwell times at potentials critical for corrosion of the carbon support [10, 36]. While some studies point towards a complete suppression of HOR on PtOx [44–46], a newer study presents an improved HOR and H_2 evolution reaction (HER) activity of synthesized Pt-(PtOx)-Nitrogen doped hybrid catalysts [47]. In a study by Iden et al. [48], the authors correlate the decrease in H_{2X} limiting current density to the increase in mass transfer losses due to the loss in effective ECSA, when Pt sites are blocked by surface oxides at elevated potentials. Whether PtOx affects HOR/HER depends on the electronic and electrochemical properties of the Pt particles, interactions with possible alloying components in and on the carbon support, the uniformity of the PtOx coverage, which

Table 1 Currents associated to the artifact (I_{Art}) and potentials of its onset (E_{Red}), peak (E_{Peak}), and completion (E_{Int}) as well as the transferred charge q_{Art} integrated from the yellow area from Fig. 4b per scan rate s

s (mV/s)	q_{Art} (mC cm^{-2})	i_{Art} (mA cm^{-2})	E_{Peak} (V)	E_{Red} (V)	E_{Int} (V)
20	107.5	17.1	0.806	0.934	0.752
100	35.9	25.1	0.758	0.863	0.673
200	20.7	25.6	0.730	0.838	0.635
300	15.0	26.0	0.709	0.811	0.611
400	12.5	26.9	0.689	0.798	0.594
500	11.7	27.8	0.673	0.785	0.561
600	10.9	29.1	0.660	0.779	0.550
700	10.8	30.6	0.649	0.775	0.528
800	10.2	31.7	0.637	0.771	0.520

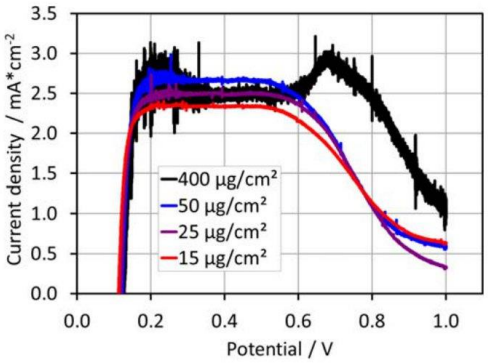

Fig. 5 LSV measurements corrected for IR (resistance from slope between 0.3 and 0.5 V). Scan rate: 1 mV/s; P_{an}/P_{ca}: 50/50 mbar; flow rate f_{an}/f_{ca}: 1/1.2 l/min

itself depends on the type and orientation of the underlying Pt particle facets [49], respectively, and if nothing else, on the medium (acidic or alkaline environment). Either way, for the LSV profiles shown in Fig. 5, it is safe to assume that the drop in current at potentials > 0.6 V can be associated with the effect of PtOx on HOR. Similarly, the decrease in current at potentials > 0.8 at scan rates < 300 mV/s in the CV profiles shown in Fig. 4 can also be linked to the decreasing H_{2X} bias overlapping the current associated to Pt oxidation. Since molecular H_2 continues to cross over through the PEM also when PtOx suppresses the HOR, the H_{2X} must accumulate in the WE. This is consistent with the observation that the artifact is suppressed once the N_2 flow is switched on and H_{2X} is purged out of the WE.

Gas Pressure Variations

To test whether crossover hydrogen (H_{2X}) is the species responsible for the artifact, CV measurements at varying gas pressures in the CE and WE (p_{CE}/p_{WE}) were conducted. Higher gas pressures in the CE as compared to the WE would lead to higher crossover rates and, therefore, are expected to affect the magnitude or transferred charge of the artifact. Figure 6 shows the CVs conducted at gas pressure variations between 50 and 600 $mbar_g$ in CE and WE for all three low-loaded electrodes (50, 25, and 15 µg/cm²).

Again, the CV profiles include currents associated to H-adsorption and H-desorption (between 0.1 and 0.3 V) as well as Pt oxidation (during anodic scan, between 0.8 and 1.4 V) and PtOx reduction (during cathodic scan, between 0.5 and 1 V). Also, for lower electrode loadings, the artifact peaks appear increased relative to currents associated to H_{UPD} or PtOx formation and reduction. Moreover, with higher pressures in the CE (600/50, 400/50, and 200/50), the CV profiles

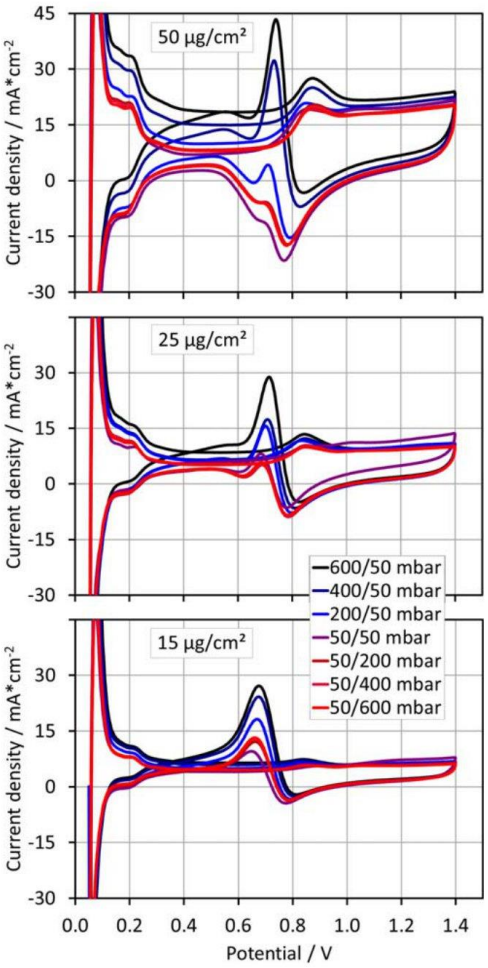

Fig. 6 Variation of gas pressures between 50 and 600 $mbar_g$ on anode/cathode for the 50, 25, and 15 mg/cm² electrodes. Scan rate: 400 mV/s

include an enhanced bias upwards from the *x*-axis as a result of an increased H_{2X} while simultaneously the artifact peaks appear enhanced for all electrode loadings. To facilitate this observation, Fig. 7 shows the artifact currents I_{Art} as well as the charges transferred q_{Art} integrated again as shown in the inset of Fig. 4b.

As can be seen, I_{Art} (solid line) and q_{Art} (dashed line) significantly increase with higher gas H_2 pressures in the CE (left hand side from p_{CE}/p_{WE} 50/50), indicating the correlation between the artifact and H_{2X}. Interestingly, slight increases in I_{Art} and q_{Art} are apparent also at higher pressures in the WE

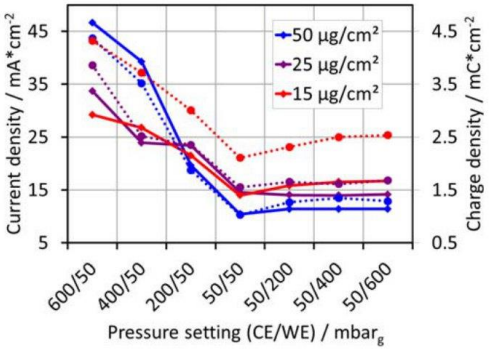

Fig. 7 Peak current (solid line) and transferred charges (dashed line) integrated as shown in the inset of Fig. 4b of all three low-loaded electrodes from CVs in Fig. 6

(right hand side from p_{CE}/p_{WE} 50/50), which could be due to an increased activity of H_{2X} at higher gas pressures in the WE and therefore increased HOR rates. Again, the values used for Fig. 7 are listed in Table 2.

From the pressure variations during the CV measurements, it is evident that with higher H_2 pressures in the CE, more H_2 crosses through the membrane and the larger the artifact peak occurs (at a given Pt loading), if the N_2 purge of the WE is switched off. Based on the findings, the artifact

a. Most likely is a Faradaic process limited by the presence of a species
b. Only appears if N_2 purge is switched off such that a gaseous species can accumulate
c. Appears for electrodes which fully passivate towards H_{2X}-related currents at oxide formation potentials
d. Increases with higher gas pressures in the CE, i.e., higher H_{2X} rates

Consequently, we hypothesize that the artifact originates from crossover hydrogen (H_{2X}), which collects at the WE as soon as the electrode is passivated due to PtOx coverage. With the reduction of the oxide during the cathodic scan, active metallic catalyst sites are freed and made available for the spontaneous HOR of the accumulated H_{2X} as shown schematically in Fig. 8.

This process occurs in three main steps; (1) PtOx formation and coverage of the Pt sites takes place in the anodic scan, while H_{2x} accumulates in the catalyst layer simultaneously; (2) a full PtOx coverage is obtained with H_{2x} accumulated in the pore space of the catalyst layer; (3) HOR of the accumulated H_{2x} commences as the potential drops during the

Table 2 Currents associated to the artifact (I_{Art}) and potentials of its onset (E_{Red}), peak (E_{Peak}), and completion (E_{Int}) as well as the transferred charge q_{Art} per pressure setting on anode/cathode

p (CE/WE) (mbar)	q_{Art} (mC cm^{-2})	i_{Art} (mA cm^{-2})	E_{Peak} (V)	E_{Red} (V)	E_{Int} (V)
50 µg/cm^2					
600/50	4.4	46.7	0.740	0.842	0.642
400/50	3.5	39.3	0.734	0.829	0.642
200/50	1.9	19.6	0.710	0.792	0.665
50/50	1.0	10.4	0.706	0.771	0.669
50/200	1.3	11.4	0.706	0.784	0.665
50/400	1.3	11.4	0.706	0.781	0.665
50/600	1.3	11.4	0.706	0.781	0.665
25 µg/cm^2					
600/50	3.9	33.7	0.713	0.618	0.822
400/50	2.5	23.9	0.710	0.611	0.809
200/50	2.4	23.4	0.703	0.614	0.798
50/50	1.6	14.5	0.686	0.604	0.778
50/200	1.7	14.1	0.689	0.622	0.784
50/400	1.6	14.0	0.689	0.622	0.784
50/600	1.7	14.2	0.686	0.611	0.784
15 µg/cm^2					
600/50	4.3	29.2	0.676	0.557	0.815
400/50	3.7	26.8	0.676	0.560	0.805
200/50	3.0	21.5	0.669	0.567	0.795
50/50	2.1	14.0	0.649	0.564	0.774
50/200	2.3	15.8	0.662	0.564	0.788
50/400	2.5	16.5	0.659	0.567	0.784
50/600	2.5	16.7	0.659	0.570	0.788

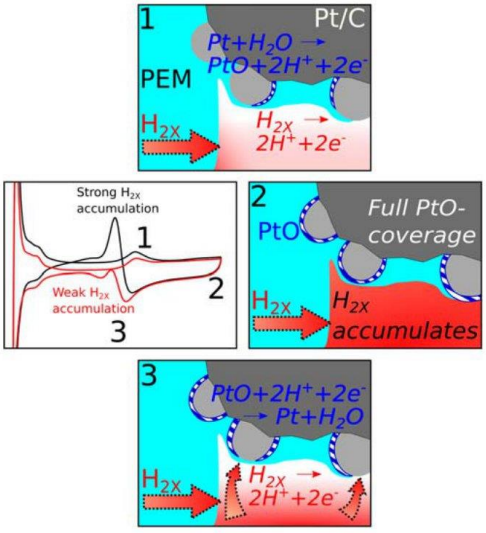

Fig. 8 Schematic of H_{2X} accumulation during PtOx formation and spontaneous HOR during PtOx reduction

cathodic scan and PtOx reduction frees metallic catalyst sites. The magnitude of the HOR peak depends on the ratio of the amount of accumulated H_{2x} in the pore spaces and the product of PtOx reduction and HOR currents. If PtOx reduction currents dominate as it is observed for higher catalyst loadings, the HOR peak appears smaller with all other conditions unchanged. Also, H_{2X} accumulations are weakened if an N_2 flow purges hydrogen out of the pore spaces in the WE. In contrary, the HOR peak increases for stronger H_{2X} accumulations caused by higher H_{2X} diffusion rates through the PEM, as it is the case for elevated gas pressures in the CE and as it is expected for lower PEM thicknesses or PEM ionomers allowing for increased hydrogen gas crossover. The upper potential limit and scan rate of the CV show mixed effects, as these parameters both determine the time for the processes of H_{2X} to accumulate and PtOx to form and, hence, the net effect depends on the relative rates of the respective processes.

Consequences for CV Analysis

Depending on the electrode material analyzed, the artifact can emerge during CV analysis of low-loaded electrodes when the N_2 purge is switched off during the measurement and the upper CV potential limit reaches into oxide formation potentials. If these requirements are met and the artifact appears, it eventually interferes with ECSA determination from H-adsorption due to difficulties in determining the starting point of H-adsorption between potentials of 0.3 and 0.6 V in the cathodic transient. Moreover, a comparison between the charges transferred during Pt oxide formation and reduction loses significance, as PtOx reduction is overlapped by the artifact. When selecting an upper potential limit below oxide formation potentials and/or employing N_2 purge rates of the WE as it is typically done for CV analysis, the artifact will not appear. However, the existence of this artifact has also consequences for the operation of low-loaded cathode CCMs. In operation conditions where PtOx is formed, we have to assume that H_{2X} can accumulate on the cathode side as it is not active enough for HOR. This can lead to safety concerns or at least to reaction heat evolution when PtOx reduction takes place with possibly enhanced degradation. It is certainly an effect to be considered carefully in operation of low-loaded CCMs.

Conclusion

In this study, we investigate an artifact peak overlapping the PtOx reduction peak measured in the cathodic transient of cyclic voltammetry analysis of ultra-low-loaded catalyst layers through a parametric analysis. Considering findings by Tahmasebi et al. [29] and Zhao et al. [30] with respect to comparable oxidation peaks, we conclude that this peak is caused by spontaneous HOR of previously accumulated crossover hydrogen (H_{2X}). Two requirements must be fulfilled for this feature to be measured. First, this feature is expected to occur predominantly during CV analysis of low and ultra-low-loaded electrodes composed of catalyst material whose oxide is completely inactive towards HOR. Second, the CV measurements must be carried out without N_2 purge of the WE. For higher loaded electrodes, the artifact is not observed as Pt or alloys including Pt are either not fully covered by an oxide layer upon reversal of the transition from anodic to cathodic transient, and/or the currents associated with the oxide reduction are much larger than the spontaneous HOR of accumulated H_{2X}. If the requirements are met and artifact appears, it can interfere with ECSA determination from H-adsorption currents and with analysis of currents associated to Pt oxide formation and reduction. With the expected cuts in noble metal loadings of catalyst-coated membranes for automotive applications, this artifact might be observed more often in the future.

Acknowledgements Open Access funding enabled and organized by Projekt DEAL.

Funding This work was supported by the German Federal Ministry for Economy and Energy within the project HAlMa, contract No. 03ET6098A.

Compliance with Ethical Standards

Conflict of Interest The authors declare that they have no conflict of interest.

References

1. W. Vielstich, A. Lamm, H.A. Gasteiger, *Handbook of Fuel Cells - Fundamentals, Technology and Applications*, vol. 3, Part 1; John Wiley & Sons, Inc.(2003)
2. G. Jerkiewicz, Electrochemical hydrogen adsorption and absorption. Part 1: Under-potential deposition of hydrogen. Electrocatalysis **1**(4), 179–199 (2010). https://doi.org/10.1007/s12678-010-0022-1
3. M. Lukaszewski, M. Soszko, A. Czerwiński, Electrochemical methods of real surface area determination of noble metal electrodes - an overview. Int. J. Electrochem. Sci *11*(6), 4442–4469 (**2016**). https://doi.org/10.20964/2016.06.71
4. S. Rudi, C. Cui, L. Gan, P. Strasser, Comparative study of the electrocatalytically active surface areas (ECSAs) of Pt alloy nanoparticles evaluated by Hupd and CO-stripping voltammetry. Electrocatalysis **5**(4), 408–418 (2014). https://doi.org/10.1007/s12678-014-0205-2
5. I.C. Halalay, S. Swathirajan, B. Merzougui, M.P. Balogh, G.C. Garabedian, M.K. Carpenter, Anode materials for mitigating hydrogen starvation effects in PEM fuel cells. J. Electrochem. Soc. **158**(3), B313 (2011). https://doi.org/10.1149/1.3530796
6. T. Binninger, E. Fabbri, R. Kotz, T.J. Schmidt, Determination of the electrochemically active surface area of metal-oxide supported platinum catalyst. J. Electrochem. Soc. **161**(3), H121–H128 (2013). https://doi.org/10.1149/2.055403jes
7. G. Jerkiewicz, G. Vatankhah, J. Lessard, M.P. Soriaga, Y.S. Park, Surface-oxide growth at platinum electrodes in aqueous H2SO4Reexamination of its mechanism through combined cyclic-voltammetry, electrochemical quartz-crystal Nanobalance, and Auger electron spectroscopy measurements. Electrochim. Acta **49**(9–10), 1451–1459 (2004). https://doi.org/10.1016/j.electacta.2003.11.008
8. G. Jerkiewicz, G. Vatankhah, S.I. Tanaka, J. Lessard, Discovery of the potential of minimum mass for platinum electrodes. Langmuir **27**(7), 4220–4226 (2011). https://doi.org/10.1021/la200153n
9. B.K. Matsutani, K. Hayakawa, T. Tada, Effect of particle size of platinum and platinum-cobalt catalysts on stability against load cycling. Platin. Met. Rev 54(4), 223–232 (2010). https://doi.org/10.1595/147106710X523698
10. K. Hengge, T. Gänsler, E. Pizzutilo, C. Heinzl, M. Beetz, K.J.J. Mayrhofer, C. Scheu, Accelerated fuel cell tests of anodic Pt/Ru catalyst via identical location TEM: new aspects of degradation behavior. Int. J. Hydrog. Energy **42**(40), 25359–25371 (2017). https://doi.org/10.1016/j.ijhydene.2017.08.108
11. M. Wesselmark, B. Wickman, C. Lagergren, G. Lindbergh, The impact of iridium on the stability of platinum on carbon thin-film model electrodes. Electrochim. Acta **111**, 152–159 (2013). https://doi.org/10.1016/j.electacta.2013.07.108
12. N. Macauley, D.D. Papadias, J. Fairweather, D. Spernjak, D. Langlois, R. Ahluwalia, K.L. More, R. Mukundan, R.L. Borup, Carbon corrosion in PEM fuel cells and the development of accelerated stress tests. J. Electrochem. Soc. **165**(6), F3148–F3160 (2018). https://doi.org/10.1149/2.0061806jes
13. S.J. Lee, S. Mukerjee, E.A. Ticianelli, J. McBreen, Electrocatalysis of CO tolerance in hydrogen oxidation reaction in PEM fuel cells. Electrochim. Acta **44**(19), 3283–3293 (1999). https://doi.org/10.1016/S0013-4686(99)00052-3
14. T. Lopes, V.A. Paganin, E.R. Gonzalez, The effects of hydrogen sulfide on the polymer electrolyte membrane fuel cell anode catalyst: H2S–Pt/C interaction products. J. Power Sources **196**(15), 6256–6263 (2011). https://doi.org/10.1016/j.jpowsour.2011.04.017
15. H. Angerstein-Kozlowska, B.E. Conway, W.B.A. Sharp, The real condition of electrochemically oxidized platinum surfaces. Electroanal. Chem. Interfacial Electrochem. **43**(1), 9–36 (1973)
16. H. Angerstein-Kozlowska, B.E. Conway, B. Barnett, J. Mozota, The role of ion adsorption in surface oxide formation and reduction at noble metals: general features of the surface process. J. Electroanal. Chem. **100**(1-2), 417–446 (1979)
17. D. Pletcher, S. Sotiropoulos, Hydrogen adsorption-desorption and oxide formation-reduction on polycrystalline platinum in unbuffered aqueous solutions. J. Chem. Soc. Faraday Trans. **90**(24), 3663–3668 (1994). https://doi.org/10.1039/FT9949003663
18. S.G. Rinaldo, W. Lee, J. Stumper, M. Eikerling, Mechanistic principles of platinum oxide formation and reduction. Electrocatalysis **5**(3), 262–272 (2014). https://doi.org/10.1007/s12678-014-0189-y
19. E.L. Redmond, B.P. Setzler, F.M. Alamgir, T.F. Fuller, Elucidating the oxide growth mechanism on platinum at the cathode in PEM fuel cells. Phys. Chem. Chem. Phys. **16**(11), 5301–5311 (2014). https://doi.org/10.1039/c3cp54740j
20. M.D. Edmundson, F.C. Busby, Overcoming artifacts in cyclic voltammetry through the use of multiple scan rates and potential windows. ECS Trans. Electrochem. Soc. **41**(1), 661–671 (2011). https://doi.org/10.1017/CBO9781107415324.004
21. R.N. Carter, S.S. Kocha, F. Wagner, M. Fay, H.A. Gasteiger, Artifacts in measuring electrode catalyst area of fuel cells through cyclic voltammetry. ECS Trans. **11**(1), 403–410 (2007). https://doi.org/10.1149/1.2780954
22. T. Biegler, D.A.J. Rand, R. Woods, Limiting oxygen coverage on platinized platinum; relevance to determination of real platinum area by hydrogen adsorption. J. Electroanal. Chem. **29**(2), 269–277 (1971). https://doi.org/10.1016/S0022-0728(71)80089-X
23. A. Kongkanand, M.F. Mathias, The priority and challenge of high-power performance of low- platinum proton-exchange membrane fuel cells. J. Phys. Chem. **7**(7), 1127–1137 (2016). https://doi.org/10.1021/acs.jpclett.6b00216
24. K. Eom, G. Kim, E. Cho, J.H. Jang, H.-J. Kim, S.J. Yoo, S.-K. Kim, B.K. Hong, Effects of Pt loading in the anode on the durability of a membrane–electrode assembly for polymer electrolyte membrane fuel cells during startup/shutdown cycling. Int. J. Hydrog. Energy **37**(23), 18455–18462 (2012)
25. Y. Hashimasa, Y. Matsuda, M. Akai, Effects of platinum loading on PEFC power generation performance deterioration by carbon monoxide in hydrogen fuel. ECS Trans. **26**(1), 131–142 (2010). https://doi.org/10.1149/1.3428984
26. S. Prass, K.A. Friedrich, N. Zamel, Tolerance and recovery of ultralow-loaded platinum anode electrodes upon carbon monoxide and hydrogen sulfide exposure. Molecules **24**(19), 1–14 (2019). https://doi.org/10.3390/molecules24193514
27. B.K. Hong, P. Mandal, J.G. Oh, S. Litster, On the impact of water activity on reversal tolerant fuel cell anode performance and durability. J. Power Sources **328**, 280–288 (2016). https://doi.org/10.1016/j.jpowsour.2016.07.002
28. X. Zhou, H. Ji, B. Li, C. Zhang, High-repetitive reversal tolerant performance of proton-exchange membrane fuel cell by designing a suitable anode. ACS Omega **5**(17), 10099–10105 (2020). https://doi.org/10.1021/acsomega.0c00638

29. S. Tahmasebi, A.A. McMath, J. van Drunen, G. Jerkiewicz, Catalytic duality of platinum surface oxides in the oxygen reduction and hydrogen oxidation reactions. Electrocatalysis **8**(4), 301–310 (2017). https://doi.org/10.1007/s12678-017-0372-z
30. Y. Zhao, X. Li, J.M. Schechter, Y. Yang, Revisiting the oxidation peak in the cathodic scan of the cyclic voltammogram of alcohol oxidation on noble metal electrodes. RSC Adv. **6**(7), 5384–5390 (2016). https://doi.org/10.1039/c5ra24249e
31. T. Unmüssig, J. Melke, A. Fischer, Synthesis of Pt@TiO2 nanocomposite electrocatalysts for enhanced methanol oxidation by hydrophobic nanoreactor templating. Phys. Chem. Chem. Phys. **21**(25), 13555–13568 (2019). https://doi.org/10.1039/c9cp00502a
32. R. Manoharan, J.B. Goodenough, Methanol oxidation in acid on ordered NiTi. J. Mater. Chem. **2**(8), 875–887 (1992). https://doi.org/10.1039/jm9920200875
33. A.M. Hofstead-Duffy, D.J. Chen, S.G. Sun, Y.J. Tong, Origin of the current peak of negative scan in the cyclic voltammetry of methanol electro-oxidation on Pt-based electrocatalysts: a revisit to the current ratio criterion. J. Mater. Chem. **22**(11), 5205–5208 (2012). https://doi.org/10.1039/c2jm15426a
34. E. Passalacqua, P.L. Antonucci, M. Vivaldi, A. Patti, V. Antonucci, N. Giordano, K. Kinoshita, The influence of Pt on the electrooxidation behaviour of carbon in phosphoric acid. Electrochim. Acta **37**(15), 2725–2730 (1992). https://doi.org/10.1016/0013-4686(92)85199-U
35. K. Kinoshita, J.A.S. Bett, Potentiodynamic analysis of surface oxides on carbon blacks. Carbon N. Y. **11**(4), 403–411 (1973). https://doi.org/10.1016/0008-6223(73)90080-8
36. S.C. Ball, S.L. Hudson, D. Thompsett, B. Theobald, An investigation into factors affecting the stability of carbons and carbon supported platinum and platinum/cobalt alloy catalysts during 1.2 V potentiostatic hold regimes at a range of temperatures. *J.* Power Sources **171**(1), 18–25 (2007). https://doi.org/10.1016/j.jpowsour.2006.11.004
37. S. Maass, F. Finsterwalder, G. Frank, R. Hartmann, C. Merten, Carbon support oxidation in PEM fuel cell cathodes. J. Power Sources **176**(2), 444–451 (2008). https://doi.org/10.1016/j.jpowsour.2007.08.053
38. J. Willsau, J. Heitbaum, The influence of Pt-activation on the corrosion of carbon in gas diffusion electrodes-a Dems study. J. Electroanal. Chem. **161**(1), 93–101 (1984). https://doi.org/10.1016/S0022-0728(84)80252-1
39. A. Pandy, Z. Yang, M. Gummalla, V.V. Atrazhev, N.Y. Kuzminyh, V.I. Sultanov, S. Burlatsky, A carbon corrosion model to evaluate the effect of steady state and transient operation of a polymer electrolyte membrane fuel cell. J. Electrochem. Soc. **160**(9), F972–F979 (2013). https://doi.org/10.1149/2.036309jes
40. L. Castanheira, W.O. Silva, F.H.B. Lima, A. Crisci, L. Dubau, F. Maillard, Carbon corrosion in proton-exchange membrane fuel cells: effect of the carbon structure, the degradation protocol, and the gas atmosphere. ACS Catal. **5**(4), 2184–2194 (2015). https://doi.org/10.1021/cs501973j
41. Y. Yamashita, S. Itami, J. Takano, K. Kakinuma, H. Uchida, M. Watanabe, A. Iiyama, M. Uchida, Degradation mechanisms of carbon supports under hydrogen passivation startup and shutdown process for PEFCs. J. Electrochem. Soc. **164**(4), F181–F187 (2017). https://doi.org/10.1149/2.0101704jes
42. H. Kumpulainen, T. Peltonen, U. Koponen, M. Bergelin, M. Valkiainen, M. Wasberg, In situ voltammetric characterization of PEM fuel cell catalyst layers. VTT Tied. - Valt. Tek. Tutkimusk, 3–28 (2002)
43. B.K. Kakati, A.R.J. Kucernak, Gas phase recovery of hydrogen sulfide contaminated polymer electrolyte membrane fuel cells. J. Power Sources **252**, 317–326 (2014). https://doi.org/10.1016/j.jpowsour.2013.11.077
44. Y. Hang Li, J. Xing, Z. Jia Chen, Z. Li, F. Tian, L. Rong Zheng, H. Feng Wang, P. Hu, H. Jun Zhao, H. Gui Yang, Unidirectional suppression of hydrogen oxidation on oxidized platinum clusters. Nat. Commun. **4**(1), 1–7 (2013). https://doi.org/10.1038/ncomms3500
45. J. Jiang, A. Kucernak, Investigations of fuel cell reactions at the composite microelectrode | solid polymer electrolyte Interface. I. Hydrogen oxidation at the nanostructured Pt | Nafion® membrane Interface. J. Electroanal. Chem. **567**(1), 123–137 (2004). https://doi.org/10.1016/j.jelechem.2003.12.018
46. N.M. Marković, S.T. Sarraf, H.A. Gasteiger, P.N. Ross, Hydrogen electrochemistry on platinum low-index single-crystal surfaces in alkaline solution. J. Chem. Soc. Faraday Trans. **92**(20), 3719–3725 (1996). https://doi.org/10.1039/FT9969203719
47. M.K. Kundu, T. Bhowmik, R. Mishra, S. Barman, Platinum nanostructure / nitrogen-doped carbon hybrid: enhancing its base media HER / HOR activity through bi- functionality of the catalyst. ChemSusChem 11(14), 2388–2401 (2018). https://doi.org/10.1002/cssc.201800856
48. H. Iden, S. Takaichi, Y. Furuya, T. Mashio, Y. Ono, A. Ohma, Relationship between gas transport resistance in the catalyst layer and effective surface area of the catalyst. J. Electroanal. Chem. **694**, 37–44 (2013). https://doi.org/10.1016/j.jelechem.2013.02.008
49. L. Wang, A. Roudgar, M. Eikerling, Ab initio study of stability and site-specific oxygen adsorption energies of Pt. J. Phys. Chem. C **113**(42), 17989–17996 (2009). https://doi.org/10.1021/jp900965q

6.2 Tolerance and recovery of ultra-low-loaded Platinum anode electrodes upon CO and H_2S Exposure

Sebastian Prass, Kaspar Andreas Friedrich, Nada Zamel

Molecules, 24 (19), 1-14 (2019)
Special Issue Proton Exchange Membrane Fuel Cells (PEMFCs)
https://www.mdpi.com/1420-3049/24/19/3514

molecules

MDPI

Article

Tolerance and Recovery of Ultralow-Loaded Platinum Anode Electrodes upon Carbon Monoxide and Hydrogen Sulfide Exposure

Sebastian Prass [1,*], Kaspar Andreas Friedrich [2,3] and Nada Zamel [1]

1 Fraunhofer Institute for Solar Energy Systems ISE, Heidenhofstr. 2, 79110 Freiburg, Germany; nada.zamel@ise.fraunhofer.de
2 German Aerospace Center, Institute of Engineering Thermodynamics, Pfaffenwaldring 38-40, 70569 Stuttgart, Germany; andreas.friedrich@dlr.de
3 University of Stuttgart, Institute of Building Energetics, Thermal Engineering and Energy Storage (IGTE), Pfaffenwaldring 31, 70569 Stuttgart, Germany
* Correspondence: sebastian.prass@ise.fraunhofer.de; Tel.: +49-761-4588-5310; Fax: +49-761-4588-9320

Academic Editors: Jean St-Pierre and Shangfeng Du
Received: 22 August 2019; Accepted: 26 September 2019; Published: 27 September 2019

Abstract: The effects of carbon monoxide (CO) and hydrogen sulfide (H_2S) in concentrations close to their respective limits in the Hydrogen Quality Standard ISO 14687-2:2012 on the performance of proton exchange membrane fuel cells (PEMFCs) with ultralow-loaded platinum anode catalyst layers (CLs) were investigated. The anodic loadings were 50, 25, and 15 μg/cm^2, which represent the current state-of-the-art, target, and stretch target, respectively, for future automotive PEMFCs. Additionally, the effect of shut-down and start-up (SD/SU) processes on recovery from sulfur poisoning was investigated. CO at an ISO concentration of 0.2 ppm caused severe voltage losses of ~40–50% for ultralow-loaded anode CLs. When H_2S was in the fuel, these anode CLs exhibited both a nonlinear decrease in tolerance toward sulfur and an improved self-recovery during shut-down and start-up (SD/SU) processes. This observation was hypothesized to have resulted from the decrease in the ratio between CL thickness and geometric cell area, as interfacial effects of water in the pores increasingly impacted the performance of ultrathin CLs. The results indicate that during the next discussions on the Hydrogen Quality Standard, a reduction in the CO limit could be a reasonable alternative considering future PEMFC anodic loadings, while the H_2S limit might not require modification.

Keywords: fuel impurities; ISO concentration; ultralow-loaded anode catalyst layer; platinum electrode; shut-down and start-up process

1. Introduction

Proton exchange membrane fuel cells (PEMFCs) are a promising clean energy alternative for applications in the transport sector, as they combine high-power density and efficiency with the significant advantage of fast system refueling times. Hydrogen (H_2) as a fuel might, however, contain low concentrations of impurities stemming from production and infrastructure. Impurities such as carbon monoxide (CO) and hydrogen sulfide (H_2S) can deteriorate the performance and lifetime of PEMFCs. Naturally, the severity of an impurity is not only affected by its concentration (or rather, dose), but also by the catalyst type, operational parameters, cross-effects, and active or passive mitigation strategies [1,2]. For example, air-bleeding is an effective strategy to provide oxygen (O_2) for the oxidation of adsorbed contaminant species in the anode electrode [3], while catalyst alloys containing platinum (Pt) and other platinum group metals (PGMs) can provide higher tolerances versus certain contaminants [4–7]. Although they are very effective, such mitigation strategies partially

come with implications about performance or durability. For example, a fraction of the O_2 introduced by air-bleeding readily reacts with H_2 in the anode compartment and thereby lowers the fuel efficiency while simultaneously accelerating membrane degradation through additional peroxide and radical formation [8]. Moreover, alloy catalysts containing PGMs or metals other than Pt usually offer a lower stability, as the alloying components exhibit higher leaching rates. What typically remains is a catalyst particle with a Pt-enriched surface [9], while the leaching cations eventually have impacts on the protonic conductivity or even integrity of the ionomer in the electrode or membrane [10].

Apart from active or passive PEMFC system internal contamination mitigation techniques, adjusting the allowed impurity limits in the Hydrogen Quality Standard ISO 14687-2:2012 poses an additional layer in accommodating enhanced PEMFC requirements versus fuel contaminants. If electrode design or system internal strategies are exhausted, the allowed impurity level for the respective contaminant could be lowered at reasonable levels based upon tangible experimental PEMFC data. Although this option eventually leads to higher H_2 production costs, it helps to avoid higher PEMFC system costs per vehicle or implications coming from internal tolerance improvement strategies.

Some of the major cost drivers in mass-produced PEMFC vehicles are the catalyst layers (CLs) attached to the membrane. The choice of CL materials, the electrode design, and production are primary levers in reducing PEMFC costs while simultaneously increasing the lifetime. Although substantial reductions in PGM catalyst loading per cell area have already been achieved, further reductions are required as a consequence of increasing PGM prizes with higher FC vehicle market penetration. The stipulated reductions range from 50% to 75% compared to the approximate state-of-the-art, resulting in PGM targets for 2020 of about 125 and 62.5 $\mu g/cm^2$ depending on the contemplated scenario [11]. In both cases, the loading of the anode electrode is expected to account for 20% (i.e., 25 and 12.5 $\mu g/cm^2$ of PGMs, respectively): this is called ultralow loading in the present study hereafter.

Generally, lower anodic catalyst loadings are less tolerant toward catalyst contaminants, as both fuel and contaminants compete for fewer active sites in the electrode. For pure Pt electrodes, the voltage drop was found to increase by 25% when the Pt-loading decreased from 400 to 50 $\mu g/cm^2$ if 1 ppm CO was introduced [12,13]. A similar trend was observed for H_2S, where the tolerance of the electrode was found to decreased proportionally with the reduction in the anode loading [14]. It is expected that this trend would continue for ultralow loadings (<50 $\mu g_{PGM}/cm^2$), but so far there has been no study in the literature that has investigated the tolerance of such ultralow anodic loadings. Additionally, processes such as the shut-down and start-up (SD/SU) of FC vehicles are expected to affect the poisoning phenomenon of the electrodes. During downtime, reactants can diffuse from the anode to the cathode, and conversely, mixed potentials arise at the electrodes and poisoned catalysts eventually recover. However, there are limited experimental data available in the literature on recovery due to SD/SU processes, which is especially of interest in the case of recovery from sulfur contamination. Cyclic voltammetry (CV)-like methods triggering oxidative processes at ~0.9–1.1 V count as a recovery strategy for sulfur-contaminated electrodes [6,15,16], but this strategy also induces carbon corrosion and therefore destruction of the electrode itself.

The study presented here therefore seeks to add to the studies by Hashimasa et al. [12,14] by investigating the tolerance of ultralow-loaded anodic platinum catalyst layers. Two different types of contaminants were selected: CO, as its poisoning effect is fully reversible, while in contrast, H_2S typically poisons the catalyst irreversibly during regular fuel cell operation. Additionally, recovery from sulfur poisoning through simple shut-down and start-up (SD/SU) processes was examined in more detail for ultralow anodic catalyst loadings.

2. Materials and Methods

2.1. Test Station and Contaminant Introduction

Single-cell tests were carried out in an in-house-built test station with an integrated potentiostat (Zahner Zennium Pro) and an electric load (Kikusui PLZ664WA) with fluidics (shown schematically in Figure 1).

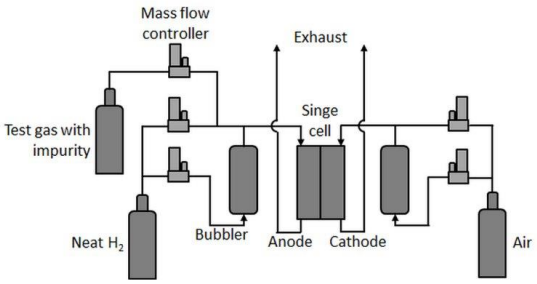

Figure 1. Single-cell test station scheme.

In principle, the test station was comparable to the one used by Hashimasa et al. [12], but with a different humidification system for the anode, a different position of the test gas feed inlet (here, the test gases were not fed through the humidifier), and no gas analysis system. In the present study, a differential cell (Baltic qCF type with automotive linear-channel flow field) with an active area of 20.25 cm^2 was employed, which allowed for the minimization of in-plane effects such as gradients in partial gas pressures, relative humidity, and temperature and therefore enhanced focus on the contamination effect at a given concentration. Although the effects of very low concentrations of impurities eventually become less visible in such a cell [17], a rather uniform coverage of the contaminant on the catalyst throughout the active area was expected.

Low concentrations of impurities were achieved by mixing precontaminated test gases with neat H_2. Therefore, carbon monoxide (CO, 10 ppm in H_2 5.0) and hydrogen sulfide (H_2S, 0.5 ppm in N_2 5.0) were mixed via mass flow controllers with house-supply high-purity hydrogen (all gases provided by Linde AG) in the required fractions.

2.2. Materials

The variations in the anode-loading on the catalyst-coated membranes (CCMs, provided by Greenerity GmbH) were achieved through different thicknesses of the anode catalyst layers (CLs), while the cathode loading was kept constant at 400 µg/cm^2. The catalyst material for both electrodes, the anode and the cathode, was pure Pt on carbon. The membrane electrode assembly (MEA) specifications are shown in Table 1.

Table 1. Membrane electrode assembly (MEA) specifications.

Active Cell Area		**20.25 cm^2**
Catalyst	Anode	Pt/C
	Cathode	Pt/C
Electrode loading	Anode	50/25/15 µg/cm^2 (named A, B, and C hereafter)
	Cathode	400 µg/cm^2
Membrane thickness		~15 µm
Gas diffusion layer		Freudenberg H23C9

2.3. Testing Procedure and Conditions

For every test with a different type of contaminant gas, a fresh MEA sample was assembled into the test cell. To measure the effect of the impurities, the test cell was operated with a constant load to detect the voltage drop associated with the contaminant species and concentration. In the following figures, the cell voltage drop is defined as the relative change based on the initial cell voltage. The effect of CO was tested at three different concentrations, namely 0.1, 0.2, and 0.4 ppm (50%, 100%, and 200% of the impurity limit noted in the H_2 Quality Standard). Before and after the actual contamination, the fuel cell was operated with neat H_2 to establish a baseline voltage and to detect eventual irreversible degradation of the electrodes. The effect of H_2S was tested at two concentrations, which were 4 and 20 ppb (100% and 500% of the limit in the Quality Standard), with neat H_2 operation only at the start of the contaminant test. The conditions during the contaminant tests are shown in Table 2.

Table 2. Operating conditions during contamination.

Cell Temperature	80 °C
Outlet pressure anode/cathode	1.2/1.2 bara
Relative humidity anode/cathode	90%/75%
Current density	1.0 A/cm^2
Stoichiometry anode/cathode	12/14

The MEAs were characterized, including cyclic voltammetry (CV) on the anode and cathode side at the beginning and end of life (BOL and EOL), as were the polarization curves at the BOL, to compare the performance between the MEA types before starting the contaminant test. The gas pressure during contamination was selected in reference to the studies by Hashimasa et al. [12,14], while the pressure during the polarization curves was chosen according to in-house standardized testing protocols. The conditions during the polarization curves are shown in Table 3.

Table 3. Polarization curve conditions.

Cell Temperature	80 °C
Outlet pressure anode/cathode	2/2 bara
Relative humidity anode/cathode	95%/75%
Gas flow anode/cathode	3/7 l/min

CV measurements were performed to determine the electrochemically active surface area (ECSA) of the CLs before and after contamination and recovery procedures, specifically from H_2S poisoning. The CVs were performed on both the anode and cathode electrodes under the conditions summarized in Table 4. To conduct an anode CV, the test cell was purged with nitrogen in order to exchange the gas supply and the electric connectors of the anode and cathode compartment and then reconditioned with fully humidified H_2 and N_2 for 12 min prior to the CV. Following the anode CV, the cell was purged again and reconnected in a regular anode/cathode configuration for subsequent tests.

Table 4. Cyclic voltammetry (CV) conditions.

Cell Temperature	80 °C
Outlet pressure anode/cathode	1.05/1.05 bara
Relative humidity anode/cathode	95%/95%
Gas flow anode/cathode	1.0/0 l/min (1.0 l/min N_2 for 12 min prior to CV on cathode)
Scan range	50–700 mV
Sweep rate	100 mV/s

An upper CV boundary of 700 mV was selected to avoid the oxidation of adsorbed foreign species, especially during the H_2S recovery tests, and to solely focus on the recovery from SD/SU processes. Moreover, the N_2 flow was stopped during the actual CV to avoid disproportionally high H_2 evolution currents during the anodic sweep, which were observed especially for the lowest anodic loading. Figure 2 shows exemplary BOL CVs of the three different anode electrodes and one cathode electrode for comparison.

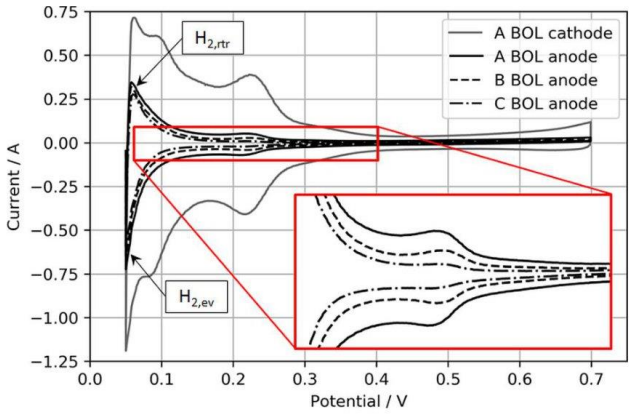

Figure 2. Anode CVs of MEA types A, B, and C with an MEA type A cathode CV for reference. The inset expands the H_2 adsorption/desorption regions of the anode catalyst layers (CLs) for visual comparison.

Normally, the ECSA is determined through integration of the charge transfer between voltage boundaries, starting from ~0.08 to 0.1 V to the minima or maxima of the respective double-layer charging current, which typically is somewhere between 0.3 and 0.6 V [18]. However, in this study, these boundaries were considered less suitable for CVs on ultralow-loaded anode CLs. High currents associated with H_2 evolution during the cathodic sweep ($H_{2,ev}$) and the coherent reverse-transport of eventually evolved H_2 during the anodic sweep ($H_{2,rtr}$) would account for relatively large errors in the ECSA. Hence, the voltage boundaries for the determination of the ECSA were chosen as 0.15 to 0.3 V, as shown in Figure 3.

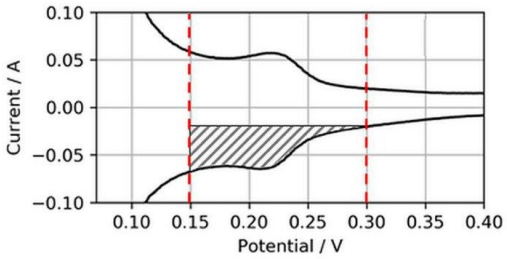

Figure 3. Electrochemically active surface area (ECSA) determination from reduced H_2 adsorption area.

Using this narrowed voltage range, the anode ECSA was determined from the anodic sweeps associated with the adsorption of H_2 on the catalyst surfaces. Although this procedure cuts the measured ECSA compared to integration between regular voltage ranges, it was found that it would

increase the accuracy of the ECSA determination and its changes in the case of ultralow-loaded anodes (as tested in the present study).

3. Results and Discussion

3.1. Performance and Stability of Ultralow-Loaded Anodic CLs

Before the actual contamination tests, the BOL performance and voltage stability of the MEA samples with ultralow-loaded anodes were established. Figure 4 shows the BOL polarization curves of the three different MEAs when neat H_2 was supplied to the test cells.

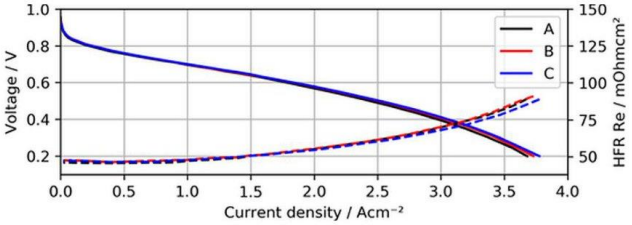

Figure 4. Polarization curves of MEA types A, B, and C using neat H_2, with high-frequency resistance (HFR) as dashed lines.

As can be seen in the figure, the polarization curves of the different MEAs overlap quite well, indicating that overpotentials arising due to a lack of active catalyst sites for the hydrogen oxidation reaction (HOR) were not significant for ultralow anodic loadings. In fact, MEA type C (15 µg/cm^2) even showed a slightly better performance at current densities above 2.5 A/cm^2, (~15 mV at 3 A/cm^2), which might have been a result of minimal differences in humidification characteristics of this specific sample and the lower measured high-frequency resistance (HFR).

In addition to the BOL performance, the cell voltage stability of the three MEA types over a testing time of 100 h of continuous operation at a constant load with neat H_2 was established, which is shown in Figure 5.

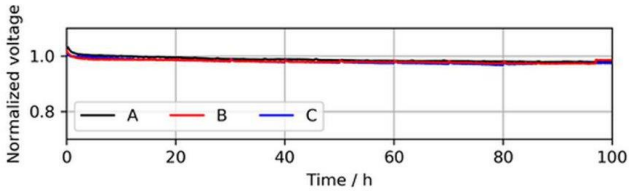

Figure 5. Voltage decay over 100 h of continuous operation in neat H_2 at 1.0 A/cm^2, showing similar voltage stabilities of the MEA types. The voltages were normalized to the initial cell voltage at time = 0 h.

During these stability tests, no significant difference between the voltage drops of the MEA types was observed. A slight voltage drop during the first ~2 h was visible for all three MEA types and was associated with the consumption of reactants, which saturated in the electrode before the current was increased.

Overall, the comparability of the different MEA types at the BOL under operation with neat H_2 was considered satisfactory and was accepted for subsequent tests with contaminants. Before each contamination test, the cell was operated for 20 h with neat H_2 to establish a baseline voltage. In the case of CO, the first concentration of contaminant was introduced and increased at time steps of 20 h,

before we finally shut off the impurity for an additional 20 h of operation with neat H_2. In the case of H_2S, after operation with neat H_2, a single concentration of H_2S was introduced until the cell voltage broke down, and subsequently SD/SU recovery tests were conducted. For all tests, the anode bubbler required a refill with fresh deionized (DI) water every 10 h. This DI water contained dissolved O_2, which was driven out as soon as it was heated in the bubbler and was consequently available for the recovery of poisoned Pt sites, which is visible as voltage peaks in the following figures.

3.2. Effect of CO on Ultralow-Loaded Anode CLs

Essentially, CO adsorbs on Pt and thereby competes with the actual HOR for active sites on the catalyst surfaces, as shown in Equations (1)–(3):

$$2Pt + H_2 \leftrightarrow 2(Pt - H), \tag{1}$$

$$Pt + CO \leftrightarrow Pt - CO, \tag{2}$$

$$2Pt + CO \leftrightarrow (Pt)_2 = CO. \tag{3}$$

Depending on the coverage of CO, each molecule blocks one or two active Pt sites via linear or bridge bonds (Equations (2) and (3), respectively) [5,19]. At lower coverages, a higher fraction of bridge bonds is expected, while at higher coverages, an adlayer with CO linear bonds dominates [20]. However, the adlayer CO structure depends on particle sizes, adsorption potentials, facet orientations, and temperature in a complex way because dipole–dipole interactions are important [21]. The effect of different CO concentrations on the voltage decay rates of the three ultralow-loaded anodic CLs is shown in Figure 6.

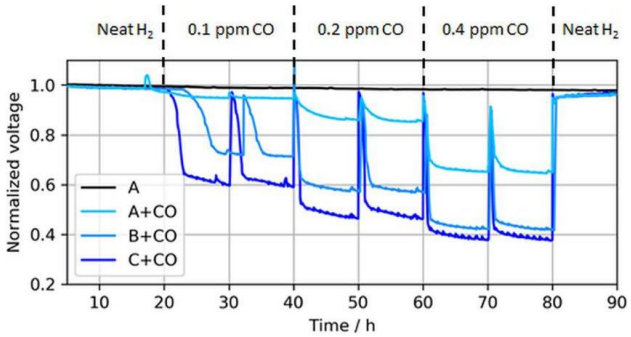

Figure 6. Voltage drops induced by different CO concentrations in MEA types A, B, and C at a constant load of 1.0 A/cm^2. The voltage peaks (every 10 h) were caused by anode bubbler refills and coherent recovery of Pt sites with O_2 dissolved in DI water. Again, the voltages were normalized to the initial cell voltage at time = 0 h, while the results are shown starting from t = 5 h.

As expected, the effect of CO in the fuel generally increased for lower anodic loadings, including both a faster and more severe voltage drop. The leveling of the potentials, i.e., the initial decline toward a plateau, depended on the contaminant concentration and the CL thickness [22,23]. For thinner CLs, the reaction front increasingly corresponded with the actual CL thickness, and therefore the local potential was more uniform while contaminants competed throughout the layer with hydrogen for adsorption sites, which resulted in a lower tolerance for thinner (and lower-loaded) CLs. At the ISO concentration (0.2 ppm), the voltage loss due to CO poisoning accounted for ~8%, 41%, and 51% when the anodic loading decreased from 50 to 25 and 15 µg/cm^2, respectively. Slight potential oscillations of the ultralow-loaded anode MEA types (type B and especially C) at high CO concentrations between

normalized voltage ratios of 0.4 and 0.6 were also visible. At these potentials, overpotentials induced by CO poisoning forced the anode potential to shift frequently toward the cathode potential and close to the oxidation potential of CO to CO_2, allowing for recovery of the electrode [24,25]. This self-recovery was the reason for the maximum coverage of the catalyst with CO in regular PEMFC operation and a flattening of the relative potential drop for lower anodic catalyst loadings with higher CO concentrations, which is partially visible in Figure 7.

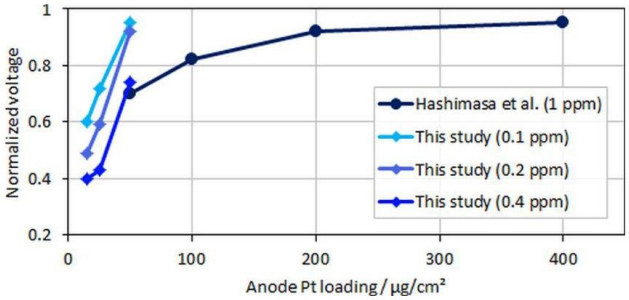

Figure 7. Normalized voltages over anodic loading; data adapted from Hashimasa et al. [12].

In the figure, relative voltage drops due to CO poisoning over the anode Pt loading from the study by Hashimasa et al. and the present study are compared. Although the test cells and the operational parameters between the two studies were different (70% fuel usage in the single cell by the Japanese Automobile Research Institute, JARI, versus 8.3% fuel usage in the differential single cell employed in the present study), a general trend for voltage decay with lower anodic loadings or higher CO concentrations can be seen. The onset of the mentioned flattening of the relative voltage drop at maximum CO coverage is visible for the lowest anodic loading and the highest tested CO concentration, where the relative change between MEA types B and C was less significant compared to types A and B.

In general, CO contamination is fairly easy to mitigate by providing O_2 to the anode via the air-bleeding technique [3]. This technique not only mitigates CO poisoning, but also partially mitigates poisoning from other contaminants, such as H_2S [16]. However, as discussed above, air bleeding also comes with disadvantages, such as a reduction in fuel efficiency and potential effects on the integrity of the ionomer in the CLs and membrane. Therefore, to minimize potentially amplified side effects from such mitigation strategies, a reduction of the limit for CO in the H_2 Quality Standard could be a reasonable option considering the severity of CO poisoning on ultralow anodic loadings, as they likely will be employed in the near future in automotive PEMFCs.

3.3. Effect of H_2S on Ultralow-Loaded Anode CLs

In contrast to CO, H_2S poisons catalyst surfaces irreversibly through dissociative adsorption on Pt via chemical or electrochemical reaction pathways, as indicated by Equations (4) and (5), respectively. The elemental sulfur on Pt cumulatively occupies active catalyst sites also via linear or bridge bonds, which eventually leads to a complete breakdown of the PEMFC performance [6,14,16]:

$$Pt + H_2S \leftrightarrow Pt - S + H_2, \tag{4}$$

$$Pt + H_2S \leftrightarrow Pt - S + 2H^+ + 2e^-. \tag{5}$$

Higher catalyst loadings provide a higher nominal ECSA and therefore a larger buffer versus such a breakdown. This decrease in tolerance with a reduction in platinum loading is partially

visible in Figure 8, which shows the operation times until the breakdown was observed for ultralow-loaded anodes.

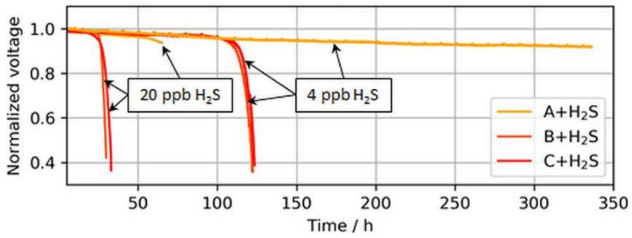

Figure 8. Voltage breakdowns induced by 4 and 20 ppb of H_2S during operation at a constant load of 1.0 A/cm^2. The operation of MEA type A was purposely stopped after ~340 h and ~70 h, while MEA types B and C stopped automatically after voltage breakdowns were observed.

The voltage breakdowns for the highest tested anodic loading (50 µg/cm^2) were not fully observed. In the case of 4 ppb of H_2S, the test was purposely interrupted after 340 h of contaminant introduction, as a voltage breakdown was not expected anymore. However, subsequent CVs revealed an almost completely sulfur-blocked ECSA, which is shown in the following sections. In the case of 20 ppb of H_2S, the test station automatically stopped at the onset of the breakdown after about ~70 h, but the start of the breakdown was still visible.

Interestingly, for both MEA types with ultralow anodic loadings (MEA types B and C), voltage breakdowns were detected after almost similar poisoning times for both tested H_2S concentrations of 4 and 20 ppb. In Figure 9, which compares the accumulated H_2S supplied until a 30-mV voltage loss was detected in the present study versus the study by Hashimasa et al., these similar poisoning times are visible as a nonproportional decline in the amount of H_2S supplied with the reduction in anodic loading.

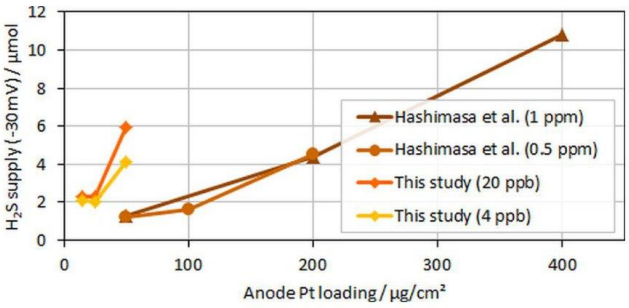

Figure 9. H_2S supplied to the cell until voltage dropped by 30 mV over anodic loading; data adapted from Hashimasa et al. [14].

Although Hashimasa et al. described their observed decline as proportional to the reduction in the loading, their data actually rather showed a slight flattening of the curve with the decrease in the anodic loading, comparable to the data from the presented study. Again, although the test cells and the operational parameters were different (70% fuel usage in JARI's single cell versus 8.3% fuel usage in the differential single cell in the present study), the general trend was still visible.

One explanation could be that some of the H_2S adsorbed on the surfaces of the test bench and cell components before actually reaching the CCM and catalyst sites. Depending on the chronology of the

tests, this latency could create delays in the voltage breakdown. On the other hand, in the present study, the CVs of lower-loaded anodes also revealed a higher degree of self-recovery from simple shut-down (SD) and start-up (SU) processes.

For these self-recovery tests, the ECSA of the anode CLs exposed to H_2S were determined at the BOL after a simulated SD/SU process, after H_2S poisoning, and again after an SD/SU process. The SD/SU included a short purge with dry nitrogen to avoid open circuit voltage (OCV) in H_2/air-atmosphere, a cooldown of the cell to 20 °C, a wait time of 3 h, and finally again heating of the cell to 80 °C and the introduction of neat H_2/air to the cell, which was kept at a fixed potential of 0.8 V during the heating. Figure 10 presents these anode CVs for the three different anodic loadings.

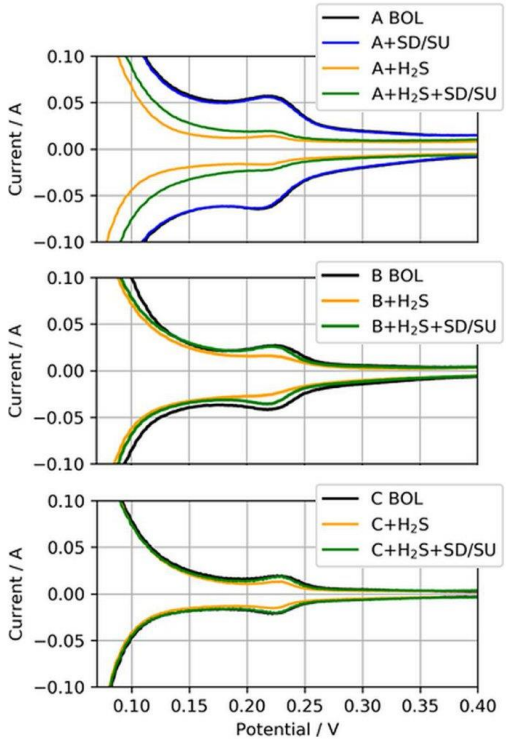

Figure 10. Anode CVs for MEA types A, B, and C (50, 25, and 15 µg/cm^2) at the beginning of life (BOL), after H_2S contamination (+H_2S), and after a subsequent shut-down/start-up (SD/SU) process (+H_2S + SD/SU). For MEA type A, the CV after SD/SU just before the contamination is also shown (A + SD/SU).

Clearly visible is the difference between the CVs at the BOL and after H_2S contamination (black to yellow CV) for all three MEA types, indicating the reduction of ECSA due to sulfur adsorbed on Pt. For MEA type A, the CV after SD/SU and before H_2S contamination (blue CV) is additionally shown to exemplarily demonstrate that the SD/SU process did not significantly affect the CV measurement and ECSA determination, as both CVs overlapped quite well. However, when the SD/SU process was carried out after H_2S contamination, the CV and therefore the ECSA gained in area compared to the poisoned ECSA (yellow to green CV), indicating a partial recovery from previously deactivated ECSA. This self-recovery was increasingly observed with the reduction in the anodic loading. Table 5 presents the nominal ECSAs and percentage changes between the test SD/SU steps.

Table 5. ECSA at the BOL and relative change after shut-down/start-up processes (SD/SU) before and after contamination with H_2S based on narrowed boundaries (integration between 150 and 300 mV). Note: the nominal ECSA was lower by about 60–70% than what would be typically expected for the specific catalyst material, while the relative ECSA changes were amplified to some degree due to the narrowed voltage boundaries and therefore the smaller area for integration.

MEA Type	ECSA (m^2/g Pt)			
	BOL	**After SD/SU**	**After H_2S**	**After H_2S + SD/SU**
A	20.5	20.0 (98%)	4.4 (22%)	7.1 (35%)
B	24.4	24.2 (99%)	16.8 (69%)	20.6 (84%)
C	19.6	19.1 (97%)	14.0 (71%)	18.4 (94%)

While only about 35% of the ECSA from MEA type A (50 µg/cm^2) could be recovered, 84% and almost a full recovery of 94% could be achieved for MEA types B (25 µg/cm^2) and C (15 µg/cm^2), respectively, through a simple SD/SU process.

The reason for the different behavior of ultralow-loaded anodes with respect to their tolerance versus H_2S contamination and the improved self-recovery during SD/SU processes might have a dimensional character in combination with the scavenging effect of water versus contaminants [26]. Studies in the literature investigating the recovery of sulfur-poisoned electrodes have often employed CV-like processes to increase the potential and thereby oxidize adsorbed sulfur either on cathode or anode electrodes [27,28]. During this oxidation, sulfur oxides such as sulfur dioxide (and in combination with water-soluble anions such as sulfate (SO^{2-}_4) or sulfite (SO^{2-}_3)) develop as shown in Equations (6)–(8) [16]:

$$Pt - S + O_2 \leftrightarrow Pt + SO_2, \tag{6}$$

$$Pt - S + 3H_2O \leftrightarrow Pt + SO_3^{2-} + 6H^+ + 4e^-, \tag{7}$$

$$Pt - S + 4H_2O \leftrightarrow Pt + SO_4^{2-} + 8H^+ + 6e^-. \tag{8}$$

Presumably, during an SD/SU process, the catalyst surfaces and adsorbed species relax, the local potential varies depending on the local equilibrium and the available species on Pt, and chemical reactions occur to the point of the formation of sulfur anions in the presence of water. It should be noted that the potential of the anodic electrode prior to and during the SD can affect the reduction state of the sulfur species, which eventually facilitates their oxidation or desorption [29]. As the different anodic loadings tested in this study were achieved through variations in CL thickness, the anode of MEA type C consequently had the lowest thickness, while the active cell area remained the same for all samples. During an SD, water condensates and eventually is driven out through hydrophobic pores of the microporous and gas diffusion layer (MPL/GDL) or collects in pores and areas, which are energetically favorable. As the interface between the MPL and CLs also contains such pores [30], sulfur in proximity to this interface might dissolve in these water accumulations in the form of soluble sulfur anions [26]. As the active cell area and therefore the CL/MPL interface area should be the same on average for all three MEA types, while the anode CL volumes are different, a higher fraction of anions could get removed for lower-loaded and therefore thinner anode electrodes. These anions dissolved in water eventually are flushed out once the PEMFC is started again. This works better so long as sulfur is weakly bonded to the Pt surface via linear bonds. With time, adsorbed sulfur develops stronger bonds to active sites and is bound more strongly to the catalyst, leading finally to the observed voltage breakdowns of the PEMFCs. Thinner CLs may also be associated with a changed ionomer structure, and the potentials within the layer are generally more homogeneous [31]. However, the differentiation of this effect is beyond the scope of this paper.

Consequently, the reduction of the anodic catalyst material down to ultralow loadings seemed to come with a nonproportional reduction in tolerance versus H_2S poisoning and an improved self-recovery during SD/SU processes. Hence, lowering the ISO limit for sulfur-containing compounds

might not be necessary with regard to ultralow-loaded anode electrodes. However, these effects should be further confirmed in large- or full-scale cell tests using realistic automotive fuel utilizations.

4. Conclusions

The key findings from this study are that the H_2 Quality Standard ISO 14687-2:2012 eventually requires partial adaption to accommodate future automotive PEMFC designs, including ultralow-loaded anodic CLs, and that ultralow-loaded anodes exhibited an improved self-recovery from sulfur poisoning from simple SD/SU processes.

As expected, CO poisoning induced significant performance losses at an increasing rate and severity with decreases in the platinum loading. At an ISO concentration of 0.2 ppm CO in the fuel, the cell voltage was about 40–50% lower compared to operation with neat H_2 for ultralow anodic loadings, which raises the question of whether the CO limit in the H_2 Quality Standard needs to be reduced with regard to future anodic loadings.

When H_2S was in the fuel, the ultralow-loaded anodic CLs exhibited a nonlinear reduction as opposed to the expected linear reduction in tolerance to the reduction in platinum loading. Simultaneously, these anodic CLs recovered to larger degrees from sulfur poisoning during the SD/SU processes. It is hypothesized that the nonlinear reduction in tolerance and improved self-recovery arose due to the decrease in the ratio between the CL thickness (and coherent ECSA) and the geometric cell area. As the ultralow-loaded anodes were also the thinner CLs, larger fractions of sulfur adsorbed on catalyst surfaces in proximity to pores at the CL–MPL interface could have dissolved in the water present in the form of anions, which were driven out of the cell during operation or during the SU of the PEMFCs.

However, to confirm these findings, the performance of ultralow-loaded anodic CLs in the presence of impurities should be further investigated, ideally in large- or full-scale PEMFCs using automotive fuel consumption rates.

Author Contributions: conceptualization, S.P.; data curation, S.P.; writing—original draft, S.P.; writing—review and editing, S.P., K.A.F., and N.Z.

Funding: This work was supported by the German Federal Ministry for Economy and Energy within the project HAlMa, contract no. 03ET6098A.

Acknowledgments: The authors thank Jean St.-Pierre at the University of Hawaii (Manoa) for technical discussions and suggestions as well as Greenerity GmbH for providing the CCM materials.

Conflicts of Interest: The authors declare no conflicts of interest. The funders had no role in the design of the study; in the collection, analysis, or interpretation of the data; in the writing of the manuscript; or in the decision to publish the results.

References

1. Cheng, X.; Shi, Z.; Glass, N.; Zhang, L.; Zhang, J.; Song, D.; Liu, Z.S.; Wang, H.; Shen, J. A Review of PEM Hydrogen Fuel Cell Contamination: Impacts, Mechanisms, and Mitigation. *J. Power Sources* **2007**, *165*, 739–756. [CrossRef]
2. Zamel, N.; Li, X. Effect of Contaminants on Polymer Electrolyte Membrane Fuel Cells. *Prog. Energy Combust. Sci.* **2011**, *37*, 292–329. [CrossRef]
3. Klages, M.; Tjønnås, J.; Zenith, F.; Halvorsen, I.J.; Scholta, J. Dual Control of Low Concentration CO Poisoning by Anode Air Bleeding of Low Temperature Polymer Electrolyte Membrane Fuel Cells. *J. Power Sources* **2016**, *336*, 212–223. [CrossRef]
4. Iezzi, R.C.; Santos, R.D.M.; da Silva, G.C.; Paganin, V.A.; Ticianelly, E.A. CO Tolerance and Stability of Proton Exchange Membrane Fuel Cells with Nafion® and Aquivion® Membranes and Mo-Based Anode Electrocatalysts. *Braz. Chem. Soc.* **2018**, *29*, 1094–1104. [CrossRef]
5. Lee, S.J.; Mukerjee, S.; Ticianelli, E.A.; McBreen, J. Electrocatalysis of CO Tolerance in Hydrogen Oxidation Reaction in PEM Fuel Cells. *Electrochim. Acta* **1999**, *44*, 3283–3293. [CrossRef]

6. Mohtadi, R.; Lee, W.-K.; Cowan, S.; Van Zee, J.W.; Murthy, M. Effects of Hydrogen Sulfide on the Performance of a PEMFC. *Electrochem. Solid State Lett.* **2003**, *6*, A272–A274. [CrossRef]
7. Gubán, D.; Tompos, A.; Bakos, I.; Vass, A.; Pászti, Z.; Szabó, E.G.; Sajó, I.E.; Borbáth, I. Preparation of CO-Tolerant Anode Electrocatalysts for Polymer Electrolyte Membrane Fuel Cells. *Int. J. Hydrogen Energy* **2017**, *42*, 13741–13753. [CrossRef]
8. Inaba, M.; Sugishita, M.; Wada, J.; Matsuzawa, K.; Yamada, H.; Tasaka, A. Impacts of Air Bleeding on Membrane Degradation in Polymer Electrolyte Fuel Cells. *J. Power Sources* **2008**, *178*, 699–705. [CrossRef]
9. Hengge, K.; Gänsler, T.; Pizzutilo, E.; Heinzl, C.; Beetz, M.; Mayrhofer, K.J.J.; Scheu, C. Accelerated Fuel Cell Tests of Anodic Pt/Ru Catalyst via Identical Location TEM: New Aspects of Degradation Behavior. *Int. J. Hydrogen Energy* **2017**, *42*, 25359–25371. [CrossRef]
10. Li, H.; Gazzarri, J.; Tsay, K.; Wu, S.; Wang, H.; Zhang, J.; Wessel, S.; Abouatallah, R.; Joos, N.; Schrooten, J. PEM Fuel Cell Cathode Contamination in the Presence of Cobalt Ion (Co2+). *Electrochim. Acta* **2010**, *55*, 5823–5830. [CrossRef]
11. Kongkanand, A.; Mathias, M.F. The Priority and Challenge of High-Power Performance of Low- Platinum Proton-Exchange Membrane Fuel Cells. *J. Phys. Chem.* **2016**, *7*, 1127–1137. [CrossRef] [PubMed]
12. Hashimasa, Y.; Matsuda, Y.; Akai, M. Effects of Platinum Loading on PEFC Power Generation Performance Deterioration by Carbon Monoxide in Hydrogen Fuel. *ECS Trans.* **2010**, *26*, 131–142. [CrossRef]
13. Matsuda, Y.; Shimizu, T.; Mitsushima, S. Adsorption Behavior of Low Concentration Carbon Monoxide on Polymer Electrolyte Fuel Cell Anodes for Automotive Applications. *J. Power Sources* **2016**, *318*, 1–8. [CrossRef]
14. Hashimasa, Y.; Matsuda, Y.; Imamura, D.; Motoaki, A. PEFC Power Generation Performance Degradation by Hydrogen Sulfi de and Ammonia—Eff Ects of Lowering Platinum Loading. *Electrochemistry* **2011**, *79*, 343–345. [CrossRef]
15. Kakati, B.K.; Kucernak, A.R.J.; Fahy, K.F. Using Corrosion-like Processes to Remove Poisons from Electrocatalysts: A Viable Strategy to Chemically Regenerate Irreversibly Poisoned Polymer Electrolyte Fuel Cells. *Electrochim. Acta* **2016**, *222*, 888–897. [CrossRef]
16. Lopes, T.; Paganin, V.A.; Gonzalez, E.R. The Effects of Hydrogen Sulfide on the Polymer Electrolyte Membrane Fuel Cell Anode Catalyst: H2S-Pt/C Interaction Products. *J. Power Sources* **2011**, *196*, 6256–6263. [CrossRef]
17. Bonnet, C.; Franck-Lacaze, L.; Ronasi, S.; Besse, S.; Lapicque, F. PEM Fuel Cell Pt Anode Inhibition by Carbon Monoxide: Non-Uniform Behaviour of the Cell Caused by the Finite Hydrogen Excess. *Chem. Eng. Sci.* **2010**, *65*, 3050–3058. [CrossRef]
18. Elgrishi, N.; Rountree, K.J.; McCarthy, B.D.; Rountree, E.S.; Eisenhart, T.T.; Dempsey, J.L. A Practical Beginner's Guide to Cyclic Voltammetry. *J. Chem. Educ.* **2018**, *95*, 197–206. [CrossRef]
19. Camara, G.A.; Ticianelli, E.A.; Mukerjee, S.; Lee, S.J.; McBreen, J. The CO Poisoning Mechanism of the Hydrogen Oxidation Reaction in Proton Exchange Membrane Fuel Cells. *J. Electrochem. Soc.* **2002**, *149*, A748–A753. [CrossRef]
20. Igarashi, H.; Fujino, T.; Watanabe, M. Hydrogen Electro-Oxidation on Platinum Catalysts in the Presence of Trace Carbon Monoxide. *J. Electroanal. Chem.* **1995**, *391*, 119–123. [CrossRef]
21. Akemann, W.; Friedrich, K.A.; Stimming, U. Potential-Dependence of CO Adlayer Structures on Pt(111) Electrodes in Acid Solution: Evidence for a Site Selective Charge Transfer. *J. Chem. Phys.* **2000**, *113*, 6864–6874. [CrossRef]
22. St-Pierre, J. PEMFC Contamination Model: Competitive Adsorption Followed by an Electrochemical Reaction. *J. Electrochem. Soc.* **2009**, *156*, B291–B300. [CrossRef]
23. St-Pierre, J. Proton Exchange Membrane Fuel Cell Contamination Model: Competitive Adsorption Followed by a Surface Segregated Electrochemical Reaction Leading to an Irreversibly Adsorbed Product. *J. Power Sources* **2010**, *195*, 6379–6388. [CrossRef]
24. Schiller, C.A.; Richter, F.; Gülzow, E.; Wagner, N. Relaxation Impedance as a Model for the Deactivation Mechanism of Fuel Cells Due to Carbon Monoxide Poisoning. *Phys. Chem. Chem. Phys.* **2001**, *3*, 2113–2116. [CrossRef]
25. Wagner, N.; Schulze, M. Change of Electrochemical Impedance Spectra during CO Poisoning of the Pt and Pt–Ru Anodes in a Membrane Fuel Cell (PEFC). *Electrochim. Acta* **2003**, *48*, 3899–3907. [CrossRef]
26. St-Pierre, J.; Wetton, B.; Zhai, Y.; Ge, J. Liquid Water Scavenging of PEMFC Contaminants. *J. Electrochem. Soc.* **2014**, *161*, E3357–E3364. [CrossRef]

27. Sethuraman, V.A.; Weidner, J.W. Analysis of Sulfur Poisoning on a PEM Fuel Cell Electrode. *Electrochim. Acta* **2010**, *55*, 5683–5694. [CrossRef]
28. Gould, B.D.; Bender, G.; Bethune, K.; Dorn, S.; Baturina, O.A.; Rocheleau, R.; Swider-Lyons, K.E. Operational Performance Recovery of SO[Sub 2]-Contaminated Proton Exchange Membrane Fuel Cells. *J. Electrochem. Soc.* **2010**, *157*, B1569. [CrossRef]
29. O'Brien, J.A.; Hinkley, J.T.; Donne, S.W.; Lindquist, S.E. The Electrochemical Oxidation of Aqueous Sulfur Dioxide: A Critical Review of Work with Respect to the Hybrid Sulfur Cycle. *Electrochim. Acta* **2010**, *55*, 573–591. [CrossRef]
30. Prass, S.; Hasanpour, S.; Sow, P.K.; Phillion, A.B.; Mérida, W. Microscale X-Ray Tomographic Investigation of the Interfacial Morphology between the Catalyst and Micro Porous Layers in Proton Exchange Membrane Fuel Cells. *J. Power Sources* **2016**, *319*, 82–89. [CrossRef]
31. Vidakovic-Koch, T.; Hanke-Rauschenbach, R.; Gonzales Martinez, I.; Sundmacher, K. Catalyst Layer Modelling. In *Handbook of Electrochemical Energy*; Springer: Berlin/Heidelberg, Germany, 2017; pp. 259–285.

Sample Availability: Not available.

6.3 Tolerance of Silicon Oxide-Coated Pt/C Catalyst Toward CO and H_2S Contamination in Hydrogen for Proton Exchange Membrane Fuel Cells

Sebastian Prass, Leon Nerlich, Rajveer Singh, Andres O. Godoy, Jasna Jankovic, Kaspar Andreas Friedrich, Nada Zamel

Energy Technology, Wiley-VCH GmbH, Weinheim (2023)
Special Issue Energy Research at Fraunhofer Institute for Solar Energy Systems ISE
https://onlinelibrary.wiley.com/doi/full/10.1002/ente.202300199

RESEARCH ARTICLE

Energy Technology
Generation, Conversion, Storage, Distribution
www.entechnol.de

Tolerance of Silicon Oxide-Coated Pt/C Catalyst Toward CO and H_2S Contamination in Hydrogen for Proton Exchange Membrane Fuel Cells

Sebastian Prass, Leon Nerlich, Rajveer Singh, Andres O. Godoy, Jasna Jankovic, K. Andreas Friedrich, and Nada Zamel**

Platinum on graphitized low surface area carbon (Pt/C) is coated with a silicon oxide thin film and is employed as anode catalyst to manipulate the tolerance of proton exchange membrane fuel cells toward carbon monoxide and hydrogen sulfide contamination. The SiO_2 coating, prepared by successive hydrolysis of 3-amino-propyl-triethoxisilane and tetraethoxysilane, forms clusters in proximity to Pt in sizes comparable to the catalyst particles, leaving most of the carbon surfaces free. The performance with and without CO is investigated in situ at relative humidities (RH) of 100%, 70%, and 40%. When operated with neat hydrogen, SiO_2-Pt/C shows marginally better performance owing to an improved protonic conduction due to the water retaining hydrophilic SiO_2. Upon operation with CO-contaminated fuel, the SiO_2-Pt/C performs worse than that of Pt/C particularly at high RH. CO stripping measurements reveal an increase in CO oxidation potential for the SiO_2-Pt/C, suggesting an increased CO coverage and consequently higher anode overpotentials during operation with CO-contaminated fuel. Upon operation with H_2S in the fuel, the SiO_2 coating extends the lifetime until the cell voltage broke down, which is attributed to the enhanced water retention due to SiO_2 and the solubility of sulfuric species.

1. Introduction

Polymer electrolyte fuel cells (PEMFCs) are a viable alternative to providing zero-emission electricity by conversion of the chemical energy stored in hydrogen via the redox reaction with oxygen. To facilitate the hydrogen oxidation reaction (HOR) and oxygen reduction reaction (ORR) in the anode and cathode electrodes, respectively, catalysts usually made from platinum group metals (PGM) are employed. As PGM catalysts are one of the main sources for the high costs of PEMFCs, effort is put into lowering the amount or even fully eliminating the use of PGMs by enhancing catalyst and support materials as well as electrode designs to ultimately meet cost, performance, and durability goals.[1] Promising materials include platinum (Pt) based alloys with optimized particle distribution or shape selected nanostructures, PGM-free catalysts based on cheaper, less scarce materials, but also catalyst supports with optimized composition and surface morphologies and furthermore ionomers with advanced properties.[2–4] The selection of electrode materials in combination with its fabrication process provides many possibilities to influence the efficiency and durability of the PEMFC. In addition to the electrode materials and design, impurities in fuel and oxidant gas streams constitute another obstacle in meeting the performance and durability goals. A broad spectrum of gaseous or solid, but dissolved species, influence reaction kinetics in the anode and cathode electrodes or impede the mass transport through pores as well as the proton conduction through the electrolyte.[5] For the fuel compartment, carbon monoxide

S. Prass, L. Nerlich, R. Singh, N. Zamel
Division Hydrogen Technologies
Department Fuel Cell
Fraunhofer Institute for Solar Energy Systems ISE
79110 Freiburg, Germany
E-mail: sebastian.prass@ise.fraunhofer.de;
nada.zamel@ise.fraunhofer.de

The ORCID identification number(s) for the author(s) of this article can be found under https://doi.org/10.1002/ente.202300199.

DOI: 10.1002/ente.202300199

A. O. Godoy, J. Jankovic
Materials Science and Engineering Department
Center for Clean Energy Engineering and Institute for Materials Science
University of Connecticut
Storrs, CT 06269, USA

K. A. Friedrich
Institute of Engineering Thermodynamics
German Aerospace Center
70569 Stuttgart, Germany

K. A. Friedrich
Institute for Building Energetics
Thermotechnology and Energy Storage
University of Stuttgart
70569 Stuttgart, Germany

(CO) inevitably present in hydrogen obtained by reforming plays a significant role as it readily adsorbs on Pt surfaces in the anode electrode, competes with the HOR for active sites, and induces a voltage loss already at low concentrations.[6] The tolerance of the anode electrode versus CO contamination can be improved by alloying the Pt catalyst with oxophilic metals such as, e.g., ruthenium (Ru), which either weaken the bond between CO and Pt and/or provide hydroxyl groups (OH) required for CO oxidation.[7] Unfortunately, oxophilic metals known to improve the CO tolerance tend to leach out of the catalyst particle leaving a Pt-enriched shell.[8–13] Furthermore, these catalysts do not work similarly when it comes to contamination with sulfuric species such as hydrogen sulfide (H_2S) potentially present in smallest concentrations in hydrogen from decarbonized fossil fuels.[14] The dissociative adsorption of H_2S on electrocatalysts leaves elemental sulfur, which also competes with HOR and results in a complete cell voltage breakdown if no recovery measures are employed.[15] Specific recovery protocols but also shut-downs and start-ups can help to recover the PEMFC performance, in which oxygen species and water play central roles for oxidation and dissolution of sulfur species; however, a delay or even elimination of a cell voltage breakdown is preferable.[16]

A promising alternative with the potential of addressing both the stability and contamination issues of electrocatalysts are thin functional coatings on catalyst and support particles. Various types of coatings made from organic polymers, inorganic carbon nano-shells, or metal oxide layers fabricated via different chemical or physical deposition processes have shown to either improve stability, selectivity, processability, or the performance of electrocatalysts at specific operating conditions.[17] One of these coatings is based on silicon oxide (referred to as SiO_2 hereinafter) applied onto the catalyst via hydrolysis of silicon-containing precursors such as 3-aminopropyl-triethoxisilane (APTES), tetraethoxysilane (TEOS), and methyltriethoxysilane (MTEOS).[18,19] When employed on electrocatalysts, such SiO_2 coatings showed to protect the catalysts from dissolution and improved the PEMFC performance particularly at low relative humidity (RH) conditions.[20–26] In these regards, Yu et al. used this coating over PtRu catalysts to protect the Ru from dissolution, such that the catalyst maintained the improved CO tolerance during accelerated stress tests.[20] Aside from the application as a coating, SiO_2 can also be integrated as an additive to the proton exchange membrane (PEM) or electrode in form of silica particles or aerogel, or as a mesoporous support for the metal catalyst.[27,28] If applied as an additive, SiO_2 affects the water retention capacity and PEMFC performance at low RH conditions,[29,30] while as a support, it eventually promotes the oxidation of CO on Pt.[31] For the latter, the silanol (Si–OH) terminated surfaces of the SiO_2 were found to provide OH groups for CO oxidation, if the catalyst particles were incorporated into the mesoporous structure of the SiO_2. However, although several features provided by a SiO_2 coating appear promising, the effect of the coating itself on the tolerance of a Pt/C catalyst versus PEMFC fuel contaminants such as CO or H_2S has not been investigated yet and therefore is objective of this work.

In the present study, commercially available Pt/C was coated with SiO_2 and employed as anode catalyst in PEMFCs operated with CO and H_2S-contaminated fuel to investigate the effect of the coating on the contaminant tolerance. The underlying hypothesis of this study is that the SiO_2 either acts as adsorption barrier or that it alters the availability of water and OH groups required for oxidation or dissolution of CO or sulfuric species adsorbed on Pt surfaces, respectively. Transmission electron microscopy (TEM) and scanning electron microscopy (SEM), both coupled with energy-dispersive X-ray spectroscopy (EDX), were employed to examine the structure and composition of the coated catalyst. The effect on performance, ECSA, and CO oxidation potentials were evaluated in a PEMFC operated with CO or H_2S-contaminated H_2 fuel and Air at various relative humidities (RH).

2. Results and Discussion

2.1. Structure of SiO_2-Coated Pt/C

Catalyst particles were analyzed by conventional TEM and STEM-EDX to assess the structure and elemental distribution of SiO_2 on the Pt/C particles. **Figure 1** shows representative particles of both uncoated (Pt/C) and coated (SiO_2-Pt/C) particles and in the insets magnifications of their carbon support surfaces.

For both, Pt/C and SiO_2-Pt/C, the dark platinum particles with diameters ranging from 2 to 10 nm are visible on the carbon supports, where they appear to be partly embedded in the multilayer graphene surface. The graphene layers shown in the insets were visible in various thicknesses throughout the carbon surfaces of Pt/C and SiO_2-Pt/C and cannot be assigned to the SiO_2 coating or an effect of the coating process. For some studies, the SiO_2 coatings could be distinguished from the carbon by their different structures. In case of carbon nanotubes (CNTs) as support, the amorphous SiO_2 could be distinguished from the regular graphene layers by the sheer structure,[19,21] whereas for studies employing carbon black (CB) as support, this was rather difficult because the carbon structures were as irregular as the SiO_2 such that the identification of the coating relied on the EDX mappings.[20,22] For all these studies, SiO_2 coating thicknesses of few, single digit nanometers were reported either in a homogeneous distribution over catalyst and support material in case of the CNTs or selectively covering the catalyst particles in case of the CB supports. For the present work, the SiO_2 distribution was also qualitatively evaluated from TEM-EDX measurements such as shown in **Figure 2** presenting elemental mappings of C, Pt, Si, and O of the Pt/C and SiO_2-Pt/C catalysts.

The Pt/C elemental maps show red Pt particles distributed in various sizes on the blue C support, with scattered green Si signals throughout the C and Pt particles. In the EDX spectra of the Pt/C particles, no Si peak (Kα lines at 1.74 keV) was visible and therefore the scattered Si signals are considered noise falsely assigned to Si. On the SiO_2-Pt/C particles, consolidated Si signals in proximity to Pt particles are visible, which in combination of significant Si peaks in the spectra were assigned to SiO_2 clusters that developed on spots favored for condensation of the Si-precursors. From the EDX-maps, SiO_2 clusters in sizes close to Pt particle sizes or layer thicknesses below 1 nm can only be estimated. During the successive hydrolysis of the precursors, the amino groups of APTES should adsorb uniformly over both catalyst and support surfaces dispersed in an alkaline matrix, while TEOS should form the multilayer SiO_2 coating on the

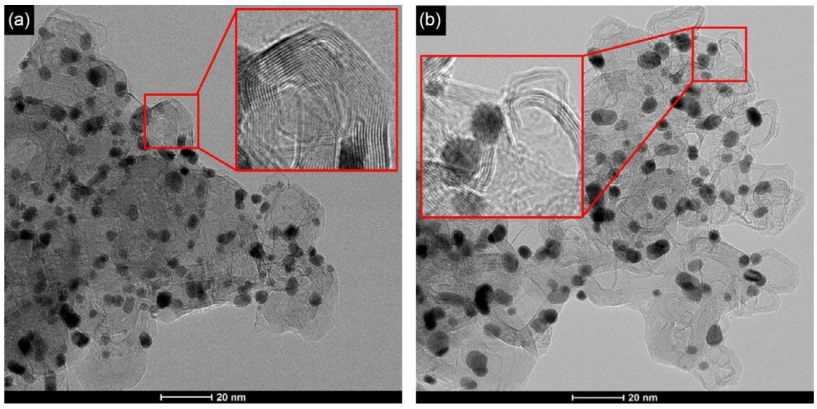

Figure 1. TEM image of a) Pt/C and b) SiO_2-Pt/C particle with insets magnifying the multilayered graphitic carbon support surfaces and black Pt particles appearing partially embedded in the carbon surfaces.

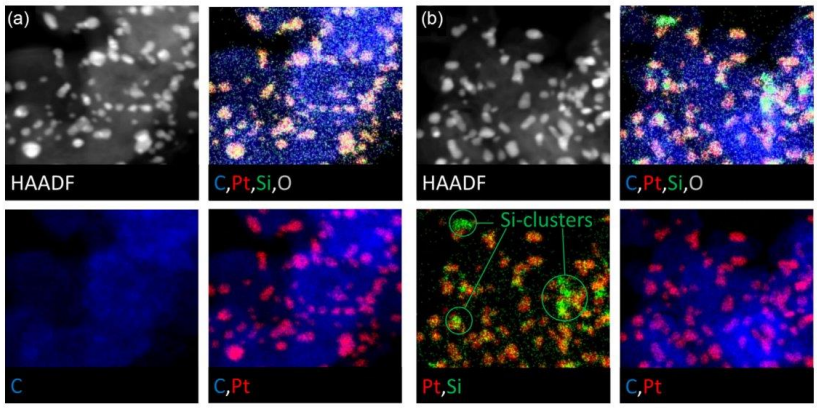

Figure 2. TEM-EDX elemental distributions of a) Pt/C and b) SiO_2-Pt/C particles, the latter showing Si-clusters in proximity to Pt particles.

nucleation sites provided by APTES. The TEM-EDX elemental mappings of multiple samples, however, showed these Si clusters in proximity to catalyst particles with most of the carbon but also Pt surfaces left free. Although this result is different from comparable studies using CNTs with graphitic surfaces as catalyst support, it is expected to be favorable for electron conduction because noncoated carbon surfaces are free of the nonconductive SiO_2 coating, while at least some Pt particles seem to be coated by or in proximity to SiO_2 clusters. From TEM images, the average Pt particle size was determined as 4.91 ± 2.2 and 5.01 ± 1.62 nm for the Pt/C and the SiO_2-Pt/C catalyst, respectively, with a marginally shifted particle size distribution for the SiO_2-Pt/C (Figure S1, Supporting Information). The slight shift in particle size distribution for the SiO_2-Pt/C can be attributed to the process steps of the SiO_2 deposition; however, the average Pt particle sizes are within the standard deviation and therefore this shift is considered insignificant. In general, the mass activity of electrocatalysts depends on the particle sizes, with a maximum activity at about 2–4 nm for ORR on polycrystalline Pt. This maximum is a result of the balance between strong and too strong adsorption of oxygen species on catalyst surfaces with decreasing particle sizes and a conversely increasing oxophilicity.[32] Extrapolated to the anode electrode operated with CO-contaminated fuel, the ability to provide more OH groups required for CO oxidation on smaller catalyst particles could be preferred and consequently, the slight shift in catalyst particle size distribution of the SiO_2-Pt/C eventually appears disadvantageous.[33] On the other hand, SiO_2 surfaces also provide the ability to

Table 1. Compositions of Pt/C and SiO_2-Pt/C catalyst powders from SEM-EDX analysis.

Catalyst	Si [wt.%]	O [wt.%]	Pt [wt.%]	C [wt.%]
Pt/C	0.0	3.3	21.6	74.7
SiO_2-Pt/C	0.6	3.3	20.3	75.8

forming Si-OH groups from dissociative chemisorption of water or hydronium ions,[34] which could benefit the CO or H_2S tolerance. Here, the morphology difference to the reported studies presumably is a result of the relatively low average Si concentration in the SiO_2-Pt/C acquired by SEM-EDX (**Table 1**).

The measured Si loading of ≈0.6 wt% is low as compared to values ranging from 0.3 to 40 wt% reported in other studies on similar types of SiO_2 coatings.[18,19,21–24,26] The comparably low concentration is assumed to either stem from adsorption of APTES and TEOS on container surfaces during the coating process or from unreacted reagent removed during the washing procedure at the end of the hydrolysis step. Whether the electrocatalyst stability and performance are enhanced, likely depends on the thickness, pore structure, and hydrophilicity of the SiO_2 coating, being a function of the precursor types, their amount and on the settings during the fabrication process. For example, a hydrogen-rich environment during calcination promotes hydrophobic Si–H rather than hydrophilic Si–OH terminated surfaces, while residual molecules can further exist in the thin film depending on the used precursors.[19,35] Coatings made from APTES and MTEOS were found to provide larger and more hydrophobic pore structures owing to methyl groups left in the coating, as compared to coatings made from APTES and TEOS, which can be beneficial for reactant transport and product discharge in the PEMFC cathode. It should be noted that these thin films comprise of non-stoichiometric SiO_2 that interact with the underlying catalyst, features ascribed to the selection of precursors and the calcination step during fabrication.[20,26] Generally, for studies with the objective to enhance catalyst stability via SiO_2 coatings, full coverage of the catalyst and support with a thick layer seems advantageous to provide complete protection versus catalyst dissolution and carbon corrosion. If the effect on the performance at varying RH conditions is in focus, thinner layers of SiO_2 could be beneficial, since the surface wettability is already affected by a low SiO_2 content or thin monolayer on the carbon and catalyst surfaces, without altering the diffusion resistances by the coating itself.[26] Similarly, a low SiO_2 thickness and consequently loading could suffice to provide the anticipated effect of the coating versus CO and H_2S contamination, and therefore, these materials were used for the in situ contamination tests.

2.2. Electrochemical Characterization of Electrodes

Figure 3 shows CV measurements of the cathode and anode electrodes with and without SiO_2, with magnified voltammograms of the anode electrodes as well as the ECSA evaluated from H_{UPD}. Redox peaks of hydrogen evolution and oxidation reaction (HER and HOR, at potentials <400 mV), Pt oxidation and reduction (>600 mV) as well as double layer charging (400–600 mV) are visible for all CVs. The measured current densities of the anode

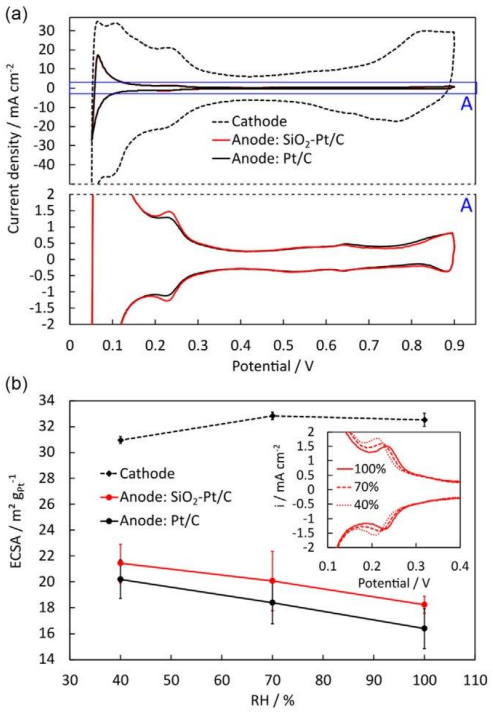

Figure 3. a) Cyclic voltammograms of each a cathode and anode electrode with and without SiO_2 at 100% RH and b) average ECSA of all characterized MEAs at 40%, 70%, and 100% RH with the inset showing the changes in the hydrogen adsorption/desorption region associated to the adsorption of SO_3^- groups.

electrodes are significantly lower as compared to the cathode electrode because the lower loaded anode electrode provides fewer catalyst and support surfaces for the electrochemical processes to occur. This circumstance can create difficulties for evaluation of the anode ECSA because artifact currents such as the signal to noise ratio and relatively augmented HER and HOR of hydrogen evolved in the WE can appear enlarged for low loaded electrodes at potentials less than 0.15 V.[36] However, when varying the potentials for integration of the charges transferred, only the magnitudes of the ECSA changed while the trends remained the same. Therefore, the ECSA presented here was evaluated from both hydrogen adsorption and desorption between the typical potentials of 90–400 mV. Consequently, the ECSA is likely overestimated due to increased HER/HOR charges at potentials below 150 mV for both anode electrode types.

From the ECSA, two observations should be noted. First, the ECSA of the SiO_2-Pt/C and Pt/C increases from ≈18.2 and 16.4 $m^2 g_{Pt}^{-1}$ to ≈21.4 and 20.2 $m^2 g_{Pt}^{-1}$ (corresponding to 17% and 23% increase), respectively, with the decrease in

humidity from 100% to 40%. Usually, the opposite is observed with catalysts on high surface area carbons, where the decrease in ECSA with lower RH is associated to catalyst particles hidden in carbon nanopores or catalyst clusters without contact to the proton conducting ionomer.[37,38] At high RH, water on surfaces and in pores inherits the proton conduction and provides the hidden catalyst particles with protons for H_{UPD}. At low RH, these protonic pathways are absent and such catalyst particles cannot be reached by protons. In this study, a Pt catalyst on graphitized carbon with low surface area was employed, where most of Pt particles are located on the carbon surfaces, ideally in contact with the ionomer and available for H_{UPD}, if the ionomer is well distributed in the electrode. In such a case, the ECSA would be expected to remain approximately constant across the RH values. However, the ECSA reported here increases, which is a consequence of the shift in the potential and current density of the peaks with lower RH values shown in Figure 3b) inset. We believe that this shift can be attributed to sulfuric acid head groups (SO_3^-) of the ionomer, which adsorb and desorb during potential sweeps in the H_{UPD} region.[39] As the adsorption strength of these anionic groups depends on the water content, the charge density at the Pt surfaces varies with RH and creates the observed increase in ECSA when the lower integration limit is kept at 90 mV. The second unexpected observation is that the SiO_2-Pt/C ECSA is about ≈10% higher than the ECSA of the Pt/C throughout the tested RH conditions, which typically comes with a lower ECSA at equal Pt loading (exact loading values 75 ± 4 versus $76 \pm 4\,\mu g_{Pt}\,cm^{-2}$ for Pt/C and SiO_2-Pt/C, respectively). Comparable studies reported a lower ECSA for SiO_2-coated catalysts and associated this to the coverage of catalyst surfaces by thick SiO_2 coatings limiting the accessibility for reactants.[20,25] In the present study, the comparably thin and nonuniformly deposited SiO_2 in combination with its hydrophilic nature, specifically when it stems from hydrolysis of APTES and TEOS,[19] could allow for improved water retention in the electrode and, thus, improve protonic connection of Pt particles which are otherwise not in contact to the ionomer. The presence of the low amounts of SiO_2 therefore could lead to an improved accessibility of the catalyst particles. In turn, this would indicate an improper distribution of ionomer indicated by the lower ECSA for the Pt/C electrodes. However, independent of the explanations for the two unexpected observations made with ECSA from H_{UPD}, the SiO_2-Pt/C electrodes providing a higher ECSA would be expected to perform better upon operation with CO-contaminated fuel, as the available ECSA is one of the crucial parameters determining the CO and H_2S tolerances.[6]

2.3. Performance in Neat H_2

Figure 4 shows polarization curves including the HFR of the Pt/C and SiO_2-Pt/C MEAs operated with neat and CO-contaminated H_2 on the anode and air on the cathode side at RH values of 100%, 70%, and 40%. For better visualization, the insets show the difference in current densities between the MEAs types at three cell voltages of 0.8, 0.5, and 0.2 V resembling activation, ohmic, and mass transport loss dominated regions, with the color signifying which MEA shows better performance.

Upon operation with neat H_2 (Figure 4a)), the MEAs with and without SiO_2 in the anode electrode show an almost similar performance considering the standard deviation represented by the error bars. A slight improvement for the SiO_2-Pt/C becomes apparent at higher current densities for all RH conditions as emphasized by the insets. This improvement is a consequence of the approximately 1%–3% lower HFR for SiO_2-Pt/C, resulting in a nearly proportional increase of the differences in current density up to about $0.06\,A\,cm^{-2}$ at 0.2 V of the polarization curve at 70% RH. Generally, SiO_2 is known to improve water retention due its comparably hydrophilic nature particularly if surfaces are terminated with OH groups, which can be of help especially during low RH operation.[30] This beneficial effect though depends on how the SiO_2 is incorporated into the electrodes or the PEM, on its concentration as well as on the operating conditions of the PEMFC. When employed as a coating such as in the present study, SiO_2 can provide improved water retention capabilities, but hinder electron conduction as it was observed in the study by Fujii et al.[22] The authors measured an increased HFR and electrode resistivity and attributed it to the electrically insulating character of the SiO_2 coating, which in their case was comparably thick (5 nm), in high concentration (40 wt% silica determined from ICP-AES) and homogeneously distributed also over the carbon support surfaces. At lower concentrations and adjusted ionomer contents in the cathode electrode, SiO_2-containing MEAs can provide better performances at low RH conditions, but also limited mass transport at high RH values and current densities.[23,24] In the present work, the effect on water retention appears to excel effect of the SiO_2 on electronic or reactant diffusion resistances visible in the slightly better performance in neat H_2.

Upon operation with 1 ppm CO in H_2 (Figure 4b)), the polarization curves show the typical trend with elevated CO concentrations, that is, (1) the regular voltage decay at low current densities arising mainly due to the activation of the catalyst for ORR in the cathode electrode, (2) a relatively sudden drop at voltages below approximately 0.7 V, and (3) the relaxation from the drop at potentials <0.4 V. Generally, CO strongly adsorbs on Pt and competes with HOR for active sites

$$Pt + CO \leftrightarrow Pt - CO_{ads} \tag{1}$$

At low current densities, the fraction of Pt covered and blocked by CO, being a function of the concentration and the rate of oxidation with OH groups or crossover oxygen, leaves yet sufficient Pt sites vacant to maintain the required HOR.[40,41] With higher current densities, the sudden drop arises as a result of the competition between HOR and CO blocking Pt sites, giving rise to a higher anode overpotential and total cell impedance with CO (e.g., Figure S2, Supporting Information, for the case of $1\,A\,cm^{-2}$). With increasing current density, the anode overpotential increases until the anode reaches potentials sufficiently high to accelerate CO oxidation. CO electrooxidation on catalysts such as Pt generally involves water adsorbing and oxidating on active catalyst sites to forming OH groups, which then oxidize adsorbed CO molecules on neighboring catalyst sites:

$$Pt + H_2O \leftrightarrow Pt - OH_{ads} + H^+ + e^- \tag{2}$$

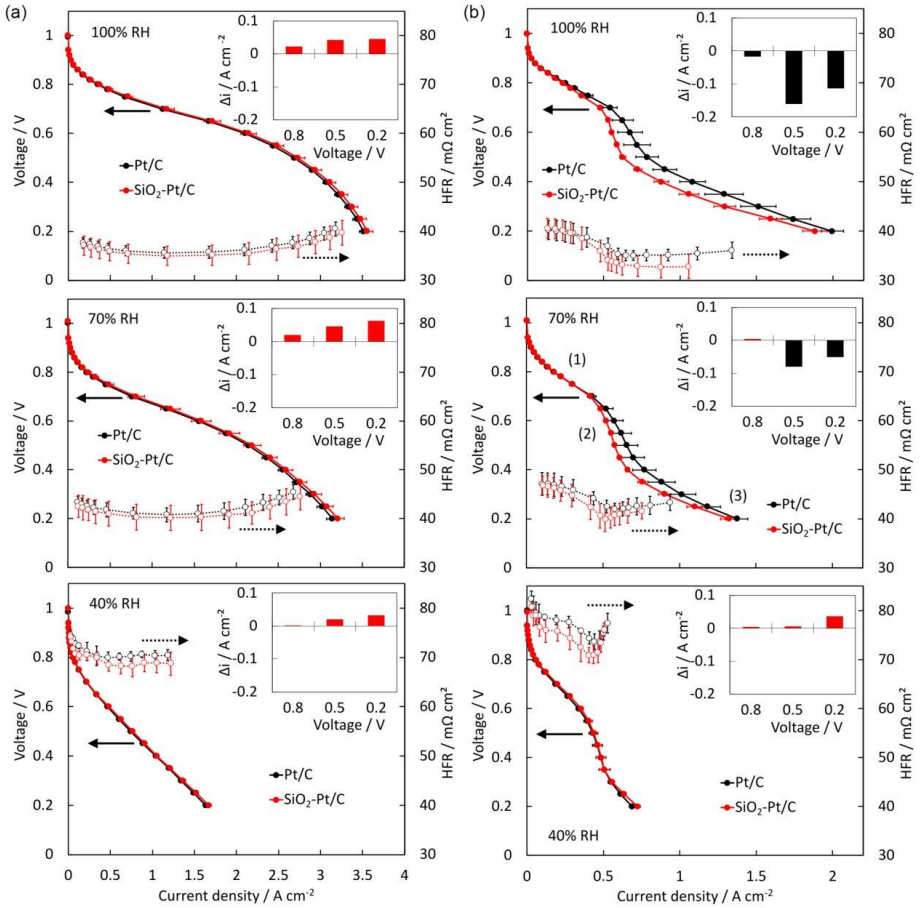

Figure 4. Polarization curves and HFR at 100%, 70%, and 40% RH with neat a) H_2 and b) 1 ppm CO supplied to the anode. Insets showing the difference between MEAs with and without SiO_2 coating (red bars—SiO_2-Pt/C exhibiting better performance).

$$Pt - CO_{ads} + Pt - OH_{ads} \leftrightarrow 2Pt + CO_2 + H^+ + e^- \quad (3)$$

The kinetics of CO oxidation on Pt and other catalysts depends on several factors such as the surface structures and compositions of both catalyst and its support, the operating temperature, and RH.[11,42–45] On Pt, the CO oxidation potential can range from approximately 0.35 to 0.7 V versus RHE for specific facets, with lower potentials indicating that less energy is required to oxidize CO.[46] From the polarization curves presented here, SiO_2 being present as a coating in the anode electrode deteriorates the PEMFC performance particularly at elevated RH values. At low current densities <0.5 A cm^{-2}, the MEAs perform practically similar; however, the drop in performance due to CO contamination commences for the SiO_2-Pt/C MEAs at lower current densities and more abruptly at intermediate potentials (between 0.65 and 0.7 V) at 70% and 100% RH. For all RH values, the HFR of the SiO_2-Pt/C MEA is lower at higher current densities and equal to the HFR of the Pt/C MEA at low current densities. The differences in current density at a given cell potential decrease with RH, e.g., from approximately 0.15, 0.08, and 0 A cm^{-2} at 0.5 V for the polarization curves at 100%, 70%, and 40% RH, respectively. With lower RH, the water retaining and HFR lowering effect of the SiO_2 supersede the negative effect on CO tolerance, such that the polarization curves at 40% RH are practically similar. These results indicate a negative impact of the SiO_2 coating toward the CO tolerance of the catalyst, which is more prominent than its beneficial effect on the

protonic conductivity of the ionomer at elevated RH values, while for low RH, these trends are counterbalanced. Considering the evaluated 10% higher ECSA for the SiO_2-Pt/C electrode determined by H_{UPD}, the coating must negatively influence the CO oxidation potential to explain this divergence. To evaluate the oxidation potential, CO stripping was conducted at 100%, 70%, and 40% RH with the SiO_2-Pt/C and Pt/C anode electrodes as WE. **Figure 5** shows the anodic and cathodic potential sweep of the first CV cycle with a focus on the CO oxidation peak between potentials of 0.55 and 0.7 V.

Upon the start of the anodic sweep at 0.1 V, close to zero charge transfer is measured until CO oxidation commences at about 0.55 V. Once CO is oxidized and catalyst surfaces are vacant, HOR of crossover H_2 occurs, until Pt oxides form above 0.7 V and passivate the catalyst for the HOR, resulting in the current density drop between 0.7 and 0.95 V.[36] During the reverse cathodic scan, Pt oxide reduction and the resumption of HOR of crossover H_2 occur from 0.8 to 0.6 V, followed by double-layer charging (between 0.3 and 0.5 V) and H_{UPD} and HER from 0.3 to 0.1 V. As can be seen in Figure 5b), the potential onset, where the CO oxidation starts, is lower for Pt/C at all RH conditions. The largest difference of approximately 20 mV (0.54 V versus 0.56 V for the SiO_2-Pt/C) is visible at 100% RH, and the difference decreases with RH to about 2–3 mV at 40% RH. Such an increase in CO oxidation potential was also observed by Yu et al., who investigated the stability enhancing effect by a SiO_2 coating on PtRu catalysts.[20] This change in the onsets of CO oxidation correlates well to trend in the polarization curves with CO-contaminated fuel measured in this work. Though the CO stripping measurements give no information on the actual CO coverage during PEMFC operation with H_2 and air, they indicate that CO on SiO_2-coated Pt/C requires more energy to oxidize and therefore will cause higher anode overpotentials. Based on the investigations by Fukuoka et al. on preferential oxidation (PROX) of CO on Pt catalysts supported on various types of (silicon based) materials, the electronic states of CO on Pt surfaces were essentially the same when applied onto different supports, but the activities of the support toward O_2 adsorption and formation of oxygenated species such as silanol were found to vary with the support.[31] Projected onto the results presented here, the higher CO oxidation potential and worse PEMFC performance would not stem from a stronger bond of CO on Pt, but rather from interactions between SiO_2 and oxygen species, possibly leading to a hindered formation or mobility of OH on catalyst or support surfaces and consequently to a complete oxidation of CO only at higher potentials. In addition, adsorption of CO on the SiO_2 surface and a spillover onto catalyst sites are possible, which could further add to the observed worse performance of SiO_2-Pt/C.[47] Considering these results in combination to the comparably low Si loading of the SiO_2-Pt/C, a positive effect of higher SiO_2 loadings on the CO tolerance seems unlikely for the silicon precursors and fabrication procedure used in this work.

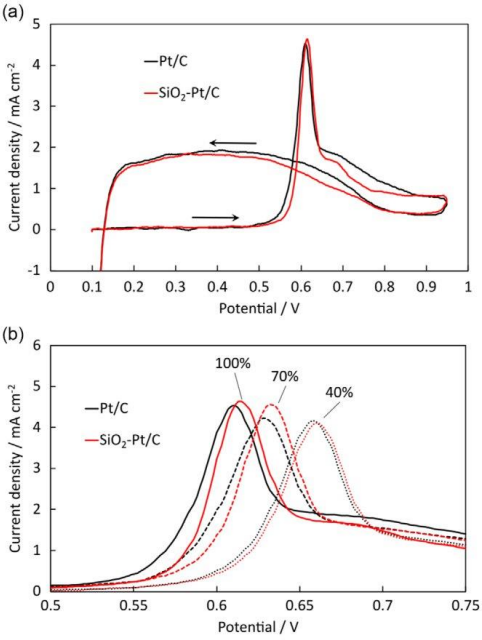

Figure 5. CO stripping voltammetry at 20 mV s^{-1} sweep rate of Pt/C and SiO_2-Pt/C electrodes a) at 100% RH and b) magnification on the CO oxidation peaks at three RH values. The CO was preadsorbed at 0.05 V for 10 min to allow for complete CO coverage before commencing the CO stripping.

2.4. H_2S Tolerance of SiO_2-Pt/C

Although the SiO_2 coating negatively affects the performance upon operation with CO-contaminated fuel, an opposite effect was visible with respect to H_2S contamination. **Figure 6** presents the cell voltage trends of Pt/C and SiO_2-Pt/C MEAs at constant galvanostatic operation of 1 A cm^{-2} and 40% RH with 75 ppb

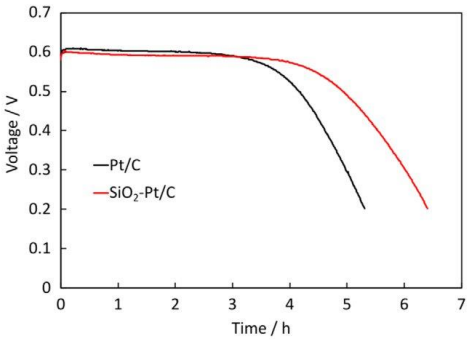

Figure 6. Cell voltages of SiO_2-Pt/C and Pt/C MEAs at 1 A cm^{-2} and 40% RH with 75 ppm H_2S in H_2, with the typically observed cell voltage breakdown due to sulfur poisoning after several hours of operation.

H_2S in the fuel showing the typical voltage drop due to sulfur poisoning of the anode electrode.

The multistep dissociative adsorption of H_2S on Pt (and other electrocatalysts) leaves elemental sulfur, which also competes with the HOR for active catalyst sites:

$$Pt + H_2S \leftrightarrow Pt - S_{ads} + 2H^+ + 2e^- \quad (4)$$

The oxidation of sulfur on Pt requires significantly higher potentials as compared to the oxidation of CO and typically shows two oxidation peaks occurring between 0.8 and 1.2 V versus RHE during CV measurement of a sulfur-contaminated electrode. These two peaks are assigned to the oxidation of linear and bridge bonded sulfur, i.e., sulfur atoms blocking one or two Pt atoms and requiring more or less energy for oxidation.[15] Sulfur adsorbed on Pt catalyst can oxidize with water toward oxidized sulfur species as proposed by Loučka et al.[48]

$$Pt - S_{ads} + 3H_2O \leftrightarrow SO_3 + Pt + 6H^+ + 6e^- \quad (5)$$

$$Pt - S_{ads} + 4H_2O \leftrightarrow SO_4^{2-} + Pt + 8H^+ + 6e^- \quad (6)$$

The formation of linear or bridge bonded sulfur depends on temperature and the water content in the electrode, and consequently their oxidation potentials varies with these parameters.[49,50] With higher temperatures and RH, the oxidation potential for sulfur on Pt shifts slightly toward lower potentials, e.g., from about 0.96 to 0.84 V versus RHE for the oxidation peak of bridge-bonded sulfur with the increase in temperature from 50 to 90 °C. Although these potentials are typically not reached by the anode electrode unless specific events like fuel starvation or cyclic voltammetry force the potential to such values, the trend with RH points toward the beneficial effect that water has on sulfur contamination in general. This can also be seen during operation of the PEMFC with H_2S-contaminated fuel, where an increase in the RH extends the durability until the voltage break down occurs.[51] During operation, a fraction of the sulfur species eventually reacts toward soluble oxidized sulfur species such as sulfate (SO_4^{2-}), allowing for scavenging with liquid water eventually and a partial recovery from the contamination.[52] In addition, a spillover of oxidized sulfur species from the Pt catalyst to the SiO_2 surfaces is possible, where further oxidation and formation of sulfate is possible.[53] This interaction between oxidized sulfur species and the SiO_2 coating and surface groups could explain the different behavior of the SiO_2 with respect to the tolerance versus CO and H_2S contamination. Ultimately, the delayed voltage drop of the SiO_2-Pt/C upon exposure to H_2S-contaminated fuel indicates a positive influence of the SiO_2 coating, which can be attributed to the enhanced water retention and a facilitated oxidation and dissolution of sulfur species due to the SiO_2 in electrode. However, instead of the rather complex coating process via hydrolysis of silicon containing precursors, the simple addition of silica or aero gel to the anode electrode during paste or ink fabrication could eventually provide a comparable water retaining and potentially H_2S tolerance enhancing effect, which would have to be confirmed in further investigations.[29]

3. Conclusion

Pt metal catalyst particles supported on graphitized carbon (Pt/C) have been coated with silicon oxide (SiO_2) to investigate the effect of the coating on the tolerance versus carbon monoxide (CO) and hydrogen sulfide (H_2S) when employed as catalyst in the anode electrode of a PEMFC. Small clusters of SiO_2 formed on and in proximity to Pt catalyst particles of comparable sizes, such that most of the carbon and Pt surfaces were uncoated. Despite similar Pt loadings per area, the SiO_2-Pt/C revealed a larger ECSA evaluated from H_{UPD} throughout relative humidities (RH) of 40%, 70%, and 100%, which is associated to the water retaining character of the SiO_2, affecting the accessibility of Pt particles during CV measurements. Upon operation in neat H_2, the SiO_2-Pt/C showed marginally better performance due to a 1%–3% lower cell resistance based on the water retaining character of SiO_2. However, the performance was worse for the SiO_2-Pt/C MEAs with 1 ppm CO in the fuel at high RH (70% and 100%), and comparable for low RH (40%) conditions despite the higher anode ECSA. CO stripping measurements revealed elevated onsets of CO oxidation for the SiO_2-Pt/C particularly at high RH, suggesting either a hindrance of OH formation or of the mobility of CO and OH on the catalyst, which are required for CO oxidation. The SiO_2 coating though extended the durability of the PEMFC upon operation with 75 ppb H_2S in the fuel by approximately 20%, which can be attributed to the water retaining character of the SiO_2, and furthermore to interactions between oxidized sulfur species and the coating. Overall, the SiO_2 coating negatively influences the CO tolerance of a Pt/C catalyst, but positively the water retention and coherent protonic resistance, and furthermore the H_2S tolerance of a PEMFC anode electrode. Hence, side effects such as a diminished or improved tolerance versus specific contaminants or enhanced water retention should to be taken into consideration when designing electrodes including SiO_2 coatings of electrocatalysts, which are intended to improve the catalyst stability versus degradation.

4. Experimental Section

Synthesis of the SiO_2-Pt/C Powder and Fabrication of the Membrane Electrode Assembly (MEA): Two types of MEAs were fabricated for this study, with the only difference being the anode electrode with or without SiO_2 coating on the carbon-supported catalyst (Pt/C). For the cathode electrodes, Umicore Pt50 0550 catalyst powder with 50 wt% Pt on carbon was used as received. For the anode electrodes, Umicore Pt20 0390 catalyst powder (both types purchased from Umicore) with 20 wt% Pt on graphitized carbon support was used as base material. The anode catalyst powder was coated with SiO_2 by successive hydrolysis of 3-aminopropyltriethoxysilane (APTES) and tetraethoxysilane (TEOS, purchased from Carl Roth Chemicals) without further optimizing the SiO_2 thickness following the procedure by Takenaka et al.[21] In brief, catalyst powder (0.7 g) was ultrasonicated in 50% ethanol and deionized (DI) water (1.4 L) for 10 min. The dispersion was heated to 60 °C and the pH adjusted to ≈11 by addition of trimethylamine (TEA, also purchased from Carl Roth Chemicals). APTES (0.077 mmol) was added to the dispersion and stirred for 1 h followed by the addition of TEOS (10.08 mmol) and further stirring for 3 h at 60 °C to allow for the hydrolysis to proceed. After hydrolysis, unreacted reagent was removed by repeated centrifugation and dispersion of the slurry in fresh DI-water. After the washing procedure, the slurry was dried overnight in air before its calcination in nitrogen (N_2) atmosphere for 3 h at 623 K to obtain SiO_2-coated Pt/C catalyst denoted

as SiO_2-Pt/C hereinafter. The reference Pt/C anode catalyst was introduced in a separate vessel in the calcination oven to exert a similar heat treatment and eventual catalyst sintering. The dry SiO_2-Pt/C powder was ball-milled to breakdown agglomerates and acquire a fine powder before preparation of the catalyst ink for the electrode printing process.

Catalyst pastes for anode and cathode electrodes were prepared in similar manner by mixing the respective catalyst powder (0.6 g) in water and alcohols (ethylene glycol, 1-methoxy-2-propanol) with Aquivion D79—25BS (25 wt% in water, purchased from Sigma-Aldrich Chemie GmbH) using an axisymmetric centrifuge (SpeedMixer, Hauschild GmbH & Co. KG) and magnetic stirring. For all pastes, the same solvents and ionomer content in the electrode (30 wt%) were employed. These pastes were screen printed onto glass fiber-reinforced PTFE decals with target loadings of 0.07 and 0.55 $mg_{Pt}\,cm^{-2}$ for anode and cathode electrodes, respectively. Each an anode and cathode decal was hot pressed (at 10 bar and 180 °C for 15 min) onto an automotive PEM (FS-715-RFS chemically and mechanically stabilized membrane with 15 µm thickness received from Fumatech BWT) to fabricate the catalyst-coated membrane (CCM). These CCMs were framed in a gasket (Teonex, purchased from CMC Klebetechnik GmbH) and assembled with two Freudenberg H23C9 gas diffusion layers (GDLs) to form the membrane electrode assembly (MEA).

Analysis of Catalyst Material: The elemental compositions of the Pt/C powders with and without SiO_2 were analyzed via scanning electron microscope coupled with energy-dispersive X-ray spectroscopy (SEM-EDX, FEI Quanta 400 with EDAX EDX) at Fraunhofer ISE. Scanning transmission electron microscopy (STEM) with EDX spectroscopy was performed at the University of Connecticut using a Thermo Fisher Scientific Talos F200X STEM, equipped with Bruker Super-X four silicon drift detectors for EDX spectrometry (Super-X SDD EDXS) to acquire structural information and local SiO_2 distribution of the coated Pt/C particles.

Electrochemical Measurements: Electrochemical measurements were conducted on an inhouse built testbench (equipped with Zahner Zennium Pro potentiostat and Kikusui PLZ664WA electric load for electrochemical and performance tests) using a baltic HighAmp qCF single cell (12 cm^2 active area and linear flow field). Polarization curves were carried out at 5 and 2 L min^{-1} air and H_2 with and without 1 ppm CO from open-circuit voltage (OCV) to 0.2 V in 10 mV (OCV–0.7 V) and 20 mV (0.7–0.2 V) decrements with sufficient hold time per load point until the current remained constant (less than 100 mA min^{-1} change, minimum 8 min hold time). For tests with 75 ppb H_2S-contaminated fuel, the cells were operated at 1 A cm^{-2} to provoke a cell voltage breakdown. The ECSA was determined from hydrogen underpotential deposition (H_{UPD}) measured via cyclic voltammetry (CV) in H_2 and N_2 atmosphere with the N_2 flow switched off during voltage sweep at a scan rate of 100 mV s^{-1}. For the CO stripping measurements, the working electrode (WE) was conditioned with 1% CO in N_2 prior to the potential sweep at a scan rate of 20 mV s^{-1}. Electrochemical impedance spectroscopy (EIS) was used for evaluation of the high-frequency resistance (HFR) during polarization curves. All measurements were carried out at 80 °C and RH conditions given in the respective plots in the following sections. For analysis of the anode electrode, the MEA was turned in the cell such that the anode became the WE and the cathode the counter electrode (CE). The polarization curves including HFR and the ECSA from H_{UPD} presented here resemble averages of three tested MEAs with the standard deviation as error bars.

Supporting Information

Supporting Information is available from the Wiley Online Library or from the author.

Acknowledgements

This work was supported by the German Federal Ministry for Digital and Transport within the project H_2 Fuel, contract No. 03B11014C.

Open Access funding enabled and organized by Projekt DEAL.

Conflict of Interest

The authors declare no conflict of interest.

Data Availability Statement

The data that support the findings of this study are available from the corresponding author upon reasonable request.

Keywords

carbon monoxide, fuel cell anodes, hydrogen sulfide, platinum on carbon catalyst, silicon oxide coating

Received: February 25, 2023
Revised: May 26, 2023
Published online:

[1] A. Kongkanand, M. F. Mathias, *J. Phys. Chem.* **2016**, *7*, 1127.
[2] Y. Sun, S. Polani, F. Luo, S. Ott, P. Strasser, F. Dionigi, *Nat. Commun.* **2021**, *12*, 5984.
[3] M. Etesami, S. Mehdipour-Ataei, A. Somwangthanaroj, S. Kheawhom, *Int. J. Hydrogen Energy* **2022**, *47*, 41956.
[4] S. Zaman, M. Wang, H. Liu, F. Sun, Y. Yu, J. Shui, M. Chen, H. Wang, *Trends Chem.* **2022**, *4*, 886.
[5] X. Cheng, Z. Shi, N. Glass, L. Zhang, J. Zhang, D. Song, Z. S. Liu, H. Wang, J. Shen, *J. Power Sources* **2007**, *165*, 739.
[6] S. Prass, K. A. Friedrich, N. Zamel, *Molecules* **2019**, *24*, 3514.
[7] S. M. M. Ehteshami, S. H. Chan, *Electrochim. Acta* **2013**, *93*, 334.
[8] K. Hengge, T. Gänsler, E. Pizzutilo, C. Heinzl, M. Beetz, K. J. J. Mayrhofer, C. Scheu, *Int. J. Hydrogen Energy* **2017**, *42*, 25359.
[9] M. Lukaszewski, M. Soszko, A. Czerwiński, *Int. J. Electrochem. Sci.* **2016**, *11*, 4442.
[10] D. Gubán, A. Tompos, I. Bakos, Vass, Z. Pászti, E. G. Szabó, I. E. Sajó, I. Borbáth, *Int. J. Hydrogen Energy* **2017**, *42*, 13741.
[11] J. X. Wang, P. He, Y. Zhang, S. Ye, *ECS Trans.* **2014**, *64*, 121.
[12] R. K. Ahluwalia, D. D. Papadias, N. N. Kariuki, J.-K. Peng, X. Wang, Y. Tsai, D. G. Graczyk, D. J. Myers, *J. Electrochem. Soc.* **2018**, *165*, F3024.
[13] R. L. Borup, A. Kusoglu, K. C. Neyerlin, R. Mukundan, R. K. Ahluwalia, D. A. Cullen, K. L. More, A. Z. Weber, D. J. Myers, *Curr. Opin. Electrochem.* **2020**, *21*, 192.
[14] B. M. Besancon, V. Hasanov, R. Benesch, M. Barrio, M. J. Mølnvik, *Int. J. Hydrogen Energy* **2009**, *34*, 2350.
[15] T. Lopes, V. A. Paganin, E. R. Gonzalez, *J. Power Sources* **2011**, *196*, 6256.
[16] J. Mitzel, Q. Zhang, P. Gazdzicki, K. A. Friedrich, *J. Power Sources* **2021**, *488*, 229375.
[17] Q. Liu, M. Ranocchiari, J. A. Van Bokhoven, *Chem. Soc. Rev.* **2022**, *51*, 188.
[18] S. Takenaka, T. Arike, H. Matsune, E. Tanabe, M. Kishida, *J. Catal.* **2008**, *257*, 345.
[19] S. Takenaka, H. Miyamoto, Y. Utsunomiya, H. Matsune, M. Kishida, *J. Phys. Chem. C* **2014**, *118*, 774.
[20] X. Yu, Z. Xu, Z. Yang, S. Xu, Q. Zhang, Y. Ling, *Nanotechnology* **2018**, *29*, 245401.
[21] S. Takenaka, N. Susuki, H. Miyamoto, E. Tanabe, H. Matsune, M. Kishida, *J. Catal.* **2011**, *279*, 381.
[22] K. Fujii, M. Ito, Y. Sato, S. Takenaka, M. Kishida, *J. Power Sources* **2015**, *279*, 100.

[23] K. Park, M. Goto, M. So, S. Takenaka, Y. Tsuge, G. Inoue, *Catalysts* **2021**, *11*, 1517.
[24] K. Park, T. Ohnishi, M. Goto, M. So, S. Takenaka, Y. Tsuge, G. Inoue, *Int. J. Hydrogen Energy* **2020**, *45*, 1867.
[25] N. Aoki, H. Inoue, H. Kawasaki, H. Daimon, T. Doi, M. Inaba, *Electrochem. Soc.* **2018**, *165*, 737.
[26] H. Su, L. Xu, H. Zhu, Y. Wu, L. Yang, S. Liao, H. Song, Z. Liang, V. Birss, *Int. J. Hydrogen Energy* **2010**, *35*, 7874.
[27] A. Kumar, V. K. Ramani, *Appl. Catal. B Environ.* **2013**, *138–139*, 43.
[28] X. Yang, Y. Wang, G. Zhang, L. Du, L. Yang, M. Markiewicz, J. Y. Choi, R. Chenitz, S. Sun, *Appl. Catal. B Environ.* **2020**, *264*, 118523.
[29] V. S. Velan, G. Velayutham, N. Hebalkar, K. S. Dhathathreyan, *Int. J. Hydrogen Energy* **2011**, *6*, 3.
[30] A. Kusoglu, A. Z. Weber, *Chem. Rev.* **2017**, *117*, 987.
[31] A. Fukuoka, J. Kimura, T. Oshio, Y. Sakamoto, M. Ichikawa, *J. Am. Chem. Soc.* **2007**, *129*, 10120.
[32] E. Antolini, *Appl. Catal. B Environ.* **2016**, *181*, 298.
[33] M. Arenz, K. J. J. Mayrhofer, V. Stamenkovic, B. B. Blizanac, T. Tomoyuki, P. N. Ross, N. M. Markovic, *J. Am. Chem. Soc.* **2005**, *127*, 6819.
[34] T. S. Mahadevan, S. H. Garofalini, *J. Phys. Chem. C* **2008**, *112*, 1507.
[35] L. Chen, X. He, H. Liu, L. Qian, S. H. Kim, *J. Phys. Chem. C* **2018**, *122*, 11385.
[36] S. Prass, J. St-Pierre, M. Klingele, K. A. Friedrich, N. Zamel, *Electrocatalysis* **2020**, *12*, 45.
[37] H. Iden, A. Ohma, *J. Electroanal. Chem.* **2013**, *693*, 34.
[38] K. K. D. Malevicha, E. Halliopa, B. A. Peppleya, J. G. Pharoaha, *ECS Trans.* **2008**, *16*, 1763.
[39] T. R. Garrick, T. E. Moylan, V. Yarlagadda, A. Kongkanand, *J. Electrochem. Soc.* **2017**, *164*, F60.
[40] J. St-Pierre, *J. Electrochem. Soc.* **2009**, *156*, B291.
[41] Y. Matsuda, T. Shimizu, S. Mitsushima, *J. Power Sources* **2016**, *318*, 1.
[42] R. W. Lindström, K. Kortsdottir, M. Wesselmark, A. Oyarce, C. Lagergren, G. Lindbergh, *J. Electrochem. Soc.* **2010**, *157*, B1795.
[43] S. Rudi, C. Cui, L. Gan, P. Strasser, *Electrocatalysis* **2014**, *5*, 408.
[44] T. Unmüssig, J. Melke, A. Fischer, *Phys. Chem. Chem. Phys.* **2019**, *21*, 13555.
[45] M. C. O. Monteiro, L. Jacobse, M. T. M. Koper, *J. Phys. Chem. Lett.* **2020**, *11*, 9708.
[46] P. Urchaga, S. Baranton, C. Coutanceau, G. Jerkiewicz, *Langmuir* **2012**, *28*, 3658.
[47] M. Eriksson, L. G. Petersson, *Surf. Sci.* **1994**, *311*, 139.
[48] T. Loučka, *J. Electroanal. Chem. Interfacial Electrochem.* **1971**, *31*, 319.
[49] R. Mohtadi, W. K. Lee, J. W. Van Zee, *Appl. Catal. B Environ.* **2005**, *56*, 37.
[50] Y. Nagahara, S. Sugawara, K. Shinohara, *J. Power Sources* **2008**, *182*, 422.
[51] F. Uribe, I. Urdampilleta, T. Rockward, E. L. Brosha, F. H. Garzon, *ECS Meet. Abstr. MA2007-02*, Washington, DC **2007**, p. 446, https://doi.org/10.1149/ma2007-02/9/446.
[52] J. St-Pierre, B. Wetton, Y. Zhai, J. Ge, *J. Electrochem. Soc.* **2014**, *161*, E3357.
[53] D. Bounechada, Z. Darmastuti, M. Andersson, L. Ojamäe, A. Lloyd Spetz, M. Skoglundh, P.-A. Carlsson, *J. Phys. Chem. C* **2014**, *118*, 29713.

7 References

(1) Pachauri, R. K.; Meyer, L. A. *IPCC, 2014: Climate Change 2014: Synthesis Report. Contribution of Working Groups I, II and III to the Fifth Assessment Report of the Intergovernmental Panel on Climate Change*; Geneva, Switzerland, 2014.

(2) UNFCCC. *Adoption of the Paris Agreement*; 2015.

(3) Johan, R.; Owen, G.; Joeri, R.; Malte, M.; Nebojsa, N.; Joachim, S. H. A Roadmap for Rapid Decarbonization. *Science (80-.).* **2017**, *355* (6331), 1269–1271. https://doi.org/10.1126/science.aah3443.

(4) *World Energy Outlook 2021*; 2021.

(5) Bundesministerium für Umwelt, Naturschutz, nukleare S. und V. *Klimaschutzplan 2050 – Klimaschutzpolitische Grundsätze Und Ziele Der Bundesregierung*.

(6) "Bundesministerium für Umwelt, Naturschutz, nukleare S. und V. Energieverbrauch nach Energieträgern und Sektoren https://www.umweltbundesamt.de/daten/energie/energieverbrauch-nach-energietraegern-sektoren#allgemeine-entwicklung-und-einflussfaktoren.

(7) Wirtschaft, B. für. *Die Nationale Wasserstoffstrategie*; 2020.

(8) International Energy Agency. The Future of Hydrogen: Seizing Today's Opportunities. *IEA Publ.* **2019**, No. June, 203.

(9) Thompson, S. T.; James, B. D.; Huya-Kouadio, J. M.; Houchins, C.; DeSantis, D. A.; Ahluwalia, R.; Wilson, A. R.; Kleen, G.; Papageorgopoulos, D. Direct Hydrogen Fuel Cell Electric Vehicle Cost Analysis: System and High-Volume Manufacturing Description, Validation, and Outlook. *J. Power Sources* **2018**, *399* (August), 304–313. https://doi.org/10.1016/j.jpowsour.2018.07.100.

(10) U.S. Department of Energy. DOE Technical Targets for Polymer Electrolyte Membrane Fuel Cell Components https://www.energy.gov/eere/fuelcells/doe-technical-targets-fuel-cell-systems-and-stacks-transportation-applications.

(11) Kongkanand, A.; Mathias, M. F. The Priority and Challenge of High-Power Performance of Low-Platinum Proton-Exchange Membrane Fuel Cells. *J. Phys. Chem.* **2016**, *7*, 1127–1137. https://doi.org/10.1021/acs.jpclett.6b00216.

(12) Abdel-Baset, T.; Benjamin, T.; Borup, R.; Martin, K. E.; Garland, N.; Hirano, S.; Kopasz, J.; Lakshmanmn, B.; Masten, D.; Mehall, M.; et al. US Drive - Fuel Cell Technical Team Roadmap. **2017**, No. November, 30. https://doi.org/10.2172/1220127.

(13) Imamura, D.; Hashimasa, Y. Effect of Sulfur-Containing Compounds on Fuel Cell Performance. *ECS Trans. Electrochem. Soc.* **2007**, *11* (1), 853–862. https://doi.org/10.1149/1.2780998.

(14) Hashimasa, Y.; Matsuda, Y.; Imamura, D.; Akai, M.; Motoaki, A. PEFC Power Generation Performance Degradation by Hydrogen Sulfide and Ammonia—Effects of Lowering Platinum Loading. *ECS Commun.* **2011**, *79* (5), 343–345. https://doi.org/10.5796/electrochemistry.79.343.

(15) Pérez, L. C.; Koski, P.; Ihonen, J.; Sousa, J. M.; Mendes, A. Effect of Fuel Utilization on the Carbon Monoxide Poisoning Dynamics of Polymer Electrolyte Membrane Fuel Cells. *J. Power Sources* **2014**, *258*, 122–128. https://doi.org/10.1016/j.jpowsour.2014.02.016.

(16) Viitakangas, J.; Auvinen, S.; Costantino, M.; Viik, S.; Ihonen, J. Effect of Toluene on PEMFC Performance. *Fuel Cells* **2020**, *20* (3), 245–252. https://doi.org/10.1002/fuce.201900075.

(17) Li, H.; Wang, H.; Qian, W.; Zhang, S.; Wessel, S.; Cheng, T. T. H.; Shen, J.; Wu, S. Chloride Contamination Effects on Proton Exchange Membrane Fuel Cell Performance and Durability. *J. Power Sources* **2011**, *196* (15), 6249–6255. https://doi.org/10.1016/j.jpowsour.2011.04.018.

(18) Kortsdottir, K.; Lindström, R. W.; Kermark, T.; Lindbergh, G. Influence of Toluene Contamination at the Hydrogen Pt/C Anode in a Proton Exchange Membrane Fuel Cell. *Electrochim. Acta* **2010**, *55* (26), 7643–7651. https://doi.org/10.1016/j.electacta.2009.11.048.

(19) Erbach, S.; Epple, S.; Heinen, M.; Toth, G.; Klages, M.; Gaudreau, D.; Ages, M.; Putz, A. CO2 Enrichment in Anode Loop and Correlation with CO Poisoning of Low Pt Anodes in PEM Fuel Cells. *Fuel Cells* **2018**, *18* (5), 613–618. https://doi.org/10.1002/fuce.201700216.

(20) Lopes, T.; Paganin, V. A.; Gonzalez, E. R. The Effects of Hydrogen Sulfide on the Polymer Electrolyte Membrane Fuel Cell Anode Catalyst: H2S--Pt/C Interaction Products. *J. Power Sources* **2011**, *196* (15), 6256–6263. https://doi.org/10.1016/j.jpowsour.2011.04.017.

(21) Papasavva, S.; Veenstra, M.; Waldecker, J.; West, T. Impact of Anode Catalyst Loadings and Carbon Supports to CO Contamination in PEM Fuel Cells. *Int. J. Hydrogen Energy* **2021**, *46* (40), 21136–

21150. https://doi.org/https://doi.org/10.1016/j.ijhydene.2021.03.204.
(22) Nachiappan, N.; Kalaignan, G. P.; Sasikumar, G. Effect of Nitrogen and Carbon Dioxide as Fuel Impurities on PEM Fuel Cell Performances. *Ionics (Kiel).* **2013**, *19* (2), 351–354. https://doi.org/10.1007/s11581-012-0730-z.
(23) Ralph, T. R.; Hards, G. A.; Keating, J. E.; Campbell, S. A.; Wilkinson, D. P.; Davis, M.; St-Pierre, J.; Johnson, M. C. Low Cost Electrodes for Proton Exchange Membrane Fuel Cells Performance in Single Cells and Ballard Stacks. **1997**, *144* (11).
(24) Inaba, M.; Sugishita, M.; Wada, J.; Matsuzawa, K.; Yamada, H.; Tasaka, A. Impacts of Air Bleeding on Membrane Degradation in Polymer Electrolyte Fuel Cells. *J. Power Sources* **2008**, *178* (2), 699–705. https://doi.org/10.1016/j.jpowsour.2007.08.040.
(25) Kneer, A.; Jankovic, J.; Susac, D.; Putz, A.; Wagner, N.; Sabharwal, M.; Secanell, M.; Fuel, A.; Cooperation, C.; Canada, V. J. Correlation of Changes in Electrochemical and Structural Parameters Due to Voltage Cycling Induced Degradation in PEM Fuel Cells. **2018**, *165* (6). https://doi.org/10.1149/2.0271806jes.
(26) Reshetenko, T. V; Bethune, K.; Rocheleau, R. Spatial Proton Exchange Membrane Fuel Cell Performance under Carbon Monoxide Poisoning at a Low Concentration Using a Segmented Cell System. *J. Power Sources* **2012**, *218*, 412–423. https://doi.org/10.1016/j.jpowsour.2012.07.015.
(27) Wang, X. L.; Zhang, H. M.; Zhang, J. L.; Xu, H. F.; Tian, Z. Q.; Chen, J.; Zhong, H. X.; Liang, Y. M.; Yi, B. L. Micro-Porous Layer with Composite Carbon Black for PEM Fuel Cells. *Electrochim. Acta* **2006**, *51* (23), 4909–4915. https://doi.org/10.1016/j.electacta.2006.01.048.
(28) Wang, W.; Wang, W.; Chen, S. The Effects of Hydrogen Dilution, Carbon Monoxide Poisoning for a Pt–Ru Anode in a Proton Exchange Membrane Fuel Cell. *Int. J. Hydrogen Energy* **2016**, *41* (45), 20680–20692. https://doi.org/https://doi.org/10.1016/j.ijhydene.2016.09.151.
(29) Lee, S. J.; Mukerjee, S.; Ticianelli, E. A.; McBreen, J. Electrocatalysis of CO Tolerance in Hydrogen Oxidation Reaction in PEM Fuel Cells. *Electrochim. Acta* **1999**, *44* (19), 3283–3293. https://doi.org/10.1016/S0013-4686(99)00052-3.
(30) Mohtadi, R.; Lee, W. -k.; Cowan, S.; Van Zee, J. W.; Murthy, M. Effects of Hydrogen Sulfide on the Performance of a PEMFC. *Electrochem. Solid-State Lett.* **2003**, *6* (12), A272. https://doi.org/10.1149/1.1621831.
(31) Schwämmlein, J. N.; Rheinländer, P. J.; Chen, Y.; Freyer, K. T.; Gasteiger, H. A. Anode Aging through Voltage Cycling Induced by H 2 -Air Fronts during System Start-Up and Shut-Down. *ECS Trans.* **2017**, *80* (8), 927–938. https://doi.org/10.1149/08008.0927ecst.
(32) Orfanidi, A.; Madkikar, P.; El-Sayed, H. A.; Harzer, G. S.; Kratky, T.; Gasteiger, H. A. The Key to High Performance Low Pt Loaded Electrodes. *J. Electrochem. Soc.* **2017**, *164* (4), F418–F426. https://doi.org/10.1149/2.1621704jes.
(33) Qi, J.; Wang, X.; Ozdemir, M. O.; Uddin, M. A.; Bonville, L.; Pasaogullari, U.; Molter, T. Effect of Cationic Contaminants on Polymer Electrolyte Fuel Cell Performance. *J. Power Sources* **2015**, *286*, 18–24. https://doi.org/10.1016/j.jpowsour.2015.03.142.
(34) Zhou, X.; Ji, H.; Li, B.; Zhang, C. High-Repetitive Reversal Tolerant Performance of Proton-Exchange Membrane Fuel Cell by Designing a Suitable Anode. *ACS Omega* **2020**. https://doi.org/10.1021/acsomega.0c00638.
(35) Banham, D.; Zou, J.; Mukerjee, S.; Liu, Z.; Yang, D.; Zhang, Y.; Peng, Y.; Dong, A. Ultralow Platinum Loading Proton Exchange Membrane Fuel Cells: Performance Losses and Solutions. *J. Power Sources* **2021**, *490* (2020), 229515. https://doi.org/10.1016/j.jpowsour.2021.229515.
(36) Ganesan, A.; Narayanasamy, M. Ultra-Low Loading of Platinum in Proton Exchange Membrane-Based Fuel Cells: A Brief Review. *Mater. Renew. Sustain. Energy* **2019**, *8* (4), 1–14. https://doi.org/10.1007/s40243-019-0156-x.
(37) Kinoshita, S. Anode Overpotential at Low Pt Loadings for Pure H2. *ECS Trans.* **2007**, *11* (1), 309. https://doi.org/10.1149/1.2780943.
(38) Shabani, B.; Hafttananian, M.; Khamani, S.; Ramiar, A.; Ranjbar, A. A. Poisoning of Proton Exchange Membrane Fuel Cells by Contaminants and Impurities: Review of Mechanisms, Effects, and Mitigation Strategies. *J. Power Sources* **2019**, *427* (December 2018), 21–48. https://doi.org/10.1016/j.jpowsour.2019.03.097.
(39) Zamel, N.; Li, X. Effect of Contaminants on Polymer Electrolyte Membrane Fuel Cells. *Prog. Energy Combust. Sci.* **2011**, *37* (3), 292–329. https://doi.org/10.1016/j.pecs.2010.06.003.

(40) Bacquart, T.; Murugan, A.; Carré, M.; Gozlan, B.; Auprêtre, F.; Haloua, F.; Aarhaug, T. A. Probability of Occurrence of ISO 14687-2 Contaminants in Hydrogen: Principles and Examples from Steam Methane Reforming and Electrolysis (Water and Chlor-Alkali) Production Processes Model. *Int. J. Hydrogen Energy* **2018**, *43* (26), 11872–11883. https://doi.org/10.1016/j.ijhydene.2018.03.084.

(41) Hashimasa, Y.; Matsuda, Y.; Akai, M. Effects of Platinum Loading on PEFC Power Generation Performance Deterioration by Carbon Monoxide in Hydrogen Fuel. *ECS Trans.* **2010**, *26* (1), 131–142. https://doi.org/10.1149/1.3428984.

(42) Cheng, X.; Shi, Z.; Glass, N.; Zhang, L.; Zhang, J.; Song, D.; Liu, Z. S.; Wang, H.; Shen, J. A Review of PEM Hydrogen Fuel Cell Contamination: Impacts, Mechanisms, and Mitigation. *J. Power Sources* **2007**, *165* (2), 739–756. https://doi.org/10.1016/j.jpowsour.2006.12.012.

(43) St-Pierre, J.; Angelo, M.; Bethune, K.; Higgins, S.; Reshetenko, T. V.; Virji, M. B. V; Zhai, Y. ECS Transactions PEMFC Contamination - Fundamentals and Outlook. *ECS Trans.* **2014**, *61* (14), 1–14.

(44) Mitzel, J.; Zhang, Q.; Gazdzicki, P.; Friedrich, K. A. Review on Mechanisms and Recovery Procedures for Reversible Performance Losses in Polymer Electrolyte Membrane Fuel Cells. *J. Power Sources* **2021**, *488* (December 2020), 229375. https://doi.org/10.1016/j.jpowsour.2020.229375.

(45) *PEM Fuel Cell Electrocatalysts and Catalyst - Fundamentals and Applications*, 1st ed.; Zhang, J., Ed.; Springer London, 2008. https://doi.org/https://doi.org/10.1007/978-1-84800-936-3.

(46) Herrera, O. E.; Wilkinson, D. P.; Mérida, W. Anode and Cathode Overpotentials and Temperature Profiles in a PEMFC. *J. Power Sources* **2012**, *198*, 132–142. https://doi.org/10.1016/J.JPOWSOUR.2011.09.042.

(47) Gasteiger, H. a.; Kocha, S. S.; Sompalli, B.; Wagner, F. T. Activity Benchmarks and Requirements for Pt, Pt-Alloy, and Non-Pt Oxygen Reduction Catalysts for PEMFCs. *Appl. Catal. B Environ.* **2005**, *56* (1-2 SPEC. ISS.), 9–35. https://doi.org/10.1016/j.apcatb.2004.06.021.

(48) Durst, J.; Simon, C.; Hasché, F.; Gasteiger, H. A. Hydrogen Oxidation and Evolution Reaction Kinetics on Carbon Supported Pt, Ir, Rh, and Pd Electrocatalysts in Acidic Media. *J. Electrochem. Soc.* **2015**, *162* (1), F190–F203. https://doi.org/10.1149/2.0981501jes.

(49) Pei, P.; Chen, H. Main Factors Affecting the Lifetime of Proton Exchange Membrane Fuel Cells in Vehicle Applications: A Review. *Appl. Energy* **2014**, *125*, 60–75. https://doi.org/10.1016/j.apenergy.2014.03.048.

(50) Baker, D. R.; Caulk, D. A.; Neyerlin, K. C.; Murphy, M. W. Measurement of Oxygen Transport Resistance in PEM Fuel Cells by Limiting Current Methods. *J. Electrochem. Soc.* **2009**, *156* (9), B991. https://doi.org/10.1149/1.3152226.

(51) Bethune, K.; St-Pierre, J.; LaManna, J. M.; Hussey, D. S.; Jacobson, D. L. Contamination Mechanisms of Proton Exchange Membrane Fuel Cells - Mass Transfer Overpotential Origin. *J. Phys. Chem. C* **2020**, *124* (44), 24052–24065. https://doi.org/10.1021/acs.jpcc.0c06233.

(52) Mandal, P.; Hong, B. K.; Oh, J. G.; Litster, S. Understanding the Voltage Reversal Behavior of Automotive Fuel Cells. *J. Power Sources* **2018**, *397* (April), 397–404. https://doi.org/10.1016/j.jpowsour.2018.06.083.

(53) Marcinkoski, J.; Spendelow, J.; Wilson, A.; Papageorgopoulos, D. DOE Hydrogen and Fuel Cells Program Record - Fuel Cell System Cost - 2017. *J. Mech. Robot.* **2017**, *9* (4), 1–9. https://doi.org/10.1115/1.4036738.

(54) Shen, G.; Liu, J.; Wu, H. Bin; Xu, P.; Liu, F.; Tongsh, C.; Jiao, K.; Li, J.; Liu, M.; Cai, M.; et al. Multi-Functional Anodes Boost the Transient Power and Durability of Proton Exchange Membrane Fuel Cells. *Nat. Commun.* **2020**, *11* (1), 1–10. https://doi.org/10.1038/s41467-020-14822-y.

(55) Joo, T.; Hu, L.; Hong, B. K.; Oh, J. G.; Litster, S. On the Origin of Deactivation of Reversal-Tolerant Fuel Cell Anodes under Voltage Reversal Conditions. *J. Power Sources* **2020**, *472*, 228439. https://doi.org/10.1016/j.jpowsour.2020.228439.

(56) Hong, B. K.; Mandal, P.; Oh, J. G.; Litster, S. On the Impact of Water Activity on Reversal Tolerant Fuel Cell Anode Performance and Durability. *J. Power Sources* **2016**, *328*, 280–288. https://doi.org/10.1016/j.jpowsour.2016.07.002.

(57) Kremliakova, N.; Eastcott, J.; Sun, D.; Jankovic, J.; Cimenti, M. Silanized OER Anode Catalyst for Improved Reversal Tolerance in Fuel Cell Stack. CA2991705A1, 2016.

(58) Fujii, K.; Ito, M.; Sato, Y.; Takenaka, S.; Kishida, M. Performance and Durability of Carbon Black-Supported Pd Catalyst Covered with Silica Layers in Membrane-Electrode Assemblies of Proton Exchange Membrane Fuel Cells. *J. Power Sources* **2015**, *279*, 100–106.

https://doi.org/10.1016/j.jpowsour.2014.12.144.
(59) Aoki, N.; Inoue, H.; Kawasaki, H.; Daimon, H.; Doi, T.; Inaba, M. Durability Improvement of Pd Core-Pt Shell Structured Catalyst by Porous SiO2 Coating. *Electrochem. Soc.* **2018**, *165* (10), 737–747. https://doi.org/10.1149/2.0131810jes.
(60) Takenaka, S.; Susuki, N.; Miyamoto, H.; Tanabe, E.; Matsune, H.; Kishida, M. Highly Durable Carbon Nanotube-Supported Pd Catalysts Covered with Silica Layers for the Oxygen Reduction Reaction. *J. Catal.* **2011**, *279* (2), 381–388. https://doi.org/10.1016/j.jcat.2011.02.008.
(61) Liu, Q.; Ranocchiari, M.; Van Bokhoven, J. A. Catalyst Overcoating Engineering towards High-Performance Electrocatalysis. *Chem. Soc. Rev.* **2022**, *51* (1), 188–236. https://doi.org/10.1039/d1cs00270h.
(62) Takenaka, S.; Arike, T.; Matsune, H.; Tanabe, E.; Kishida, M. Preparation of Carbon Nanotube-Supported Metal Nanoparticles Coated with Silica Layers. *J. Catal.* **2008**, *257* (2), 345–355. https://doi.org/10.1016/j.jcat.2008.05.016.
(63) Yu, X.; Xu, Z.; Yang, Z.; Xu, S.; Zhang, Q.; Ling, Y. SiO2 Decoration Dramatically Enhanced the Stability of PtRu Electrocatalysts with Undetectable Deterioration in Fuel Cell Performance. *Nanotechnology* **2018**, *29*, 245401–245410. https://doi.org/https://doi.org/10.1088/1361-6528/aabbfa.
(64) Park, K.; Ohnishi, T.; Goto, M.; So, M.; Takenaka, S.; Tsuge, Y.; Inoue, G. Improvement of Cell Performance in Catalyst Layers with Silica-Coated Pt/Carbon Catalysts for Polymer Electrolyte Fuel Cells. *Int. J. Hydrogen Energy* **2020**, *45* (3), 1867–1877. https://doi.org/10.1016/j.ijhydene.2019.11.097.
(65) Park, K.; Goto, M.; So, M.; Takenaka, S.; Tsuge, Y.; Inoue, G. Influence of Cathode Catalyst Layer with SiO2-Coated Pt/Ketjen Black Catalysts on Performance for Polymer Electrolyte. *Catalysts* **2021**, *11* (1517). https://doi.org/doi.org/10.3390/catal11121517.
(66) Takenaka, S.; Miyamoto, H.; Utsunomiya, Y.; Matsune, H.; Kishida, M. Catalytic Activity of Highly Durable Pt/CNT Catalysts Covered with Hydrophobic Silica Layers for the Oxygen Reduction Reaction in PEFCs. *J. Phys. Chem. C* **2013**, *118* (2), 774–783. https://doi.org/10.1021/jp407928m.
(67) Igarashi, H.; Fujino, T.; Watanabe, M. Hydrogen Electro-Oxidation on Platinum Catalysts in the Presence of Trace Carbon Monoxide. *J. Electroanal. Chem.* **1995**, *391* (1–2), 119–123. https://doi.org/10.1016/0022-0728(95)03914-3.
(68) Wang, J. X.; He, P.; Zhang, Y.; Ye, S. Can CO-Tolerant Anodes Be Economically Viable for PEMFC Applications with Reformates? *ECS Trans.* **2014**, No. 4, 4–10.
(69) Kusoglu, A.; Weber, A. Z. New Insights into Perfluorinated Sulfonic-Acid Ionomers. *Chem. Rev.* **2017**, *117* (3), 987–1104. https://doi.org/10.1021/acs.chemrev.6b00159.
(70) Jones, D. J. Perfluorosulfonic Acid Membranes for Fuel Cell and Electrolyser Applications. *Aldrich Mater. Sci.* **2015**, *10* (3), 88–99.
(71) Nepel, T. C. M.; Lopes, P. P.; Paganin, V. A.; Ticianelli, E. A. CO Tolerance of Proton Exchange Membrane Fuel Cells with Pt/C and PtMo/C Anodes Operating at High Temperatures: A Mass Spectrometry Investigation. *Electrochim. Acta* **2013**, *88*, 217–224. https://doi.org/https://doi.org/10.1016/j.electacta.2012.10.039.
(72) Lindström, R. W.; Kortsdottir, K.; Wesselmark, M.; Oyarce, A.; Lagergren, C.; Lindbergh, G. Active Area Determination of Porous Pt Electrodes Used in Polymer Electrolyte Fuel Cells: Temperature and Humidity Effects. *J. Electrochem. Soc.* **2010**, *157* (12), B1795. https://doi.org/10.1149/1.3494220.
(73) Bonnet, C.; Franck-Lacaze, L.; Ronasi, S.; Besse, S.; Lapicque, F. PEM Fuel Cell Pt Anode Inhibition by Carbon Monoxide: Non-Uniform Behaviour of the Cell Caused by the Finite Hydrogen Excess. *Chem. Eng. Sci.* **2010**, *65* (10), 3050–3058. https://doi.org/10.1016/j.ces.2010.01.029.
(74) Ehteshami, S. M. M.; Chan, S. H. A Review of Electrocatalysts with Enhanced CO Tolerance and Stability for Polymer Electrolyte Membarane Fuel Cells. *Electrochim. Acta* **2013**, *93*, 334–345. https://doi.org/10.1016/j.electacta.2013.01.086.
(75) Contractor, A. Q.; Lal, H. Formic Acid Oxidation at Platinized Platinum Electrodes: Part V. A Further Study of Catalytic Effect of Preadsorbed Sulfur. *J. Electroanal. Chem. Interfacial Electrochem.* **1979**, *103* (1), 103–117. https://doi.org/10.1016/S0022-0728(79)80482-9.
(76) Sethuaraman, V. A.; Weidner, J. W. Analysis of Sulfur Poisoning on a PEM Fuel Cell Electrode. *Electrochim. Acta* **2010**, *55* (20), 5683–5694. https://doi.org/10.1016/0002-9378(60)90090-9.
(77) Shi, W.; Yi, B.; Hou, M.; Jing, F.; Ming, P. Hydrogen Sulfide Poisoning and Recovery of PEMFC Pt-Anodes. *J. Power Sources* **2007**, *165* (2), 814–818. https://doi.org/10.1016/J.JPOWSOUR.2006.12.052.
(78) Gould, B. D.; Bender, G.; Bethune, K.; Dorn, S.; Baturina, O. A.; Rocheleau, R.; Swider-Lyons, K. E.

Operational Performance Recovery of SO2-Contaminated Proton Exchange Membrane Fuel Cells. *J. Electrochem. Soc.* **2010**, *157* (11), B1569. https://doi.org/10.1149/1.3483108.

(79) O'Brien, J. A.; Hinkley, J. T.; Donne, S. W.; Lindquist, S. E. The Electrochemical Oxidation of Aqueous Sulfur Dioxide: A Critical Review of Work with Respect to the Hybrid Sulfur Cycle. *Electrochim. Acta* **2010**, *55* (3), 573–591. https://doi.org/10.1016/j.electacta.2009.09.067.

(80) Uribe, F.; Urdampilleta, I.; Rockward, T.; Brosha, E. L.; Garzon, F. H. PEMFC Poisoning with H2S: Dependence on Operating Conditions. *ECS Meet. Abstr.* **2007**, *MA2007-02* (9), 446–446. https://doi.org/10.1149/ma2007-02/9/446.

(81) Kakati, B. K.; Kucernak, A. R. J. Gas Phase Recovery of Hydrogen Sulfide Contaminated Polymer Electrolyte Membrane Fuel Cells. *J. Power Sources* **2014**, *252*, 317–326. https://doi.org/10.1016/j.jpowsour.2013.11.077.

(82) Mohtadi, R.; Lee, W. K.; Van Zee, J. W. The Effect of Temperature on the Adsorption Rate of Hydrogen Sulfide on Pt Anodes in a PEMFC. *Appl. Catal. B Environ.* **2005**, *56* (1-2 SPEC. ISS.), 37–42. https://doi.org/10.1016/j.apcatb.2004.08.012.

(83) Lopes, T.; Paganin, V. A.; Gonzalez, E. R. Hydrogen Sulfide Tolerance of Palladium–Copper Catalysts for PEM Fuel Cell Anode Applications. *Int. J. Hydrogen Energy* **2011**, *36* (21), 13703–13707. https://doi.org/10.1016/J.IJHYDENE.2011.07.126.

(84) Rau, M.; Cremers, C.; Tübke, J. Development of Anodic Materials for HT-PEMFCs with High Tolerance to H2S. *Int. J. Hydrogen Energy* **2015**, *40* (15), 5439–5443. https://doi.org/10.1016/J.IJHYDENE.2015.01.036.

(85) Iezzi, R. C.; Santos, R. D. M.; da Silva, G. C.; Paganin, V. A.; Ticianelly, E. A. CO Tolerance and Stability of Proton Exchange Membrane Fuel Cells with Nafion® and Aquivion® Membranes and Mo-Based Anode Electrocatalysts. *Brazilian Chem. Soc.* **2018**, *29* (5), 1094–1104. https://doi.org/10.21577/0103-5053.20170230.

(86) Matsuda, Y.; Shimizu, T.; Mitsushima, S. Adsorption Behavior of Low Concentration Carbon Monoxide on Polymer Electrolyte Fuel Cell Anodes for Automotive Applications. *J. Power Sources* **2016**, *318*, 1–8. https://doi.org/10.1016/j.jpowsour.2016.03.104.

(87) Wagner, N.; Schulze, M. Change of Electrochemical Impedance Spectra during CO Poisoning of the Pt and Pt--Ru Anodes in a Membrane Fuel Cell (PEFC). *Electrochim. Acta* **2003**, *48* (25–26), 3899–3907. https://doi.org/10.1016/S0013-4686(03)00528-0.

(88) Kundu, S.; Fowler, M. W.; Simon, L. C.; Grot, S. Morphological Features (Defects) in Fuel Cell Membrane Electrode Assemblies. *J. Power Sources* **2006**, *157* (2), 650–656. https://doi.org/10.1016/j.jpowsour.2005.12.027.

(89) Tavassoli, A.; Lim, C.; Kolodziej, J.; Lauritzen, M.; Knights, S.; Wang, G. G.; Kjeang, E. Effect of Catalyst Layer Defects on Local Membrane Degradation in Polymer Electrolyte Fuel Cells. *J. Power Sources* **2016**, *322*, 17–25. https://doi.org/10.1016/j.jpowsour.2016.05.016.

(90) Lowde, D. R.; Williams, J. O.; McNicol, B. D. The Characterisation of Catalyst Surfaces by Cyclic Voltammetry. *Appl. Surf. Sci.* **1978**, *1* (2), 215–240. https://doi.org/10.1016/0378-5963(78)90016-8.

(91) Elgrishi, N.; Rountree, K. J.; McCarthy, B. D.; Rountree, E. S.; Eisenhart, T. T.; Dempsey, J. L. A Practical Beginner's Guide to Cyclic Voltammetry. *J. Chem. Educ.* **2018**, *95* (2), 197–206. https://doi.org/10.1021/acs.jchemed.7b00361.

(92) Carter, R. N.; Kocha, S. S.; Wagner, F.; Fay, M.; Gasteiger, H. A. Artifacts in Measuring Electrode Catalyst Area of Fuel Cells through Cyclic Voltammetry. *ECS Trans.* **2007**, *11* (1), 403–410. https://doi.org/10.1149/1.2780954.

(93) Edmundson, M. D.; Busby, F. C. Overcoming Artifacts in Cyclic Voltammetry Through the Use of Multiple Scan Rates and Potential Windows. *ECS Trans. Electrochem. Soc.* **2011**, *41* (1), 661–671. https://doi.org/10.1017/CBO9781107415324.004.

(94) Prass, S.; St-Pierre, J.; Klingele, M.; Friedrich, K. A.; Zamel, N. Hydrogen Oxidation Artifact During Platinum Oxide Reduction in Cyclic Voltammetry Analysis of Low-Loaded PEMFC Electrodes. *Electrocatalysis* **2020**, *12* (1), 45–55.

(95) Tahmasebi, S.; McMath, A. A.; van Drunen, J.; Jerkiewicz, G. Catalytic Duality of Platinum Surface Oxides in the Oxygen Reduction and Hydrogen Oxidation Reactions. *Electrocatalysis* **2017**, *8* (4), 301–310. https://doi.org/10.1007/s12678-017-0372-z.

(96) Zhao, Y.; Li, X.; Schechter, J. M.; Yang, Y. Revisiting the Oxidation Peak in the Cathodic Scan of the Cyclic Voltammogram of Alcohol Oxidation on Noble Metal Electrodes. *RSC Adv.* **2016**, *6* (7), 5384–

5390. https://doi.org/10.1039/c5ra24249e.
(97) Morel, S. ISO/TC 197 Hydrogen technologies https://www.iso.org/committee/54560.html.
(98) SAE International. Hydrogen Fuel Quality Screening Test of Chemicals for Fuel Cell Vehicles Normen-Download-Beuth-Fraunhofer-Institut. 2022.
(99) Prass, S.; Friedrich, K. A.; Zamel, N. Tolerance and Recovery of Ultralow-Loaded Platinum Anode Electrodes upon Carbon Monoxide and Hydrogen Sulfide Exposure. *Molecules* **2019**, *24* (19), 1–14. https://doi.org/10.3390/molecules24193514.
(100) Kinoshita, S. Anode Overpotential at Low Pt Loadings for Pure H2. *ECS Meet. Abstr.* **2007**, *MA2007-02* (9), 488–488. https://doi.org/10.1149/ma2007-02/9/488.
(101) Koski, P.; Viitakangas, J.; Ihonen, J. Dynamic Load Cycle Effects on PEMFC Stack CO Tolerance under Fuel Recirculation and Periodic Purge. *J. Electrochem. Soc.* **2022**, *169* (1), 14507. https://doi.org/10.1149/1945-7111/ac439c.
(102) Reshetenko, T. V; Bethune, K.; Rubio, M. A.; Rocheleau, R. Study of Low Concentration CO Poisoning of Pt Anode in a Proton Exchange Membrane Fuel Cell Using Spatial Electrochemical Impedance Spectroscopy. *J. Power Sources* **2014**, *269*, 344–362. https://doi.org/10.1016/j.jpowsour.2014.06.146.
(103) Gazdzick, P.; Mitzel, J.; Garcia Sanchez, D.; Schulze, M.; Friedrich, K. A. Evaluation of Reversible and Irreversible Degradation Rates of Polymer Electrolyte Membrane Fuel Cells Tested in Automotive Conditions. *J. Power Sources* **2016**, *327*, 86–95. https://doi.org/10.1016/j.jpowsour.2016.07.049.
(104) Steinberger, M.; Geiling, J.; Oechsner, R.; Frey, L. Anode Recirculation and Purge Strategies for PEM Fuel Cell Operation with Diluted Hydrogen Feed Gas. *Appl. Energy* **2018**, *232* (May), 572–582. https://doi.org/10.1016/j.apenergy.2018.10.004.
(105) Mokmeli, A.; Asghari, S. An Investigation into the Effect of Anode Purging on the Fuel Cell Performance. *Int. J. Hydrogen Energy* **2010**, *35* (17), 9276–9282. https://doi.org/10.1016/j.ijhydene.2010.03.079.
(106) Viitakangas, J.; Ihonen, J.; Koski, P.; Reinikainen, M.; Aarhaug, T. A. Study of Formaldehyde and Formic Acid Contamination Effect on PEMFC. *Electrochem. Soc.* **2018**, *165*, F718–F727. https://doi.org/10.1149/2.1381809jes.
(107) Esposito, D. V. Membrane-Coated Electrocatalysts - An Alternative Approach to Achieving Stable and Tunable Electrocatalysis. *ACS Catal.* **2018**, *8* (1), 457–465. https://doi.org/10.1021/acscatal.7b03374.
(108) Prass, S.; Nerlich, L.; Singh, R.; Godoy, A. O.; Jankovic, J.; Friedrich, K. A.; Zamel, N. Tolerance of Silicon Oxide-Coated Pt/C Catalyst Toward CO and H2S Contamination in Hydrogen for Proton Exchange Membrane Fuel Cells. *Energy Technol.* **2023**. https://doi.org/10.1002/ente.202300199.
(109) Su, H.; Xu, L.; Zhu, H.; Wu, Y.; Yang, L.; Liao, S.; Song, H.; Liang, Z.; Birss, V. Self-Humidification of a PEM Fuel Cell Using a Novel Pt/SiO2 /C Anode Catalyst. *Int. J. Hydrogen Energy* **2010**, *35*, 7874–7880. https://doi.org/10.1016/j.
(110) Kaneko, K.; Tsushima, S.; Hirai, S. Effect of SO2 Concentration and Relative Humidity on Contamination of Cathode and Anode in PEMFC. *ECS Trans.* **2009**, *25* (1), 1279. https://doi.org/10.1149/1.3210683.
(111) Tsushima, S.; Kaneko, K.; Morioka, H.; Hirai, S. Influence of SO2 Concentration and Relative Humidity on Electrode Poisoning in Polymer Electrolyte Membrane Fuel Cells. *J. Therm. Sci. Technol.* **2012**, *7* (4), 619–632. https://doi.org/10.1299/jtst.7.619.
(112) Bounechada, D.; Darmastuti, Z.; Andersson, M.; Ojamäe, L.; Lloyd Spetz, A.; Skoglundh, M.; Carlsson, P.-A. Vibrational Study of SOx Adsorption on Pt/SiO2. *J. Phys. Chem. C* **2014**, *118*, 29713–29723. https://doi.org/10.1021/jp506644w.
(113) Acheampong, R.; Esfahani, R. A. M.; Moghaddam, R. B.; Easton, B. An Organosilane-Based Fuel Cell Ionomer That Mitigates Carbon Corrosion Communication. *Electrochem. Soc.* **2020**, *167*. https://doi.org/10.1149/1945-7111/ab7a0a.
(114) Robinson, J. E.; LAbrador, N. Y.; Chen, H.; Sartor, B. E.; Esposito, D. V. Silicon Oxide-Encapsulated Platinum Thin Films as Highly Active Electrocatalysts for Carbon Monoxide and Methanol Oxidation. *ACS Catal.* **2018**, *8*, 11423–11434.
(115) Labrador, N. Y.; Songcuan, E. L.; De Silva, C.; Chen, H.; Kurdziel, S. J.; Ramachandran, R. K.; Detavernier, C.; Esposito, D. V; Bestellung, D.; Labrador, N. Y.; et al. Hydrogen Evolution at the Buried Interface between Pt Thin Films and Silicon Oxide Nanomembranes. *ACS Catal.* **2018**, *8* (3), 1767–1778. https://doi.org/10.1021/acscatal.7b02668.
(116) Velan, V. S.; Velayutham, G.; Hebalkar, N.; Dhathathreyan, K. S. Effect of SiO2 Additives on the PEM

Fuel Cell Electrode Performance. **2011**, *6* (288), 3–10. https://doi.org/10.1016/j.ijhydene.2011.03.041.
(117) Fukuoka, A.; Kimura, J.; Oshio, T.; Sakamoto, Y.; Ichikawa, M. Preferential Oxidation of Carbon Monoxide Catalyzed by Platinum Nanoparticles in Mesoporous Silica. *J. Am. Chem. Soc.* **2007**, *129* (33), 10120–10125. https://doi.org/https://doi.org/10.1021/ja0703123.
(118) Liu, H.; Li, D.; Guo, J.; Li, Y.; Liu, A.; Bai, Y.; He, D. Recent Advances on Catalysts for Preferential Oxidation of CO. *Nano Res.* **2022**. https://doi.org/10.1007/s12274-022-5182-9.

List of abbreviations

Acronym	Meaning
ALD	Atomic layer deposition
APTES	3-aminopropyltriethoxysilane
BEV	Battery electric vehicle
BOL	Begin-of-life
CCM	Catalyst coated membrane
CE	Counter electrode
CL	Catalyst layer
CNT	Carbon nanotube
CV	Cyclic voltammetry
DOE	Department of Energy
ECSA	Electrochemically active surface area
EDX	Energy dispersive X-ray spectroscopy
EOT	End-of-test
FCEV	Fuel cell electric vehicle
GDL	Gas diffusion layer
GHG	Greenhouse gas
HER	Hydrogen evolution reaction
HOR	Hydrogen oxidation reaction
HT	High temperature
ICP-MS	Inductively coupled plasma - mass spectrometry
ISE	Fraunhofer Institute for Solar Energy Systems
ISO	International organisation for standardization
LT	Low temperature
MEA	Membrane electrode assembly
MFC	Mass flow controller
MTEOS	Methyltriethoxysilane
NDA	Non-disclosure agreement
OCV	Open circuit voltage
OER	Oxygen evolution reaction
OH	Hydroxyl group
ORR	Oxygen reduction reaction
PEM	Proton exchange membrane
PEMFC	Proton exchange membrane fuel cell
PFSA	Perfluorinated sulfonic acid
PGM	Platinum group metal
PHEV	Plug-in electric vehicle

PNP	1-Propoxy-2-propanol
POX	Partial oxidation
PROX	Preferential oxidation
PSA	Pressure swing adsorption
PTFE	Polytetrafluorethylene
RE	Reference electrode
RHE	Reversible hydrogen electrode
RTA	Reversal tolerance additive
SD/SU	Shut-down/start-up
SEM	Scanning electron microscopy
SHE	Standard hydrogen electrode
SME	Steam methane reformation
TEM	Transmission electron microscopy
TEOS	Triethoxysilane
TSA	Temperature swing adsorption
WE	Working electrode

List of publications

Published manuscripts

- Prass, Sebastian; Friedrich, Kaspar Andreas; Zamel, Nada. “Tolerance and recovery of ultra-low-loaded platinum anode electrodes upon carbon monoxide and hydrogen sulfide exposure”. Molecules, 24 (19), 1-14 (2019).
- Prass, Sebastian; St-Pierre, Jean; Klingele, Matthias; Friedrich, Kaspar Andreas; Zamel, Nada: “Hydrogen Oxidation Artifact During Platinum Oxide Reduction in Cyclic Voltammetry Analysis of Low-loaded PEMFC Electrodes”. Electrocatalysis, 12, 45-55 (2020).
- Prass, Sebastian; Nerlich, Leon; Singh, Rajveer; Ortiz Godoy, Richard; Jancovic, Jasna; Friedrich, Kaspar Andreas; Zamel, Nada. “Tolerance of silicon oxide coated Pt/C catalyst versus CO and H2S contamination in hydrogen for PEMFCs”. Energy Technology (under revision at Energy Technology, Wiley-VCH GmbH, Weinheim)
- Hou, Yuze; Prass, Sebastian; Li, Xing; Du, Qing; Jiao, Kui; Zamel, Nada. “Pore-Scale Modeling of Anode Catalyst Layer Tolerance upon Hydrogen Sulfide Exposure in PEMFC”. Electrocatalysis, 12, 403-414 (2021).

Conferences

- Prass, Sebastian; Zamel, Nada; Groos, Ulf. “Effect of fuel impurities (CO, CO2, H2S) on PEMFCs with ultra-low-loaded anodic catalyst layers”. Fundamentals & Development of Fuel Cells FDFC2019, Nantes, 2019.

List of figures

Figure 1 Trend in anode and cathode PGM loading, and the DOE targets for PEMFCs in automotive applications. Adapted from selected publications including in-situ PEMFC testing on contamination [11,12,21–30,13,31–34,14–20] 3

Figure 2 Schematic PEMFC polarization curve and voltage loss domains (I activation, II ohmic and III diffusion) 9

Figure 3 Illustration of Pt/C particle fully or partially covered with SiO_2 13

Figure 4 Test bench schematic with two MFCs for impurities (GasX.1 and GasX.2) and SilcoNert® coated tubing (in blue), and the PEMFC with anode and cathode catalyst layers (CLs) 21

Figure 5 Alternatives of cell preparation for CV analysis of the anode electrode, a) MEA rotation, b) switch of gas supply and electrical connections and c) H_2 pumping and N_2 purge of both electrodes, closure of back pressure valves and subsequent CV in negative potential ranges (e.g. from -0.05 – 0.9 V) 22

Figure 6 SEM images of a) the SiO_2-Pt/C agglomerates after calcination and b) the dried electrode surface on the decal after ball milling, paste fabrication and printing 26

Figure 7 CV measurements of high loaded cathode and low-loaded anode electrodes (400 vs. 50 µg/cm² Pt/C, respectively) with the variation range in ECSA based on total ECSA value due to N_2 purge on or off (dark vs. bright transparent areas) for different lower charge integration limits U.int shown in the inset 30

Figure 8 CV measurements of low loaded anode electrode (50 µg/cm² Pt/C) with and without N_2 purge and upper potential limit (U.lim) of 0.9 V, with the ratio of H-desorption vs. adsorption charges shown in the inset (U.int for ECSA determination 0.15 V). The oxidation peak in the cathodic transient leads to the increase in the ratio if N_2 purge is switched off, while the concentration cell effect causes the decrease with purge switched on. 31

Figure 9 CV profiles of a) Pt(poly) in 0.5 M aqueous H_2SO_4 saturated with H_2, and b) of methanol oxidizing on a Pd electrode taken from Tahmasebi et al. [95] and Zhao et al. [96], respectively, with the oxidative peak marked in red. 32

Figure 10 Schematic of the influence of dynamic vs. static load cycling (DLC vs. SLC) on CO fuel contamination, where periodic high anode overpotentials lead to electrochemical oxidation of CO and to higher performance for the DLC at equal average current density, taken from Koski et al. [101]. 36

Figure 11 H_2S contamination tests showing a) cell voltage drop due to H_2S, where no (significant) recovery upon introduction of neat H_2 can be seen, but OCV-hold recovered the cell performance, and b) polarization curves of Pt (full symbols, e.g. ♦) and PtRu (open symbols ◊) anode electrodes, each one before and after H_2S contamination, 24 h recovery at 0.67 – 0.69 V potentiostatic operation in neat H_2 and after sulfur oxidation via CV, taken from Imamura et al. [13] and Mohtadi et al. [30] 37

Figure 12 Average cell voltage drops of stacks in chronoamperometric measurements at 0.6 A/cm² upon operation with a) HCOH and b) HCOOH as compared to the voltage drop in neat H_2 and reference measurement with 2 ppm CO, taken from Viitakangas et al. [106]. 38

Figure 13. Mechanisms on how functional coatings can affect reaction mechanisms on an active metal (M). Depicted is the reduction of an oxidant species (O_1) to forming the reductant species (R_1). Contamination mechanisms can be affected by a) size-selection and repelling of a competing oxidant

species (O_c) with spheres symbolizing hydration spheres, b) charge-selection, c) overlayer-assisted electrocatalysis and d) confinement of a reactant species (here: CO molecule) buried at the interface between metal M and the coating, taken from Esposito [107].....39

Figure 14 Investigations on Pt and Ti thin films supported on a Si-wafer and coated with SiO_2 of thickness t_{SiOx}, a) CO stripping measurements showing the shift in CO oxidation towards lower potentials for thicker SiO_2-coatings, and b) HER rate at -5 mA/cm² with and without copper sulfate ($CuSO_4$) forming Cu^{2+} in aqueous solution as model contaminant, with SEM images of catalyst surfaces showing contaminant deposition after testing, taken from Robinson et al. [114] and Labrador et al. [115].....43

Figure 15 CO stripping measurements showing the 90 and 200 mV shifts in CO oxidation towards higher potentials and stability enhancing effect (solid lines for fresh catalyst, dashed lines for degraded) for SiO_2-coated catalyst materials, taken from a) Yu et al. for a PtRu/C catalyst evaluated per RDE in 0.5 M H_2SO_4 [63], and b) Takenaka et al. for a Pd/CNT catalyst also evaluated per RDE in 0.1 $HClO_4$ [60].....45

Figure 16 Influences of water and SiO_2 on contamination by sulfur species, a) ECSA of anode and cathode electrodes after exposure of the cathode to SO_2 at different relative humidities taken from Tsushima et al. [111], and b) schematic cross-section of the Pt catalyst supported on SiO_2, and representation of terminal silanol groups (A-C), siloxane (D) and surface sulfate groups (E) on SiO_2, taken from Bounechada et al. [112].....46

List of tables

Table 1 Specific enthalpy and entropy for O_2, H_2 and H_2O in gaseous (g) or liquid (l) states.....8

Table 2 Hydrogen for automotive application: ISO 14687:2019 fuel purity standard [40] 15

Table 3 Operating parameter ranges.....23

Table 4 Cell platform and MEA specifications.....25

Table 5 Publications on CO and H_2S contamination, and effects contributing to a recovery thereof. ...35

Table 6 Publications on SiOx serving as coating, additive or support in electrocatalysis.....42

Danksagung

Zu Beginn möchte ich meinem Doktorvater Professor Dr. K. Andreas Friedrich für die wissenschaftliche Begleitung meiner Promotion, sowie für die Bereitschaft, mich als externen Doktoranden anzunehmen, bedanken. Darüber hinaus gilt mein Dank Professor Dr. Markus Hölzle für die Übernahme des Zweitgutachtens.

Im Besonderen möchte ich Ulf Groos für die Möglichkeit zur Promotion am Fraunhofer ISE danken. Unser Treffen in Vancouver, währenddessen wir über Lebenspfade plauderten und die Doktorandenstelle am ISE wie ein dicker Zaunpfahl winkte, ist mir noch sehr gut in Erinnerung, und ich bin sehr glücklich, dass sich unsere Pfade dort wieder trafen.

Dr. Nada Zamel möchte für ihre wissenschaftliche Unterstützung, aber auch insbesondere für ihre humoristische Art danken, mit der Sie mir die Welt der Forschung inklusive der Fachpublikation zugänglicher machte. Als Doktorand verliert man sich manchmal im Detail und somit den Überblick, und in solchen Situationen waren unsere Gespräche immer sehr willkommen.

Herzlich möchte ich mich bei meinen Kollegen bedanken, die mich fachlich, kritisch und ebenfalls mit Humor in den letzten Jahren im Labor und am Schreibtisch unterstützten. Das gilt im Besonderen für Jens Theobald, der mit Ruhe und Systematik (wovon ich mir eine Scheibe abschneiden sollte) in aller Regel meine Wünsche und Probleme am Teststand lösen und somit erst verschiedenste Messungen ermöglichen konnte. Dieser Dank gilt jedoch ebenso allen meiner Kolleginnen und Kollegen, die ich nicht einzeln auflisten möchte, da mich jede unserer Diskussionen zu chemisch-physikalischen Vorgängen, zum Betrieb von Brennstoffzellen, zur Fluidik und Sicherheit drum herum, ja, grundsätzlich zu allem Technikrelevanten weiterbrachte, und, das ist ganz wichtig, schlicht Spaß machte!

Zu guter Letzt gilt mein größter Dank jedoch meiner Familie, meinen Eltern Volker und Eleonore und Schwestern Anna und Maria, sowie meiner Partnerin fürs Leben Zazie, deren moralisch, seelische Unterstützungen mich erst am Ball haben bleiben lassen. Natürlich gibt es Phasen, in denen der eigene Pfad in Frage gestellt wird, aber mit solch einem familiären und partnerschaftlichen Hintergrund fällt alles einfach leichter – vielen Dank!